

University of Louisville

ThinkIR: The University of Louisville's Institutional Repository

Electronic Theses and Dissertations

8-2017

Characterization of *Porphyromonas gingivalis* Mfa1 fimbriae.

Jae Yong Lee

University of Louisville

Follow this and additional works at: <https://ir.library.louisville.edu/etd>



Part of the [Bacteriology Commons](#), and the [Biochemistry, Biophysics, and Structural Biology Commons](#)

Recommended Citation

Lee, Jae Yong, "Characterization of *Porphyromonas gingivalis* Mfa1 fimbriae." (2017). *Electronic Theses and Dissertations*. Paper 2766.

<https://doi.org/10.18297/etd/2766>

This Doctoral Dissertation is brought to you for free and open access by ThinkIR: The University of Louisville's Institutional Repository. It has been accepted for inclusion in Electronic Theses and Dissertations by an authorized administrator of ThinkIR: The University of Louisville's Institutional Repository. This title appears here courtesy of the author, who has retained all other copyrights. For more information, please contact thinkir@louisville.edu.

CHARACTERIZATION OF *PORPHYROMONAS GINGIVALIS* MFA1 FIMBRIAE

By

Jae Yong Lee

A Dissertation

Submitted to the Faculty of the

School of the Interdisciplinary and Graduate Studies of the University of Louisville

in Partial Fulfillment of the Requirements

for the Degree of

Doctor of Philosophy in Interdisciplinary Studies

School of Interdisciplinary and Graduate Studies

University of Louisville

Louisville, KY

August 2017

CHARACTERIZATION OF *PORPHYROMONAS GINGIVALIS* MFA1 FIMBRIAE

By

Jae Yong Lee

A Dissertation Approved on August 7th, 2017

by the following Dissertation Committee

Dr. Richard Lamont, Chair

Dr. Donald Demuth

Dr. Matthew Lawrenz

Dr. Jan Potempa

Dr. David Scott

ACKNOWLEDGEMENTS

I would like to thank my mentor Dr. Richard Lamont for giving me the invaluable opportunity to work in his lab and guiding me throughout this project during my three years as a PhD student in the DMD/PhD dual-degree program. I would also like to express my gratitude to my other committee members Dr. Demuth, Dr. Lawrenz, Dr. Potempa, and Dr. Scott for their insights during committee meetings. Finally, I would like to thank my parents and family members for their unconditional support.

ABSTRACT

CHARACTERIZATION OF *PORPHYROMONAS GINGIVALIS* MFA1 FIMBRIAE

Jae Yong Lee

August 7, 2017

Porphyromonas gingivalis, an obligate anaerobic bacterium associated with chronic periodontitis, utilizes various virulence factors to achieve pathogenicity, one of which is the Mfa1 fimbriae. As a surface structure comprising Mfa1 major subunit along with accessory fimbrial proteins Mfa2-5, the Mfa1 fimbriae has been shown to mediate the adherence of *P. gingivalis* to antecedent bacterial colonizers of the oral cavity to cause increased virulence. However, the spatial relationships amongst the individual subunits and their assembly mechanism have remained unclear. Through immunoelectron microscopy, Mfa1-4 were localized on the surface of *P. gingivalis* with Mfa1 localizing throughout the fimbriae and Mfa2 in the base. Mfa3 and Mfa4 were both localized in the distal portion of the Mfa1 fimbriae. ELISA-based binding experiments with recombinant Mfa proteins and whole-cell ELISA experiments with wild-type and isogenic individual *mfa* mutants showed intricate interactions amongst Mfa proteins that implicated Mfa3 as the adaptor protein interlinking other fimbrial subunits with the fimbrial assembly initiating within the periplasm. Binding assays also demonstrated that

the inter-subunit interactions occur independently of the proteolytic processing known to take place on the surface for Mfa1, Mfa3, and Mfa4 by an arginine specific protease Rgp. However, immunoblotting of Mfa1 proteins corresponding to pre- or post-Rgp processed forms indicated that the polymerization is initiated upon the proteolytic processing on the surface and that both N- and C-terminal regions of post-Rgp processed Mfa1 protein are crucial for its polymerization. Mfa1 polymerization assay with *rgpA/B* mutant also confirmed that the pre-Rgp processed form is unable to polymerize. Furthermore, substitutions of alternating hydrophobic amino acid residues in the terminal regions of recombinant Mfa1 with charged residues yielded Mfa1 proteins that failed to polymerize, reminiscent of a distinct polymerization present in type I and P pili systems of *E. coli* termed donor-strand exchange (DSE). Collectively, the fimbrial subunits may initiate the assembly within the periplasm prior to the proteolytic processing on the surface with Mfa3 serving as an adaptor protein between Mfa1 and other accessory fimbrial proteins and that the polymerization of Mfa1 necessitates a DSE-like process with the terminal regions forming the binding interface between Mfa1 subunits.

TABLE OF CONTENTS

	Page
Acknowledgements.....	iii
Abstract.....	iv
List of Tables.....	vi
List of Figures.....	vii
Introduction.....	1
Materials and Methods.....	17
Results.....	38
Discussion.....	92
Conclusion.....	101
References.....	102
Curriculum Vita.....	106

LIST OF TABLES

Table	Page
1. Bacterial strains used in this study.....	29
2. Plasmids used in this study.....	30
3. Primers used for cloning, RT-PCR, and site-directed mutagenesis.....	33
4. Estimated apparent dissociation constants (K_D) from the saturation binding ELISA with pre-Rgp processed recombinant Mfa proteins.....	49

LIST OF FIGURES

Figure	Page
1. Localization of Mfa1 via immuno-negative stain TEM.....	40
2. Localization of Mfa2 via immuno-negative stain TEM.....	41
3. Localization of Mfa3 via immuno-negative stain TEM.....	42
4. Localization of Mfa4 via immuno-negative stain TEM.....	43
5. Binding ELISA between pre-Rgp processed Mfa3 and other pre-Rgp processed Mfa proteins.....	46
6. Pre-Rgp processed Mfa saturation binding ELISA.....	48
7. Binding ELISA between Mfa2 and other pre-Rgp processed Mfa proteins.....	51
8. Binding ELISA between pre-Rgp processed Mfa1 and Mfa2.....	52
9. Secondary structure estimation of recombinant Mfa proteins via circular-dichroism (CD) spectroscopy.....	59
10. Binding ELISA between post-Rgp processed Mfa3 and other post-Rgp processed Mfa proteins.....	61
11. Binding ELISA between Mfa2 and other post-Rgp processed Mfa proteins	62

12. Mfa surface presentation and expression in <i>mfa</i> mutants via whole cell ELISA and immunoblotting analyses.....	67
13. Homology search of <i>E. coli</i> DegP against the <i>P. gingivalis</i> 33277 genome via NCBI BLAST.....	70
14. Transcriptional analyses of <i>mfa</i> gene cluster in <i>mfa</i> mutants.....	71
15. Mfa1 polymerization in <i>mfa</i> mutants.....	75
16. Predicted secondary structure of Mfa1.....	79
17. Mfa1 polymerization assay with recombinant Mfa1 proteins.....	80
18. Mfa1 polymerization assay with 33277, <i>mfa1</i> mutant, <i>rgpA/B</i> mutant, and <i>kgp</i> mutant.....	81
19. Mfa1 polymerization assay with N-terminal or C-terminal beta-strand disrupted Mfa1.....	83
20. CD spectra of post-Rgp processed recombinant Mfa1 and its derivative with N-terminal or C-terminal beta-strand disruption.....	85
21. Predicted biochemical characteristics of Mfa1 termini.....	89
22. Beta-strand disruption and hydrophobicity alteration on post-Rgp processed rMfa1 termini.....	90
23. Mfa1 polymerization with hydrophobicity altered post-Rgp processed recombinant Mfa1.....	91
24. Proposed assembly model of Mfa1 fimbriae.....	100

CHAPTER 1 INTRODUCTION

Periodontitis and *P. gingivalis*

Chronic adult periodontitis is a prevalent oral inflammatory disease affecting approximately half the US adult population (1). Clinically, severe disease manifests with alveolar bone resorption and loss of periodontal ligaments and can be accompanied by tooth loss in affected sites. The cause of chronic adult periodontitis is microbial in nature and involves an excessive host inflammatory response to subgingival bacterial plaque and biofilm. A prevailing theory suggests that a few opportunistic pathogens that reside within the subgingival biofilm can alter the profile of the surrounding microbial communities from commensal to pathogenic through synergistic and cooperative processes with other normally commensal bacteria to ultimately render the host's immune system less effective in bacterial clearance (2). Increased bacterial load then gives rise to sustained inflammation and subsequently elicits damage to the periodontium through the actions of osteoclasts and components of the host innate immune system.

One of the oral organisms thought to participate in such pathogenic process is *Porphyromonas gingivalis*, a Gram-negative obligate anaerobe. As a low-abundance opportunistic pathogen in the subgingival environment, *P. gingivalis* employs various intricate mechanisms to promote pathogenic community development with already existing subgingival microbiome (2). Specifically, *P. gingivalis* attaches to oral streptococci that are established on salivary pellicles on the tooth surface. Such oral

streptococci are hence considered primary colonizers with *P. gingivalis* considered secondary colonizers. The interaction between a member of oral streptococci, *S. gordonii*, and *P. gingivalis* leads to subgingival biofilm development that provides anaerobic environment and important metabolites for *P. gingivalis* with interbacterial communication mediated by autoinducer molecules such as AI-2 (2, 3). For instance, 4-aminobenzoate (pABA) generated by *S. gordonii* can be used by *P. gingivalis* to be entered through the histidine degradation pathway, which ultimately results in elevated pathogenic profile of *P. gingivalis* (3). Furthermore, *P. gingivalis* bestows *S. gordonii* and other surrounding members of the subgingival biofilm an increased protection from the host innate immune system by degrading complement proteins and undermining the phagocytic ability of neutrophils (2). To facilitate such pathogenic processes, *P. gingivalis* specifically utilizes virulence factors including its lipopolysaccharides (LPS), capsule, proteases, and fimbriae.

LPS

Lipopolysaccharides (LPS) are Gram-negative surface structures composed of lipid A, core polysaccharides, and O-antigen. The lipid A endotoxins, can elicit severe inflammatory response by the host and contribute to septic shock when recognized by the host's pattern recognition receptors including toll-like receptors 2 and 4 (4, 5). Structurally, core polysaccharides of *P. gingivalis* LPS are conserved, whereas *P. gingivalis* lipid A and O-antigen exhibit variations depending on the number of acylation on lipid A and the biochemical nature of repeating polysaccharides that constitute the O-antigen. Specifically, lipid A of *P. gingivalis* LPS has been shown to be either tetra-acylated or penta-acylated, and the O-antigen can exhibit either tetrasaccharide or anionic polysaccharide as repeating units, designated as O-LPS and A-LPS respectively (6). Furthermore, tetra-acylated lipid

A exhibits an antagonistic effect (i.e. innate immune suppressive) on TLR4 (7), whereas penta-acylated lipid A displays a weak agonistic effect (i.e. innate immune evasive) on TLR4 (8). Interestingly, the conversion between different acylation states of lipid A is dependent on the concentration of hemin, an important nutrient for *P. gingivalis*, with high hemin concentration leading to tetra-acylation and low hemin-concentration to penta-acylation, and *P. gingivalis* lipid A phosphatase, an activity of which is dependent on hemin concentration, has also been shown to be directly involved in the conversion process (9). In addition, variations in O-antigen modifications have important functional implications. For instance, A-LPS confers resistance to complement system by hindering depositions of complement proteins on the bacterial surface (10). Furthermore, A-LPS provides a covalent attachment site for some of the exported proteins of *P. gingivalis*, thereby anchoring them on the surface (11).

Capsule

Capsule, or capsular polysaccharide, is the outermost layer in a number of *P. gingivalis* strains with six reported serotypes K1-6 (12). The precise structure and composition of each of the serotypes are not completely defined. Despite the structural uncertainty, mounting evidence has demonstrated elevated virulence and pathogenicity with encapsulated strains compared to non-encapsulated ones. Specifically, a reduced level of pro-inflammatory cytokines (IL-1 β , IL-6, and IL-8) was observed when human gingival fibroblasts were infected with a *P. gingivalis* mutant lacking a capsule compared to the wild-type that produces a capsule (13). It was also shown in an animal model that encapsulated strains elicit more severe pathogenic outcomes compared to non-encapsulated strains, as mice infected with encapsulated strains exhibited more systemic

spread of infection with necrosis and body weight loss compared to the localized nature of infection and abscess formation in mice infected with non-encapsulated strains (14).

Proteases

P. gingivalis possesses three known cysteine proteases, which are also referred to as gingipains. They include arginine-specific proteases RgpA and RgpB that cleave the peptide bond following an arginine residue, and the lysine-specific protease Kgp that cleaves a peptide bond after a lysine residue (15). Importantly, gingipains contain conserved domains on the C-terminus that are cleaved by the PorU signal peptidase upon translocation to the surface, and the translocation from cytoplasm to the surface is facilitated by Type IX secretion system that comprises several Por proteins: conserved C-terminal domains are characteristic of proteins utilizing the Type IX secretion system (16). Upon translocation, gingipains are thought to be anchored onto the surface through covalent attachment to A-LPS catalyzed by a putative sortase PG0026, which is also designated as PorU signal peptidase (11). In addition, gingipains are produced as an enzymatically inactive form, and their conversion into the active form necessitates proteolytic processing following the transport onto the surface, where Kgp and RgpA form into a complex while RgpB remains as a monomer (15). Functionally, gingipains participate (i) in processing of nutrients including proteins, some of which containing heme moieties, to accommodate the inability of *P. gingivalis* to metabolize carbohydrates and its requirement for porphyrin and iron, (ii) in enhancing the virulence of *P. gingivalis* by serving as ligands to extracellular matrix proteins and host cells via hemagglutinin-adhesin domains found in RgpA and Kgp, (iii) by processing its own fimbrial proteins to facilitate their assembly on the surface, and (iv) by undermining the host immune system through

proteolysis of various complement proteins and immunologically important host cell surface receptors (15).

Fimbriae

The FimA fimbria is a proteinaceous structure protruding from throughout the surface of *P. gingivalis* and is composed of FimA major subunit protein (43 kDa) that forms an oligomeric backbone with its length varying from 0.3 micron to 3 micron (17). The fimbria is expressed from a gene cluster that includes *fimA*, *fimB*, *fimC*, *fimD*, and *fimE*, with the last four genes encoding for accessory fimbrial proteins (18). The fimbria functions as an adhesive unit that enables *P. gingivalis* to adhere to host cells and other oral bacteria. For instance, FimA has been shown to interact with β 1-intgerin surface protein of gingival epithelial cells and the GAPDH surface protein of streptococci (19, 20). Moreover, accessory fimbrial proteins FimC and FimD were shown to adhere to extracellular matrix proteins including fibronectin and collagen (21). While no adhesive role has been reported for FimE, the protein was shown to serve as a recruiting protein that binds both FimC and FimD for their assembly into the FimA fimbriae (21). FimB, on the other hand, was shown to regulate fimbrial length as Δ *fimB* mutants produce a longer FimA fimbria, suggesting FimB's role in fimbrial assembly and elongation (22).

Mfa1 fimbria is another proteinaceous structure extending from throughout the surface of *P. gingivalis* and ranges in length from 60 nm to 500 nm, with Mfa1 constituting the major subunit (75 kDa) in an oligomeric form (23, 24). Mfa1 fimbria also serves an adhesive role for *P. gingivalis* with pathogenic implications. Specifically, Mfa1 binds to SspB surface protein of *Streptococcus gordonii* through a 26-amino acid region within the C-terminus domain of SspB spanning amino acid residues 1167 to 1250 termed BAR (Ssp**B**

Adherence Region) (25, 26). The interaction between Mfa1 and SspB has been shown to be the main driving force in interbacterial adhesion and subsequent dual-species community development between *P. gingivalis* and *S. gordonii* (24). Furthermore, the dual-species community between *P. gingivalis* and *S. gordonii* induced more alveolar bone resorption in mice model of periodontitis than either organism alone, suggesting synergistic pathogenicity by the *P. gingivalis*-*S. gordonii* community (27). Interestingly, alveolar bone resorption level and hence the pathogenicity of the dual-species community were significantly diminished in the presence of peptide derived from BAR domain in the same mice model, demonstrating the importance of Mfa1-SspB interaction in the progression of virulence (27). Another reported binding partner for Mfa1 fimbriae is DC-SIGN (dendritic cell-specific ICAM-3 grabbing nonintegrin) receptor of human dendritic cells (28). Interaction between Mfa1 and DC-SIGN facilitates the entry of *P. gingivalis* into dendritic cells and subsequent persistence of *P. gingivalis* within the cells, leading to blocked maturation of dendritic cells, stimulation of Th2 effector response, and diminished level of pro-inflammatory cytokines (28).

Mfa1 fimbrial components are expressed from a gene cluster that includes *mfa1*, *mfa2*, *mfa3*, *mfa4*, and *mfa5*, and the latter four encode for accessory fimbrial proteins Mfa2-5, respectively (29, 30). Transcriptional analysis of the *mfa* gene cluster revealed *mfa1-4* are co-transcribed and that *mfa1-4* constitute an operon, whereas *mfa5* is transcribed independently of *mfa1-4* (22). The purified Mfa1 fimbria has been shown to comprise Mfa1 (67 kDa), Mfa3 (40 kDa), Mfa4 (37 kDa), and Mfa5 (120 kDa) (31). However, studies have also demonstrated that Mfa1 co-immunoprecipitates with Mfa2 in cell lysates of *P. gingivalis*, suggesting either a direct or indirect interaction between the

two proteins and hence a potential incorporation of Mfa2 into the Mfa1 fimbria (31, 32). Furthermore, Mfa2 has been shown to regulate fimbrial length as a $\Delta mfa2$ mutant has been shown to produce longer Mfa1 fimbriae, further suggesting that Mfa2 may be a component of a fully assembled Mfa1 fimbria and may serve as an assembly and elongation terminator (31, 32). Consistent with Mfa2's putative role as an assembly terminator, the protein was localized in the basal portion of the Mfa1 fimbriae in immune-electron microscopy (31). Other accessory fimbrial proteins Mfa3, Mfa4, and Mfa5 have been shown to participate in the fimbrial assembly process as the absence of any one of the three proteins resulted in purified Mfa1 fimbriae that lack all three accessory fimbrial proteins, suggesting a direct interaction amongst Mfa3-5 to yield a supramolecular complex (30, 33, 34). Moreover, Mfa3 has been shown to localize in the distal tip portion of the Mfa1 fimbriae in immunoelectron microscopy, suggesting its potential role as a ligand to receptors on host cells and other oral bacteria (33). However, the location of Mfa4 and the binding interactions amongst Mfa proteins have not been previously examined.

Mfa1 fimbrial biogenesis/assembly and Mfa1 major subunit polymerization

It is evident that as one of the crucial virulence factors of *P. gingivalis*, the Mfa1 fimbria has been actively investigated in both *in vitro* and *in vivo* settings with some studies showing therapeutic implications for Mfa1 fimbria-mediated pathogenic processes (24, 27, 35-37). Such findings on Mfa1-mediated interbacterial adherence mechanism of *P. gingivalis* and *S. gordonii* have led to significant advancements with regards to functional insights into the fimbria and some of its component Mfa proteins. Yet, much is still unknown regarding the mechanism by which Mfa proteins assemble into a complete structure upon translocation into the periplasm and beyond. Specifically, binding partners

amongst Mfa proteins both within the periplasm and on the surface to yield a supramolecular complex, and the role of accessory Mfa proteins in expression and surface presentation of individual Mfa fimbrial proteins, have remained elusive. In addition, the biochemical mechanism by which individual Mfa proteins (especially the Mfa1 major subunit) adhere to each other has only recently begun to unravel with groundbreaking crystallizations of FimA and Mfa4 (32, 38). Nonetheless, the Mfa1 major subunit polymerization mechanism is still an active avenue of investigation due to a paucity of biochemical and structural evidence. As further insights into the assembly and polymerization mechanism of Mfa1 fimbria may provide a model that can be generalized to other Gram-negative bacterial pili systems and may also reveal specific targets within the assembly or polymerization process for therapeutics delivery to prevent or treat chronic adult periodontitis, it is imperative to further examine both Mfa1 fimbrial assembly and polymerization processes.

Overview of *P. gingivalis* Mfa fimbrial biogenesis and assembly

Biogenesis and assembly of Mfa1 fimbriae entail multiple steps from their initial transcription to the final assembly on the surface. Upon transcription and translation in the cytoplasm, nascent Mfa fimbrial proteins, apart from Mfa5, are thought to be transported into the periplasmic space via SecYEG translocon located in the inner membrane, guided by their N-terminal signal peptides of approximately 20 amino acids in length (30, 39). It has been proposed that upon translocation into the periplasmic space, signal peptides of the fimbrial proteins are cleaved by type II signal peptidase, which specifically targets a cysteine residue on the C-terminus of the signal peptide, and the cysteine residue is then lipidated by another periplasmic enzyme Lgt to yield a lipoprotein (39). The now lipidated

fimbrial proteins are proposed to be transported to the outer membrane via a largely unknown mechanism that may resemble a lipoprotein-outer membrane-localization pathway, which proposes a chaperone-like protein that directly associates with the lipoproteins and guides them to the outer membrane; once at the outer membrane, either a pore-like channel protein or a dynamic transporter protein termed flippase export them onto the surface (40). The fimbrial proteins, Mfa1, Mfa3, and Mfa4, are then further processed by arginine-specific proteases (RgpA and RgpB) and assemble into a complete fimbrial structure (22, 30, 32, 34, 38).

Role of intrinsic proteases in processing/maturation of fimbrial proteins

Previous studies have demonstrated the essential role played by RgpA/B and, to lesser extent, the lysine-specific protease Kgp in biogenesis and processing of Mfa proteins (32, 38, 39, 41, 42). Mfa1 produced in a double Rgp and Kgp knock-out strain exhibited two distinct molecular weights in an immunoblot of cell lysates with one corresponding to the mature form of 67 kDa and another at a higher molecular weight corresponding to an immature/precursor form, demonstrating a direct involvement of proteases in biogenesis and processing of Mfa1 (34, 39, 41). Localization of proteolytic processing was pinpointed to the N-terminal region of Mfa1, as autoradiographic analysis of [³H] palmitic acid labeled cell lysates of *rgp/kgp* knock-out strain detected only the higher molecular weight form (immature form) of Mfa1 but not the mature form of Mfa1, suggesting that upon lipidation of N-terminal cysteine residue, a subsequent proteolytic processing by intrinsic proteases leads to a removal of the lipidated N-terminal region of Mfa1 to yield the mature form (39). Interestingly, only one of the two Rgp is required for processing of Mfa1, as single mutants still leads to proteolytic processing of Mfa1 (41). Specifically, the C-

terminal peptide bond of arginine 49 of Mfa1 is predicted to be cleaved by Rgp, yielding a mature form starting with alanine 50 (39). In contrast, the accessory fimbrial protein Mfa2 does not undergo proteolytic processing by either RgpA or RgpB and remains as a lipoprotein on the surface with lipidation at cysteine 28 playing a role in efficient surface presentation of Mfa2 (32). Mfa3 and Mfa4 have been shown to also undergo proteolytic processing by Rgps at arginine 43 and arginine 53, respectively (33, 34). In the case of Mfa4, it has been shown that Kgp may also be involved in processing, as a replacement of arginine 53 with alanine for Mfa4 still led to the production of Mfa4 with a molecular weight intermediate of mature and precursor form in *P. gingivalis* lysate with its N-terminal amino acid analysis suggesting a proteolytic processing following lysine 50 (38). Consequently, Mfa4 was proposed to undergo two rounds of processing, first by Kgp at lysine 50 and then by Rgp at arginine 53 (38). Interestingly, Kgp was also shown to rescue processing of Mfa4. Replacement of arginine 53 with lysine led to a production of mature form of Mfa4 in *P. gingivalis* lysate, suggesting an intricate rescuing mechanism in the processing of fimbrial proteins when one type of protease is not functional or absent (38). On the other hand, Rgps were shown not to be essential in the processing of Mfa5 (30). However, Mfa5 has been reported to utilize the Type IX secretion system that entails a cleavage of conserved peptide located on the C-terminus of Mfa5 (from amino acid residues 1,207 to 1,228) by the PorU signal peptidase and export of the protein through a dedicated secretion channel, which comprises several Por proteins which mostly reside in the outer membrane (30).

Expression and surface presentation of Mfa1 fimbria and its components

Because Mfa1 fimbria is a heteropolymeric complex consisting of Mfa1, Mfa3, Mfa4, Mfa5, and potentially Mfa2, it is possible that each of the fimbrial components may affect expression, processing, and surface presentation of other Mfa component proteins. For instance, Mfa4 has been shown to be essential in proper incorporation of Mfa3 and Mfa5 into the Mfa1 fimbria, and the lack of Mfa4 prevents Mfa3 from being properly processed (34). Additionally, while Mfa3 does not affect proteolytic processing of Mfa4 and Mfa5, the absence of Mfa3 prevents the incorporation of Mfa4 and Mfa5 into Mfa1 fimbria (33). Interestingly, it has been reported that the surface presentation of Mfa1 major subunit protein is reduced in isogenic mutants of *P. gingivalis* lacking either *mfa4* or *mfa5*, suggesting an intricate role played by accessory fimbrial proteins in assembly and surface presentation of Mfa1 fimbria (30, 34). Therefore, to further understand the mechanism by which Mfa proteins assemble into a complete fimbrial structure, the role of accessory proteins Mfa2-5 in expression, processing, and surface presentation of Mfa1 fimbrial components must be examined, preferably in individual *mfa* mutants of *P. gingivalis* with intact FimA fimbria to more definitively characterize the function of each *mfa* gene product.

Polymerization mechanisms in bacterial pili/fimbrial system

Polymerization of major fimbrial subunits to produce a rod-like structure on the surface represents a pivotal step in fimbrial biogenesis as it determines the physical and, to an extent, biochemical nature of the bacterial surface. Thus, it has been actively studied in the field of microbiology in many of the Gram-positive and Gram-negative bacterial fimbrial systems. The majority of Gram-positive and Gram-negative pili/fimbriae are composed of major subunit protein forming a homopolymeric structure that extends from

the surface with accessory/minor proteins often capping the tip portion or completing the fimbrial structure at the basal portion (43). In Gram-positive bacteria, the polymerization mechanism of major subunit proteins entails formation of inter-subunit covalent bonds catalyzed by a sortase (43). In Gram-negative bacteria, polymerization of the major subunit is mediated by non-covalent bond formation between subunits that may involve a combination of hydrophobic, polar, or electrostatic interactions (43).

One of the well-characterized fimbrial polymerization mechanisms in bacteria is termed donor-strand exchange (DSE) (44). DSE has been shown to be essential in the biogenesis of the chaperone-usher mediated fimbrial/pili system including type I/P pili of *E. coli* (43-45). In type I and P pili systems, fimbrial proteins possess a conserved, incomplete IgG fold, that lacks a β -strand in the C-terminus of the fimbrial proteins (44). The incomplete IgG fold creates a hydrophobic groove on the C-terminus and renders the fimbrial proteins unstable and consequently insoluble (44). However, an N-terminal β -strand present in the type I/P fimbrial proteins interacts with the C-terminal hydrophobic groove of another fimbrial subunit by forming intersubunit non-covalent bonds, thereby completing the IgG fold and stabilizing the proteins (44). Upon interaction between the N-terminal β -strand of a major subunit and C-terminal hydrophobic groove of another major subunit, a dimeric structure is formed. The processive interactions between the two termini of nascent major subunits yielding a polymeric backbone of the type I/P pili (44). In particular, the N-terminal β -strand is designated as the donor-strand or N-terminal extension, and exhibits distinct biochemical characteristics. Specifically, crystallographic evidence has shown that the donor-strand in type P pili system contains alternating

hydrophobic residues that are crucial in DSE, as they interact with hydrophobic pockets residing on the C-terminal hydrophobic groove (44).

Recently solved crystal structures of the FimA major subunit of FimA fimbriae and Mfa4 accessory subunit of Mfa1 fimbriae suggest *P. gingivalis* may utilize DSE for its fimbrial polymerization and biogenesis (32, 38). FimA consists of two domains termed the N-terminal domain (NTD) and C-terminal domain (CTD), with each domain comprising seven β -strands that form β -sheets (32). Furthermore, the NTD and CTD both contain hydrophobic grooves that interact with β -strands, and such grooves have been shown to be aligned with each other, thereby giving rise to a continuous groove that extends across both domains (32). Thus, the continuous groove interacts with two distinct β -strands, one stemming from NTD (N-terminal β -strand) and another from CTD (C-terminal β -strand). Additionally, an extra β -strand extends from the C-terminal β -strand, however this β -strand does not interact with the CTD groove (32). Furthermore, the N-terminal β -strand includes a loop region with an Rgp cleavage site, and the C-terminal β -strand lies directly under this loop (32). According to the FimA polymerization model proposed by Xu *et al*, the N-terminal β -strand that was occupying the NTD groove would dissociate from the protein upon Rgp processing of FimA and subsequently uncover the NTD groove (32). Next, the C-terminal β -strand that was occupying the CTD groove would undergo a conformational change to assume an extended conformation along with an extra β -strand into the solvent away from the protein core (32). The C-terminal β -strand and the consecutive extra β -strand would then interact with NTD groove and CTD groove, respectively, of another Rgp-processed/mature FimA to form a dimer, thereby initiating FimA polymerization. Additional experiments involving cysteine substitution based crosslinking of the FimA

polymer in *P. gingivalis* lysates confirmed the interaction between C-terminal β -strand and NTD groove (32). While the location of putative donor-strand is on the C-terminus rather than on the N-terminus, as is the case in type I/P pili system of *E. coli*, the completion of β -sheet structures by incoming β -strands from another major subunit docking into a hydrophobic groove, supports the DSE as a likely polymerization mechanism of FimA. Interestingly, the crystal structure of Mfa4 revealed that Mfa4 does not possess the two C-terminal β -strands involved in putative DSE in FimA, positioning Mfa4 as a putative tip pilin as it is unable to continue the DSE process due to the lack of donor-strands (32, 38). However, Mfa4 has been shown to possess an Rgp cleavage site, and similar to FimA, cleavage by Rgp removes N-terminal β -strands and uncovers a hydrophobic groove that can accept an incoming donor-strand, thereby enabling Mfa4 to partake in the DSE albeit only as an acceptor subunit (32). While Mfa4 does not possess the C-terminal β -strands found in FimA, it does exhibit N-terminal β -strands following the Rgp cleavage site (38). It has been proposed that such N-terminal β -strands may be able to participate in DSE by undergoing a conformational change to assume an extended position into the solvent. This would allow Mfa4 to not only accept an incoming fimbrial subunit but also insert its own putative N-terminal donor-strands to another subunit during fimbrial biogenesis (38). However, whether such DSE is possible in the Mfa1 major subunit of Mfa1 fimbriae has not been experimentally shown.

Additional functional roles for Rgp proteases in fimbrial biogenesis apart from simple cleavage of N-terminal residues has been implied from the structural evidence of FimA and Mfa4 (32, 38). Prior to processing by an Rgp, the C-terminal β -strands of FimA remain folded close to the protein core while the N-terminal β -strands cover the

hydrophobic groove necessary for DSE, according to the FimA crystallographic evidence (32). Similarly, in a study examining the structure of Mfa4, Klopsteck *et al.* proposed that the N-terminal β -strands prior to the Rgp cleavage site may serve as an intrinsic chaperone by improving the solubility and stability of Mfa4, likely by covering the hydrophobic groove by the N-terminal β -strands (38). Hence, Rgp processing of N-terminal residues in *P. gingivalis* fimbrial proteins most likely serves to improve protein stability and solubility to ultimately preserve the fimbrial proteins in a monomeric state prior to initiation of polymerization on the bacterial surface following Rgp processing. However, direct biochemical evidence demonstrating Rgp roles in maintaining the fimbrial proteins in monomeric form is largely lacking, and in particular the role of Rgp processing in polymerization initiation of the Mfa1 major subunit fimbriae has not been extensively studied.

Aims and Experimental Approach

In this study, assembly and polymerization mechanisms of Mfa fimbria were investigated using a combination of biochemical and molecular approaches based on the central hypothesis that accessory Mfa proteins mediate expression and surface presentation of Mfa1 fimbria, and that polymerization of the Mfa1 major subunit requires a select hydrophobic amino acid residues residing on the protein termini reminiscent of DSE of type 1 and P pili systems of *E. coli*. To gain a better understanding of spatial relationships of Mfa1 fimbrial components and to identify potential interacting partners along the assembly pathway, recombinant Mfa proteins were generated and their binding interactions amongst each other were examined through enzyme-linked immunosorbent assays, in addition to localization of individual Mfa proteins on the surface of *P. gingivalis* via

immuno-transmission electron microscopy. Furthermore, relative binding affinities amongst pairs exhibiting binding activity were estimated via saturation binding ELISA, and the secondary structure content of recombinant Mfa proteins were approximated through circular-dichroism spectroscopy. Individual *mfa* deletion mutants were also generated to further examine the expression of Mfa1-4 within the whole cell lysates, and their surface presentation via immunoblotting and whole cell ELISA. Lastly, Mfa1 polymerization mechanism was studied through truncation and amino acid substitution-based assays using various recombinant Mfa1 proteins and *rgpA/B* mutant with the polymerization pattern examined via immunoblotting.

CHAPTER 2 MATERIALS AND METHODS

Bacterial strains and growth conditions

All bacterial strains used in this study are listed in Table 1. *P. gingivalis* ATCC33277 strain and its isogenic mutants were grown anaerobically at 37°C without shaking in Trypticase-soy broth supplemented with 1 g/L yeast extract, 5 mg/L hemin, and 1 mg/L menadione. For solid medium, 1.5% agar and 5% sheep blood were added. Erythromycin (10 µg/mL) or tetracycline (1 µg/mL) was included in the culture media as needed.

E. coli BL21 Star (DE3) strain (Invitrogen) was cultured aerobically at 37°C with shaking in Luria-Bertani (LB) Broth, or on LB agar plates. Kanamycin (50 µg/mL) or ampicillin (200 µg/mL) was included in the culture media as needed.

Plasmid construction for recombinant proteins

All *P. gingivalis* 33277 genes amplified via polymerase chain reactions (PCR) and plasmids used for cloning are listed in Table 2. All primers (Sigma) used in this study are listed in Table 3. pGEX6P::*mfa2* and pHIS101::*mfa3* were kindly provided by Dr. Yoshiaki Hasegawa (Aichi Gakuin University, Japan) and Dr. Karina Persson (Umea University, Sweden), respectively. For cloning of *mfa* genes, TOPO cloning kits (Thermo Fisher) were used, and the manufacturer's instructions included in the kits were followed. Briefly, a gene was amplified with Pfx polymerase (Thermo Fisher) or Phusion polymerase (New

England Biolabs) with the genomic DNA isolated from *P. gingivalis* 33277 through a genomic DNA purification kit (Promega) as a template. PCR products were then purified through a PCR purification kit (Qiagen) and were incubated with a TOPO plasmid, followed by transformation into chemically competent *E. coli* via heat-shock at 42°C. The resulting transformants were plated on LB agar plates with an appropriate antibiotic for overnight growth at 37°C. A single colony was picked, and plasmids were extracted with the plasmid miniprep kit (Qiagen) from the overnight growth culture of the colony. To ensure sequence integrity, plasmids were isolated from transformed *E. coli* with a plasmid miniprep kit (Qiagen) with plasmid concentrations measured through NanoDrop spectrophotometer (Thermo Fisher Scientific), and regions encompassing the inserts on the resulting constructs were sequenced through the Center for Genetics and Molecular Medicine DNA Facility Core at the University of Louisville. Sequence information was checked against *P. gingivalis* 33277 nucleotide sequences encoding for recombinant proteins through NCBI blastn (https://blast.ncbi.nlm.nih.gov/Blast.cgi?PAGE_TYPE=BlastSearch).

Protein expression and purification

Expression of hexahistidine (His)-tagged or glutathione-S-transferase (GST)-tagged recombinant proteins in transformed *E. coli* strains was induced for 3-4 h at 37°C with either 0.1 mM isopropyl β -D-1-thiogalactopyranoside (IPTG) or 0.2% lactose when optical density at absorbance 600nm (OD₆₀₀) of the culture was approximately 0.4-0.8 as measured by a Genesys30 Visible Spectrophotometer (Thermo Fisher Scientific). For expression of Mfa5, the culture was grown to OD₆₀₀ of 0.4-0.8 at 37°C and was induced at 15°C for 24 h with either 0.1mM IPTG.

His-tagged recombinant proteins were purified by immobilized metal ion chromatography using a nickel-charged resin. Briefly, *E. coli* cells were harvested by centrifugation at 5,000xg for 10 min followed by resuspension in phosphate-buffered saline (PBS) pH 7.4. Cells were then lysed through sonication on ice (6 min/500 ml culture; 5 sec on; 10 sec off; 40% amplitude; 120 kHz). Lysates were centrifuged at 7,000xg, and the supernatant was passed through the nickel-charged agarose resin (Qiagen) in either a gravity flow column or in a HisTrapFF Crude column (GE Healthcare Life Sciences) connected to the ÄKTA start chromatography system (GE Healthcare Life Sciences). Unbound proteins were washed off with running buffer (pH 8.0, 300 mM NaCl, 10 mM imidazole). Hexahistidine-tagged proteins were eluted from the resin with elution buffer (pH 8.0, 300 mM NaCl, 250 mM imidazole). The eluted protein was buffer-exchanged into PBS through Amicon Ultra centrifugal filters (EMD Millipore) by centrifugation at 5,000xg. When appropriate, His-tagged proteins were processed with either enterokinase (Genscript) or TEV protease (Genscript) for his-tag removal, and manufacturer's instruction was followed.

GST-tagged protein was purified through affinity chromatography using glutathione agarose resin (Genscript). Cell preparation and lysis steps were identical to those of His-tagged recombinant proteins. After passing the soluble fraction of lysate through the resin, unbound proteins were washed off with PBS (pH 7.4). Bound proteins were eluted with 50 mM Tris-HCl (pH 8.0) containing 10 mM reduced glutathione. For cleavage of GST tag, purified protein was buffer-exchanged to cleavage buffer (50 mM Tris-HCl (pH 7.0), 150 mM NaCl, 1 mM EDTA, and 1 mM DTT) and was incubated overnight at 4°C with GST-tagged PreScission Protease (Genscript). The reaction was

passed through the glutathione resin to remove the cleaved GST tag and the protease. The resulting flow-through containing the tag-free protein was buffer-exchanged to PBS through Amicon Ultra centrifugal filters (EMD Millipore) by centrifugation at 5,000xg.

For purification of post-Rgp processed form of recombinant Mfa4, the precursor His-tagged Mfa4 was first purified as described above. Upon purification and buffer exchange into PBS, His-tagged RgpB purified from *P. gingivalis* (gift from Dr. Jan Potempa, University of Louisville, USA) was incubated with Mfa4 overnight at room temperature and subsequent proteolytic cleavage was confirmed with SDS-PAGE. The cleaved N-terminal segment and His-tagged RgpB were removed by passing the reaction through the gravity flow column containing Ni-resin and by collecting the flow-through.

Measurement of protein concentration

Protein concentration was measured through the bicinchoninic acid (BCA) assay kit (Thermo Fisher Scientific), following the manufacturer's protocol. Briefly, 25 μ L of a bovine serum albumin (BSA) dilution series (2 mg/mL to 0 mg/mL) and the protein of unknown concentration were immobilized on a 96-well polystyrene microplate from Corning (flat/clear bottom, high binding capacity, full/round well) in technical duplicates and were immediately incubated with 200 μ L of 1:50 ratio of Reagents A and B provided with the kit for 30 min at 37°C. A standard curve was generated from absorbance 595 nm signals measured through the Victor X3 plate reader (PerkinElmer). A linear equation was derived from the standard curve using Microsoft Office Excel's *Add Trendline* function, and the unknown protein concentration was calculated by inserting its averaged absorbance at 595nm values into the equation.

Immuno-negative stain transmission electron microscopy

Ten mL of overnight bacterial culture were harvested by centrifugation at 3,000xg for 10 min and washed with 1 mL PBS. OD₆₀₀ of the washed culture was measured, and the cell density was diluted in PBS to OD₆₀₀ of 1. Ten µL of the bacterial solution was placed on parafilm, and a 200-mesh nickel grid with formvar/carbon film (Ted Pella) was suspended on the bacterial drop for 2 min, with the film side touching the drop. The grid was then suspended on 10µL 1% BSA in PBS for 1 h to block non-specific binding sites. The grid was placed on 10 µL diluted primary rabbit antibodies in 1% BSA for 1 h followed by washing in drops of 10 µL 1% BSA. Bacterial cells were probed with 10 µL of diluted secondary 10 nm gold particle-conjugated anti-rabbit goat IgG (Sigma Aldrich) for 1 h followed by washing in drops of 10 µL 1% BSA. The grid was fixed by incubating on 10 µL 2.5% glutaraldehyde (diluted from 8% glutaraldehyde, EM grade, Electron Microscopy Sciences) in PBS for 10 min prior to negative staining by suspending the grid on 10 µL 1% ammonium molybdate (Sigma Aldrich) in distilled water for 1 min. Negatively stained grids were then washed in distilled water, and any excess liquid was blotted with filter paper. The grid was then observed through a Hitachi HT7700 transmission electron microscope at 80 kV.

Protein-protein interaction enzyme-linked immunosorbent assay (ELISA)

Recombinant proteins were diluted in PBS and were immobilized on a 96-well polystyrene microplate from Corning (flat/clear bottom, high binding capacity, full/round well) in 100 µL volumes for 1 h at room temperature in technical duplicates. Wells were then washed with 200 µL PBS with 0.1% Tween (PBST), and blocked with 100 µL 10% skim milk in PBS for 1 h at room temperature. Potential binding partner recombinant

proteins were diluted to an appropriate concentration in PBST and were added to appropriate wells in 100 μ L volumes for 1 h incubation at room temperature. Wells were subsequently washed twice with 200 μ L PBST. Primary antibodies diluted in 1% skim milk in PBST were added into appropriate wells in 100 μ L volumes for 1 h incubation at room temperature. Wells were washed twice with 200 μ L PBST. Horseradish peroxidase-linked secondary antibodies (Cell Signaling Technology) diluted in 1:5000 ratio in 1% skim milk in PBST were then added into appropriate wells in 100 μ L volumes for 1 h incubation at room temperature. After washing wells twice with 200 μ L PBST, 100 μ L of 3,3',5,5'-tetramethylbenzidine (TMB; Thermo Fisher Scientific) substrate solution were added into each well for 10 min incubation at room temperature. The reaction was stopped with 100 μ L 0.16 M sulfuric acid (Thermo Fisher Scientific), and signals were measured at absorbance 450 nm on a Victor X3 plate reader.

Whole cell ELISA

Ten mL of overnight bacterial culture was harvested by centrifugation at 3,000xg for 10 min and washed with 1mL PBS. The OD₆₀₀ of the washed culture was measured, and the cell density was diluted to OD₆₀₀ of 1. One hundred μ L of the bacterial solution were immobilized on a 96-well polystyrene microplate from Corning (flat/clear bottom, high binding capacity, full/round well) in technical duplicates for 1 h at room temperature. Wells were then washed with 200 μ L PBST, and blocked with 100 μ L 10% skim milk in PBS for 1 h at room temperature. Primary antibodies diluted in 1% skim milk in PBST were added into appropriate wells in 100 μ L volumes for 1 h incubation at room temperature, followed by two rounds of washing with 200 μ L PBST. Horseradish peroxidase (HRP)-linked secondary antibodies (Cell Signaling Technology) diluted in

1:5000 ratio in 1% skim milk in PBST were then added into appropriate wells in 100 μ L volumes for 1 h incubation at room temperature. After washing wells twice with 200 μ L PBST, 100 μ L of 3,3',5,5'-tetramethylbenzidine (TMB; Thermo Fisher Scientific) substrate solution were added into each well for 10 min incubation at room temperature. The reaction was stopped with 100 μ L 0.16M sulfuric acid (Thermo Fisher Scientific), and signals were measured at absorbance 450nm on a Victor X3 plate reader.

Circular-dichroism spectroscopy and secondary structure estimation

Circular dichroism spectra of recombinant Mfa proteins in PBS were obtained from a Jasco J-810 circular dichroism spectropolarimeter from absorbance 190 nm to 260 nm at 25°C using a cuvette with a lightpath of 0.1mm. Data pitch, sensitivity, DIT/bandwidth, accumulations, and scanning speed were configured as 1 nm, standard, 1 nm, 4, and 100 nm/min respectively. Baseline spectra (in mdeg) measured from blank PBS (pH 7.4, 137 mM NaCl, and 2.7 mM KCl) were subtracted from the spectra of the recombinant proteins. The subtracted spectra values along with their corresponding absorbance values, protein molar concentrations in micromolar, number of amino acid residues, and pathlength information were inputted into the BeStSel server at <http://bestsel.elte.hu> to estimate secondary structure of the recombinant proteins.

SDS-PAGE and Western blot

For sodium dodecyl sulfate-polyacrylamide gel electrophoresis (SDS-PAGE), a resolving gel with 0.375 M Tris-HCl pH 8.8, 0.1% SDS, and 10% polyacrylamide in distilled water was polymerized by the addition of ammonium persulfate (APS) and tetramethylethylenediamine (TEMED) in Mini-PROTEAN plates (BioRad) at room

temperature for 20 min with an overlay of distilled water. Upon polymerization of the resolving gel, the distilled water was decanted, and a stacking gel with 0.125 M Tris-HCl pH 6.8, 0.1% SDS, and 5% polyacrylamide in distilled water was polymerized above the resolving gel by the addition of APS and TEMED for 20 min at room temperature with a loading comb inserted. Sample buffer with 0.083 M Tris-HCl pH 6.8, β -mercaptoethanol, 0.17% bromophenol blue, 0.33 mM NaOH, 23% glycerol, and 1.3% SDS in distilled water was added to samples prior to incubation at 100°C in a dry-bath incubator (Fisher Scientific) for 10 min. Samples were loaded into the gel in 10-15 μ L volumes and were electrophoresed through the gel in running buffer containing 0.025 mM Tris, 0.192 mM glycine, and 0.01% SDS at 120V for 90 min.

For Western blotting, a nitrocellulose membrane (BioRad) and an electrophoresed SDS-PAGE gel were equilibrated in transfer buffer (0.025 mM Tris, 0.192 mM glycine, and 15% methanol) for 10 min. Upon equilibration, the membrane was placed on the gel and covered in filter paper on both sides, followed by placement in a cassette with sponge. The cassette was submerged in a tank containing transfer buffer and an ice pack, and the transfer was carried out for 2h at 70V on ice. The membrane was then blocked with 10 mL 10% skim milk in PBST for either 1 h with rocking at room temperature or overnight at 4°C. Following blocking, the membrane was washed with 10 mL PBST. Membranes were probed with primary antibodies diluted to an appropriate dilution in 10 ml in PBST containing 1% skim milk for 1 h at room temperature with rocking, followed by two washes with 10 mL PBST each. Membranes were then probed with HRP-linked anti-rabbit IgG (Cell Signaling Technology) diluted to 1:5000 ratio in 10 ml 1% skim milk in PBST for 1 h at room temperature with rocking, followed by two washes with 10 mL PBST each. The

membrane was incubated in Pierce ECL Western Blotting Substrate with 2.5 ml each of Reagents A and B for 10 sec (Thermo Fisher Scientific). The blot was developed for 5-10 min in ChemiDoc XRS+ with ImageLab software (BioRad).

Site-directed mutagenesis

A Q5 Site-Directed Mutagenesis kit (New England Biolabs) was used for introduction of amino acid substitutions into the His-tagged Mfa1 expressed from pEXP5NT::*mfa1N*. Primers for site-directed mutagenesis were designed through NEBaseChanger (<http://nebasechanger.neb.com/>). The manufacturer's instructions were followed with minor modifications. Briefly, PCRs were carried out with Q5 polymerase using pEXP5NT::*mfa1N* as a template. The resulting reaction was then incubated with the KLD enzyme mix for template plasmid reduction and re-circularization of plasmids containing amino acid substitutions. The plasmids were introduced into *E. coli* BL21 Star (DE3) via heat-shock transformation at 42°C, and the resulting transformants were plated on LB agar plates with ampicillin for overnight growth at 37°C. A single colony was picked, and plasmids were extracted with the plasmid miniprep kit (Qiagen) from the overnight growth culture of the colony, with plasmid concentrations measured with a NanoDrop spectrophotometer. Amino acid substitutions were confirmed by sequencing the region encompassing the *mfa1* gene at the Center for Genetics and Molecular Medicine DNA Facility Core at the University of Louisville. Sequence information was checked against the *P. gingivalis* 33277 nucleotide sequences through NCBI blastn.

Reverse-transcriptase PCR of *mfa* mutants

Total RNA was extracted from 10 ml overnight bacterial culture using a RNeasy Mini kit (Qiagen) and following the manufacturer's instructions. Briefly, cells were harvested by centrifugation at 3,000xg for 10 min at room temperature and washed with 1 ml PBS. Cells were then homogenized using glass beads in an Omni bead ruptor (OMNI International). Seventy percent ethanol was added to the homogenate, and the resulting solution was passed through an RNeasy spin column by centrifugation at 8,000xg for 15 sec. Three rounds of washing were carried out with washing buffer provided with the kit by centrifugation at 8,000xg for 15 sec. RNA was eluted from the column in distilled water by centrifugation at 8,000xg for 15sec. Genomic DNA levels in the total RNA sample were minimized using TURBO DNA-free kit (Invitrogen) through two rounds of DNase treatment in a 50µl reaction volume. DNase was removed with the DNase inactivation reagent provided with the kit, and the reaction was centrifuged at 15,000xg for 1.5 min. The RNA concentration in the supernatant was measured on a NanoDrop spectrophotometer.

cDNA was synthesized through the High-Capacity cDNA Reverse Transcription Kit (Thermo Fisher Scientific) following the manufacturer's instructions. Briefly, reactions with or without reverse transcriptase were prepared in 10 µl volumes along with random primer mix provided with the kit to which 10 µl of DNase-treated RNA samples were added. The reactions were initiated in a thermal cycler in the following sequence: 25°C 10 min, 37°C 2 h, 85°C 5 min, with a final hold at 4°C. The DNA concentration was then measured on a NanoDrop spectrophotometer, and the reactions were diluted to 100 ng/µl. One µl of the diluted reaction was used in subsequent PCRs with RT-PCR primers listed in Table 3. PCRs for 33277, *Δmfa1*, *Δmfa2*, *Δmfa3*, and *Δmfa4* were carried out in

a thermal cycler in the following the settings/sequence with GoTaq polymerase (Promega): one cycle of 95°C for 30 sec followed by 35 cycles of 95°C 30 sec, 60°C 30 sec, and 72°C 30 sec followed by one cycle of 72°C 30 sec and a final hold at 4°C. PCR conditions for *Δmfa5* were identical to those described above apart from the second cycle number, which was reduced to 33. PCR samples were electrophoresed at 100V for 40 min in a 2% agarose gel stained and stained with SYBR Safe (Invitrogen). Gel images were acquired through a ChemiDoc XRS+ with ImageLab software (BioRad).

Secondary structure prediction of Mfa1

PSIPRED version 3.3 (<http://bioinf.cs.ucl.ac.uk/psipred/>) and RaptorX Property (<http://raptorx.uchicago.edu/StructurePropertyPred/predict/>) were used for estimation of Mfa1 secondary structure. Full-length amino acid sequences of Mfa1 from *P. gingivalis* 33277 were inputted into each web server.

Mfa1 polymerization assay of *mfa* mutants

Overnight bacterial cultures were harvested by centrifugation at 3,000xg for 10 min and washed in 1 ml PBS. OD₆₀₀ of the bacterial suspension in PBS was measured and diluted in PBS to OD₆₀₀ of 1. One ml of diluted bacterial solution was sonicated on ice for cell lysis (2 min, 5 sec on; 10 sec off; 40% amplitude; 120 watts; 20 kHz). 15 μl SDS sample buffer were added to 15 μl whole cell sonicates, and the resulting sample was processed at 65°C, 80°C, or 100°C for 10 min in a dry-bath incubator (Fisher Scientific) prior to loading onto a SDS-PAGE gel in a 10 μl volume. Electrophoresis and Western blotting procedures described in *SDS-PAGE and Western blot* section of this chapter were followed.

Mfa1 polymerization assay of purified recombinant Mfa1s

Recombinant Mfa1 proteins were purified according to *Protein Expression and Purification* procedures described in this chapter. Recombinant proteins (0.1 µg) in SDS sample buffer in 10 µl volume were incubated at either 60°C or 100°C for 10 min in a dry-bath incubator and separated by SDS-PAGE gel. Electrophoresis and Western blotting procedures described in *SDS-PAGE and Western blot* section of this chapter were followed.

Mfa1 polymerization assay of amino-acid substituted recombinant Mfa1s

Overnight cultures of *E. coli* BL21(DE) strains expressing amino-acid substituted recombinant Mfa1s were sub-cultured into 5 ml LB broth containing ampicillin, and were grown at 37°C until the OD₆₀₀ of the cultures reached 0.4-0.8, at which point 125 µl of 8% lactose were added for induction for 3 h at 37°C. One ml of bacterial solution was sonicated on ice for cell lysis (2 min, 5 sec on; 10 sec off; 40% amplitude; 120 watts; 20 kHz). The sample was then centrifuged at 21,000xg for 1 min. SDS sample buffer (15µl) were added to an equal volume of the supernatant, and the resulting sample was processed at 60°C or 100°C for 10 min in a dry-bath incubator prior to separation by SDS-PAGE. Electrophoresis and Western blotting procedures described in *SDS-PAGE and Western blot* section of this chapter were followed.

Antisera generation and purification

Antisera to recombinant Mfa2 and Mfa3 were generated through the custom rabbit polyclonal antibody service of Abgent (San Diego, CA). Antisera to recombinant Mfa4 were generated through the custom rabbit polyclonal antibody service of Enzymax (Lexington, KY).

Antisera were purified using Protein A resin (Genscript) in gravity flow columns following the manufacturer's instructions. Briefly, antisera were clarified by centrifugation at 7,000xg for 10 min, and the supernatant was buffered with PBS at 1:1 ratio and passed through the resin, followed by washing with PBS. Bound IgGs were eluted with 0.1 M glycine pH 2 and were immediately neutralized with 1.5 M Tris-HCl pH8.5.

Statistics

Statistical analyses were carried out using GraphPad Prism version 6.04. Ordinary one-way ANOVA or two-way ANOVA and Tukey's multiple comparison test were performed, and p values less than 0.05 were considered significant.

Table 1. Bacterial strains used in this study.

Bacteria/strain	Comment	Source
<i>P. gingivalis</i>		
ATCC 33277	wild-type, gentamicin resistant	ATCC
$\Delta mfa1$	<i>mfa1</i> -deletion mutant of 33277, erythromycin resistant	This study
$\Delta mfa2$	<i>mfa2</i> -deletion mutant of 33277, erythromycin resistant	This study
$\Delta mfa3$	<i>mfa3</i> -deletion mutant of 33277, erythromycin resistant	This study
$\Delta mfa4$	<i>mfa4</i> -deletion mutant of 33277, erythromycin resistant	This study
$\Delta mfa5$	<i>mfa5</i> -deletion mutant of 33277, erythromycin resistant	This study
<i>Escherichia coli</i>		

BL21 Star (DE3)	Recombinant protein expression strain (inducible by IPTG via <i>lacUV</i> promoter and T7 polymerase)	Invitrogen
-----------------	-------------------------------------------------------------------------------------------------------	------------

Table 2. Plasmids used in this study.

Plasmid	Comment	Source
pET200	TOPO cloning vector with kanamycin resistance marker and N-terminal hexahistidine-tag	Invitrogen
pET200:: <i>mfa1NS</i>	Derivative of pET200 encoding <i>mfa1</i> (amino acids 21-563)	This study
pET200:: <i>mfa4NS</i>	Derivative of pET200 encoding <i>mfa4</i> (amino acids 21-333)	This study
pET200:: <i>mfa5NT</i>	Derivative of pET200 encoding <i>mfa5</i> (amino acids 21-1044)	This study

pGEX-6P:: <i>mfa2</i>	Vector encoding <i>mfa2</i> Dr. Yoshiaki Hasegawa (amino acids 41-325); (Aichi Gakuin University, Contains ampicillin Japan) resistance marker and N- terminal GST tag
pET-His1a:: <i>mfa3</i>	Vector encoding <i>mfa3</i> Dr. Karina Persson (Umea (amino acids 23-446); University, Sweden) contains kanamycin resistance marker and N- terminal hexahistidine tag
pEXP5NT	TOPO cloning vector with Invitrogen ampicillin resistance marker and N-terminal hexahistidine tag
pEXP5CT	TOPO cloning vector with Invitrogen ampicillin resistance marker and C-terminal hexahistidine tag
pEXP5NT:: <i>mfa1N</i>	Derivative of pEXP5NT This study encoding <i>mfa1</i> (amino acids 50-563)

pEXP5CT:: <i>mfa1C</i>	Derivative of pEXP5NT encoding <i>mfa1</i> (amino acids 50-563)	This study
pEXP5NT:: <i>mfa1NT</i>	Derivative of pEXP5NT encoding <i>mfa1</i> (amino acids 50-563)	This study
pEXP5NT:: <i>mfa1CT</i>	Derivative of pEXP5NT encoding <i>mfa1</i> (amino acids 50-563)	This study
pEXP5NT:: <i>mfa1NAsp</i>	Derivative of pEXP5NT encoding <i>mfa1</i> (amino acids 50-563)	This study
pEXP5NT:: <i>mfa1NSer</i>	Derivative of pEXP5NT encoding <i>mfa1</i> (amino acids 50-563)	This study
pEXP5NT:: <i>mfa1NAla</i>	Derivative of pEXP5NT encoding <i>mfa1</i> (amino acids 50-563)	This study
pEXP5NT:: <i>mfa1CAsp</i>	Derivative of pEXP5NT encoding <i>mfa1</i> (amino acids 50-563)	This study

pEXP5NT:: <i>mfa1CSer</i>	Derivative of pEXP5NT encoding <i>mfa1</i> (amino acids 50-563)	This study
pEXP5NT:: <i>mfa1NAla</i>	Derivative of pEXP5NT encoding <i>mfa1</i> (amino acids 50-563)	This study
pEXP5NT:: <i>mfa1NB</i>	Derivative of pEXP5NT:: <i>mfa1N</i> (amino acids 50-563)	This study
pEXP5NT:: <i>mfa1CB</i>	Derivative of pEXP5NT:: <i>mfa1N</i> (amino acids 50-563)	This study
pEXP5NT:: <i>mfa2</i>	Derivative of pEXP5NT encoding <i>mfa2</i> (amino acids 29-324)	This study
pEXP4NT:: <i>mfa3</i>	Derivative of pEXP5NT encoding <i>mfa3</i> (amino acids 44-446)	This study

Table 3. Primers used for cloning, RT-PCR, and site-directed mutagenesis

Primer name	Primer sequence	Comments
287NSF	CACCAGTAAAGAGGGCAATGGCC	For expression of Mfa1NS
287NSR	TTAGAGATCAACCTCATAGGAATGAAC	For expression of Mfa1NS
290NSF	CACCAAGAACAATCCTAGCGAGCC	For expression of Mfa4NS
290NSR	TCAAATCTCGACTTCGTA CTGTAC	For expression of Mfa4NS
291NTF	CACCTTTCAAATAAAAAGCTCGCCCT	For expression of Mfa5NT
291NTR	TTAGTCGAATCCGAACGAAAG	For expression of Mfa5NT
1N50F	GATGATGATGAT <u>AAA</u> GCGGGTGACGGACAGGAT	For expression of Mfa1N and Mfa1NT
1N563R	TTAGAGATCAACCTCATAGGAATGAAC	For expression of Mfa1N and Mfa1CT
1C50F	ATGGATGATGATGAT <u>AAA</u> GCGGGTGACGGACAGGAT	For expression of Mfa1C
1C563R	GAGATCAACCTCATAGGAATGAAC	For expression of Mfa1C
1R543	TTACGTATCCTGATCAGGCAAGG	For expression of Mfa1NT
1F92	GATGATGATGAT <u>AAA</u> GCTGAAGATCTTGATTTGGC	For expression of Mfa1CT
YMFA1RTF	GCTTGTGGAGAGTGCTGAAG	For RT-PCR of <i>mfa1</i>
YMFA1RTR	TTGCCGACAGCAGAATTAAC	For RT-PCR of <i>mfa1</i>

YMFA2RTF	ATAGATGGGACGACCCTTTG	For RT-PCR of <i>mfa2</i>
YMFA2RTR	ACACTCACCGTCACACGATT	For RT-PCR of <i>mfa2</i>
RT289F	TGGCCTCGATCGTGAACAAA	For RT-PCR of <i>mfa3</i>
RT289R	ATTGTTTTCTCCGTCCGGCT	For RT-PCR of <i>mfa3</i>
MFA4RTF	TGCTGCCGAAAGGCTCATTA	For RT-PCR of <i>mfa4</i>
MFA4RTR	CCAGCCTCGGATTGTGTCAT	For RT-PCR of <i>mfa4</i>
291RTF2	GGCTTCGATGCGGATAAGGA	For RT-PCR of <i>mfa5</i>
291RTR2	CTGCCGATTCAACCCACTCT	For RT-PCR of <i>mfa5</i>
M1NHF	CGATTACATGGATCCTCAGGGTGGCCCTGGG	For placement of aspartic acids in N-terminal Mfa1N
M1NHR	CTATCTTTCTCATCTTTGTCTTTTCCTGCCCACTCTCCTAC	For placement of aspartic acids in N-terminal Mfa1N
M1NSF	CTCTTACATGTCTCCTCAGGGTGGCCCTGGG	For placement of serines in N-terminal Mfa1N
M1NSR	CTAGATTTCTCAGATTTGTCTTTTCCTGCCCACTCTCCTAC	For placement of serines in N-terminal Mfa1N
M1NAF	CGCTTACATGGCTCCTCAGGGTGGCCCTGGG	For placement of alanines in N-terminal Mfa1N
M1NAR	CTAGCTTTCTCAGCTTTGTCTTTTCCTGCCCACTCTCCTAC	For placement

MICHF	TACAGATTTGCCTTGAAAGTTCATTC	of alanines in N- terminal Mfa1N For placement of aspartic acids in C- terminal Mfa1N
MICHR	TCCTCATCCGACATGAACGTATCCTG	For placement of aspartic acids in C- terminal Mfa1N
MICSF	TACATCTTTGCCTTGAAAGTTCATTC	For placement of serines in C- terminal Mfa1N
MICSR	GACTCAGACGACATGAACGTATCCTG	For placement of serines in C- terminal Mfa1N
MICAF	TACAGCTTTGCCTTGAAAGTTCATTC	For placement of alanines in C- terminal Mfa1N
MICAR	GCCTCAGCCGACATGAACGTATCCTG	For placement of alanines in C- terminal Mfa1N
MINBF	GGGTGGCCCTGGGCTTGTGCCAAGTGCTGAAGATCTTGATTTTG	For placement of prolines in N- terminal Mfa1N
MINBR	TGAGGCACCATGTAGATGCTTGGTTTCTCAATTTTGTCTTTTCC	For placement of prolines in N- terminal Mfa1N
MICBF	CCTTGAAACCACATTCCTATGAGGTTGATCTC	For placement of prolines in C-

M1CBR	CAAAACTGTTGGCTCAACCGACATGAACGTATC	terminal Mfa1N For placement of prolines in C- terminal Mfa1N
2N29F	GATGATGATGATAAA TGTGATAAGATGATTTATGACAATTACG	For expression of Mfa2
2N324R	TTAAAGTTCTATTTTCGTA ACTATGTATCAACC	For expression of Mfa2
3N44F	GATGATGATGAT <u>AAA</u> GCAGCACATACGAATGGC	For expression of Mfa3
3N446R	CTATTTCTTGATAAAA <u>ACTTTATCCGG</u>	For expression of Mfa3

Enterokinase P1 site is bolded and underlined.

CHAPTER 3 RESULTS

Surface localization of Mfa proteins

To fully understand the mechanisms underlying Mfa fimbrial biogenesis, it is essential to determine locations of individual Mfa proteins as this may provide insights into interacting partners amongst Mfa proteins and their putative functions as either assembly initiators, mediators, or terminators. Previous immuno-TEM experiments have shown the Mfa1 major subunit protein localizing throughout the fimbrial structure with Mfa3 capping the tip portion and Mfa2 completing the structure at the base (31, 33). However, the location of Mfa4 has not been examined. Because Mfa4 exhibits similar quantitative abundance within the purified Mfa1 fimbriae as Mfa3 and based on the crystal structure of Mfa4 that is reminiscent of a tip pilin (31, 32), we hypothesized that Mfa4 localizes with Mfa1 fimbriae on the surface of *P. gingivalis* near Mfa3 in the tip portion of the fimbriae. Surface localization of Mfa1-4 was thus carried out via immuno-negative stain TEM with antibodies specific to each of the Mfa proteins. Given the extracellular nature of the fimbriae and to maximize the retention of native fimbrial structure during sample processing, immuno-negative stain TEM was deemed more technically appropriate than the traditional immuno-TEM involving ultrathin-sectioning. Hence, TEM images shown in this study represent structurally intact cells without any sectioning. In addition, specificity of the antibodies was validated through the inclusion of isogenic *mfa* mutants in TEM experiments as controls and through immunoblotting analyses of recombinant Mfa

proteins. Consistent with previous results (31, 33), Mfa1 was localized throughout the fimbrial structure (Figure 1), whereas Mfa2 was localized in the proximal portion of the fimbriae (Figure 2). Intriguingly, localization of Mfa3 and Mfa4 was either distal or throughout the fimbriae depending on the immuno-labelled cells being examined (Figures 3 and 4). However, considering the technical nature of immuno-negative stain TEM that involves structurally intact cells and given the variable reported length of Mfa1 fimbriae along with its peritrichous nature, it is likely that gold particles appearing to localize throughout the fimbriae in the case of Mfa3 and Mfa4 are in fact localizing at the tip portion of the fimbriae which by chance is overlapping with one or more fimbriae nearby. Therefore, we conclude that Mfa3 localizes in the distal portion of the Mfa1 fimbriae, in agreement with the previous result. Similarly, we conclude Mfa4 localizes in the distal portion of the fimbriae. Collectively, the results suggest Mfa3 and Mfa4 serve as tip pilins of Mfa1 fimbriae whose oligomeric backbone is composed solely of Mfa1 major subunit protein with Mfa2 serving as a base pilin.

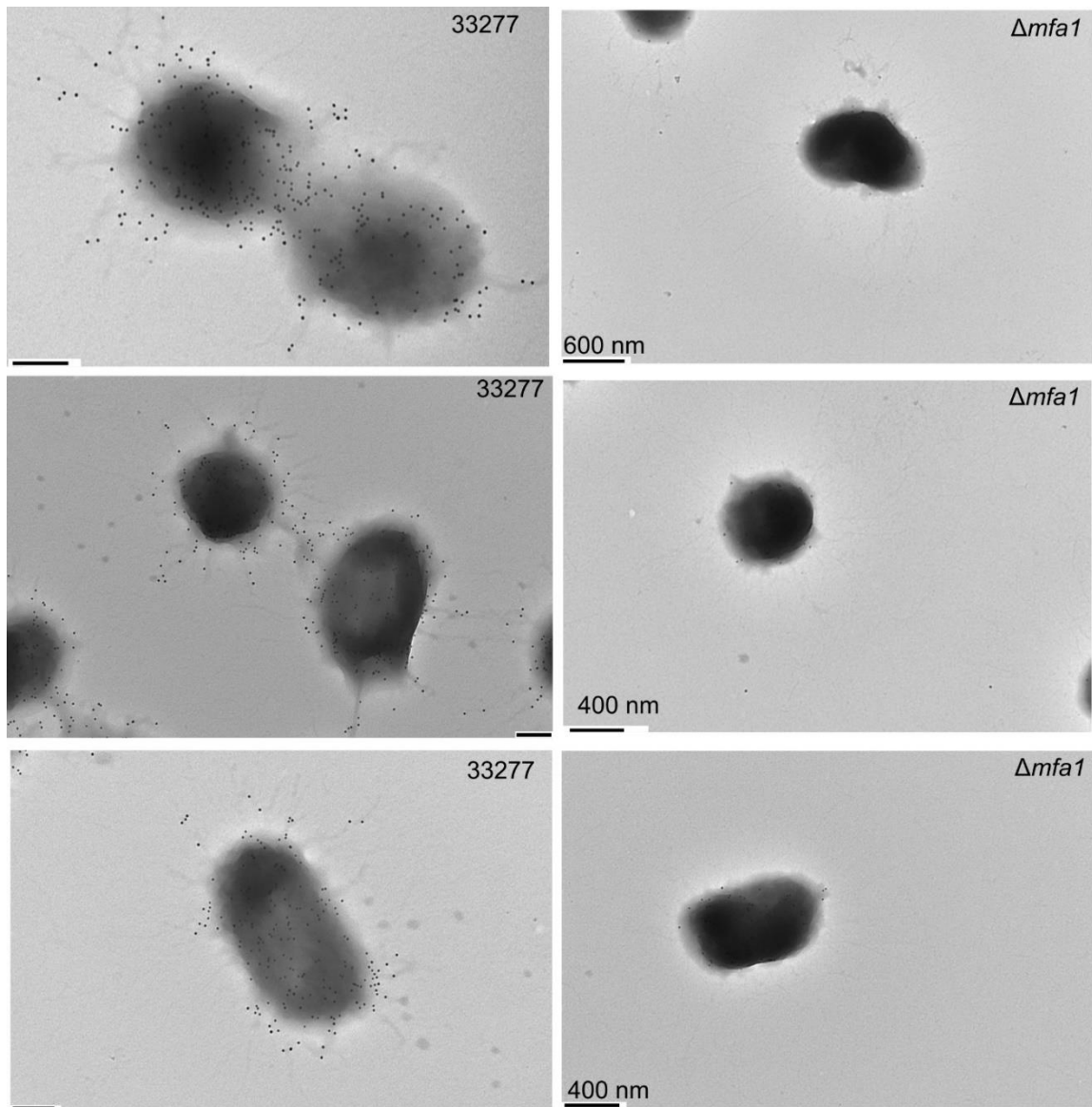


Figure 1. Localization of Mfa1 via immuno-negative stain TEM. *P. gingivalis* 33277 (left side) or *mfa1* mutant (right side) whole cells were probed with IgG-enriched antibodies to Mfa1 (diluted to 1:100) followed by 10 nm gold particle-conjugated anti-rabbit IgG antibodies (diluted to 1:500). Cells were negatively stained with 1% ammonium molybdate prior to viewing under a transmission electron microscope and representative images are presented. Black bars indicate 200 nm unless otherwise noted.

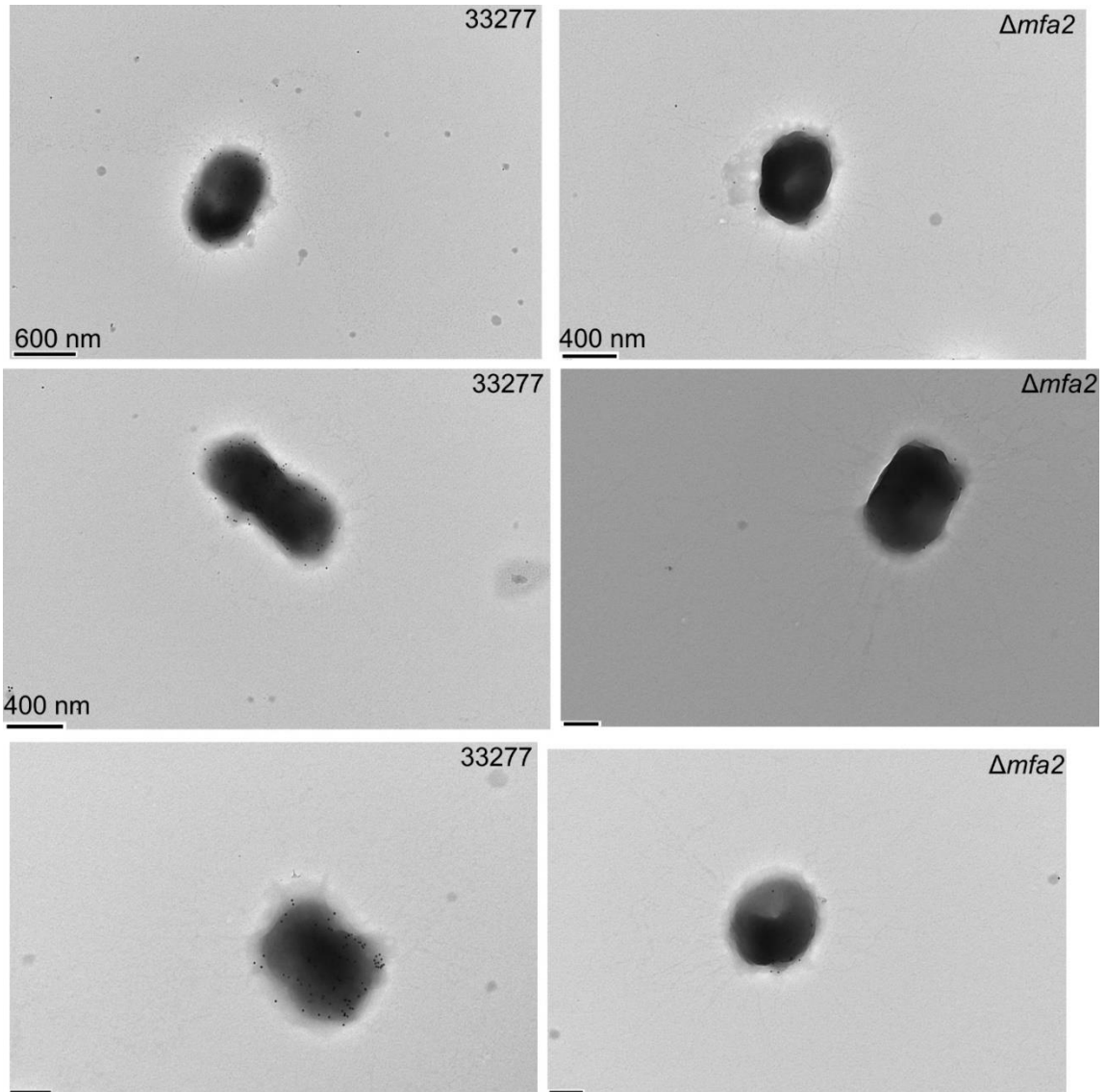


Figure 2. Localization of Mfa2 via immuno-negative stain TEM. *P. gingivalis* 33277 and *mfa2* mutant whole cells were probed with IgG-enriched antibodies to Mfa2 (diluted to 1:500) followed by 10nm gold particle-conjugated anti-rabbit IgG antibodies (diluted to 1:500). Cells were negatively stained with 1% ammonium molybdate prior to viewing under a transmission electron microscope. Black bars indicate 200nm unless otherwise noted.

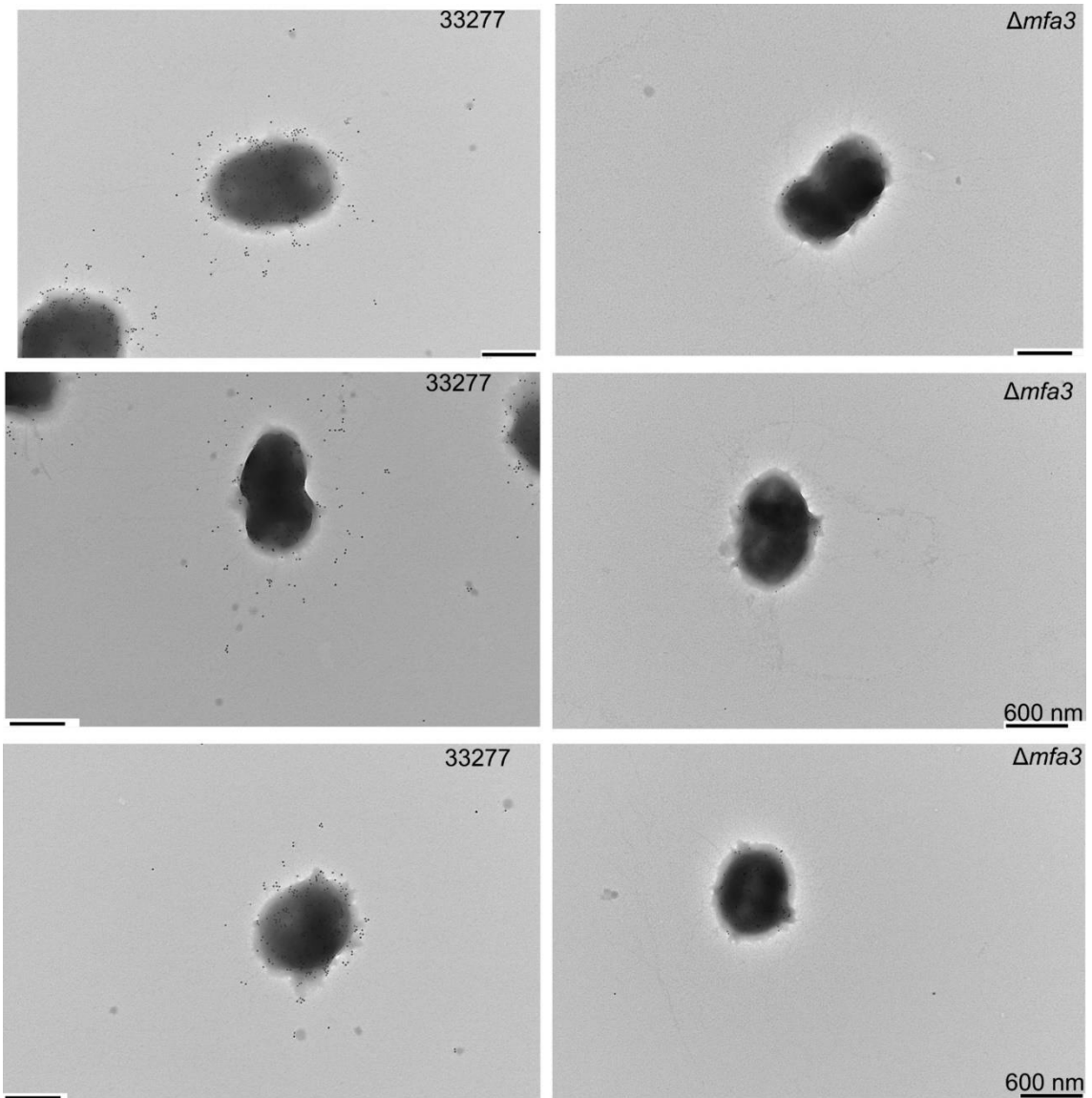


Figure 3. Localization of Mfa3 via immuno-negative stain TEM. *P. gingivalis* 33277 and *mfa3* mutant whole cells were probed with IgG-enriched antibodies to Mfa3 (diluted to 1:500) followed by 10nm gold particle-conjugated anti-rabbit IgG antibodies (diluted to 1:500). Cells were negatively stained with 1% ammonium molybdate prior to viewing under a transmission electron microscope. Black bars indicate 400nm unless otherwise noted.

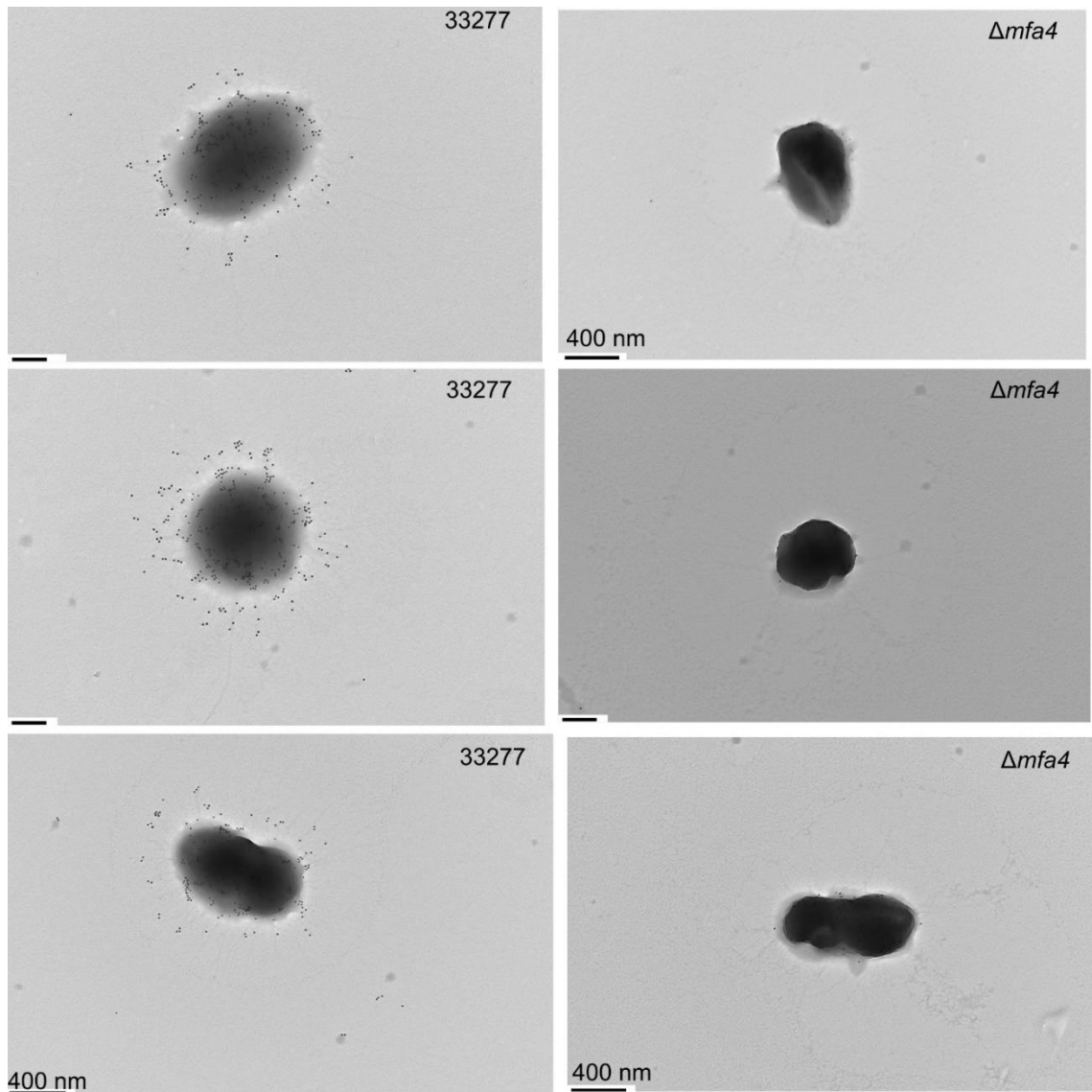


Figure 4. Localization of Mfa4 via immuno-negative stain TEM. *P. gingivalis* 33277 and *mfa4* mutant whole cells were probed with IgG-enriched antibodies to Mfa4 (diluted to 1:500) followed by 10nm gold particle-conjugated anti-rabbit IgG antibodies (diluted to 1:500). Cells were negatively stained with 1% ammonium molybdate prior to viewing under a transmission electron microscope. Black bars indicate 200nm unless otherwise noted.

Binding interactions amongst pre-Rgp processed Mfa proteins

The binding interactions among spatially related Mfa proteins have remained elusive. Furthermore, it has been unclear whether Mfa proteins initiate a direct association with each other as precursor forms (apart from Mfa2 and Mfa5 which do not undergo processing by Rgp and hence do not have precursor forms) in the periplasm prior to processing by arginine-specific gingipains (Rgps). Results from the localization of Mfa proteins suggest a direct association between Mfa1 major subunit protein and either Mfa3 or Mfa4 accessory proteins. Additionally, according to the fimbrial polymerization model proposed by Xu *et al*, Mfa3 may serve as an adaptor protein at the tip of the fimbriae interlinking Mfa1 and Mfa4 (32). This model is supported by our localization experiments in which Mfa3 and Mfa4 were both localized in the distal portion of the fimbriae, suggesting a direct interaction between Mfa3 and Mfa4. Hence, we hypothesized that the assembly of the Mfa1 fimbriae is initiated through the interaction of precursor Mfa proteins prior to processing by Rgps and that Mfa3 serves as an adaptor protein that interlinks other fimbrial subunits for their incorporation into the Mfa1 fimbriae. We further hypothesized that Mfa2 serves as an assembly terminator and hence at least interacts with Mfa1 but may also bind other fimbrial subunits to form a heteromeric complex on the base of the Mfa1 fimbriae. Hereafter, the terms “precursor” and “pre-Rgp processed” will be used interchangeably to denote Mfa proteins that lack the N-terminal signal peptides but retain the N-terminal extension regions prior to the Rgp cleavage site. Similarly, the terms “mature” and “post-Rgp processed” will signify Mfa proteins that lack both the signal peptides and the N-terminal extension regions prior to the Rgp cleavage site. Mfa2 and Mfa5 will not be subjected to such nomenclature as they are not known to be processed by

Rgps (30, 34). Furthermore, all recombinant Mfa proteins used in this study lack the putative signal peptides on their N-termini. For Mfa5, a C-terminal region was truncated to aspartic acid at amino acid residue 1044 (denoted as D) to improve its solubility as determined by the Recombinant Protein Solubility Prediction server (46). Because Mfa5 is a known CTD protein that has its C-terminus peptides cleaved by PorU as part of the maturation process (30), the functional consequence of such truncation is lessened.

Binding of precursor Mfa3 to other pre-Rgp processed Mfa proteins was examined using recombinant Mfa proteins and through ELISA-based binding assays. To control for non-specific binding, interactions between Mfa3 and an irrelevant eukaryotic protein, bovine serum albumin (BSA), was also examined. Consistent with our hypothesis, recombinant pre-Rgp processed Mfa3 exhibited concentration-dependent binding activity to recombinant precursor Mfa1 and Mfa4. Interestingly, Mfa3 also adhered to Mfa2 and Mfa5 in a concentration-dependent manner (Figure 5).

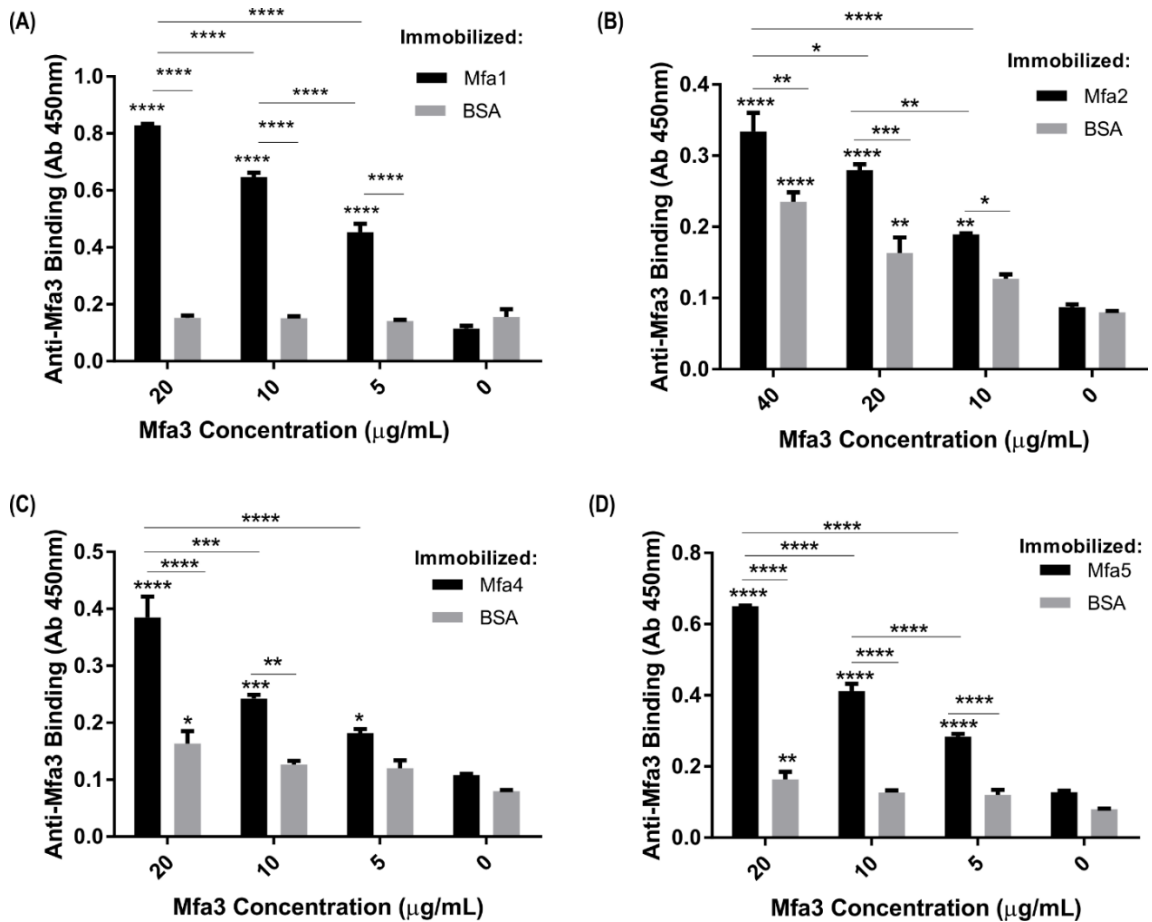


Figure 5. Binding ELISA between pre-Rgp processed Mfa3 and other pre-Rgp processed Mfa proteins. Recombinant Mfa1, Mfa3, and Mfa4 representing pre-Rgp processed forms and Mfa2 and Mfa5 (1 μg each) were immobilized on a plate through passive absorption. BSA (1 μg) was also immobilized as a specificity control. Binding of recombinant Mfa3 at various concentrations to the immobilized proteins was detected with antibodies to Mfa3 (1:5000) followed by secondary anti-rabbit IgG HRP-linked antibodies (1:5000). Signals were developed for 10 min with the TMB substrate and stopped with 0.1 M sulfuric acid. Absorbance values were measured at 450 nm. Error bar = SD (measured in technical duplicates). One representative result of two independent experiments is shown. Statistical significance was tested via two-way ANOVA. Asterisk(s) directly above a bar indicates statistical significance compared to the background control.

To further characterize the binding interactions, relative affinity information was derived via saturation ESLIA binding experiments, in which one-site binding was assumed. Mfa3-Mfa5 pair showed the highest affinity and therefore the strongest binding interaction as evidenced by the lowest estimated apparent dissociation constant, closely followed by Mfa3-Mfa1 and Mfa3-Mfa4 (Figure 6 and Table 3). Consistent with relatively weak binding activity observed in binding ELISA, Mfa3-Mfa2 exhibited weakest affinity and hence the highest estimated apparent dissociation constants (Figure 6 and Table 3). All Mfa-Mfa interactions were stronger than the Mfa3-BSA interaction. It must be noted that the absolute accuracy of dissociation constants derived from the saturation binding ELISA hinges on the assumption that one-site binding holds true amongst the binding pairs, which may or may not be valid and is inferred from the goodness of fit, R^2 . Considering there is no established R^2 threshold value at or above which an assumption is rendered valid, the affinity of binding pairs, at least presently, can only be concluded in relative terms rather than in absolute terms. Nonetheless, the reported dissociation constants in the submicromolar range amongst the binding pairs here are within the range of dissociation constants reported for the periplasmic binding pairs of Type I pili of *E. coli*, for which dissociation constants of micromolar range were observed (47). The assumption of one-site binding for Mfa binding pairs here is therefore likely valid.

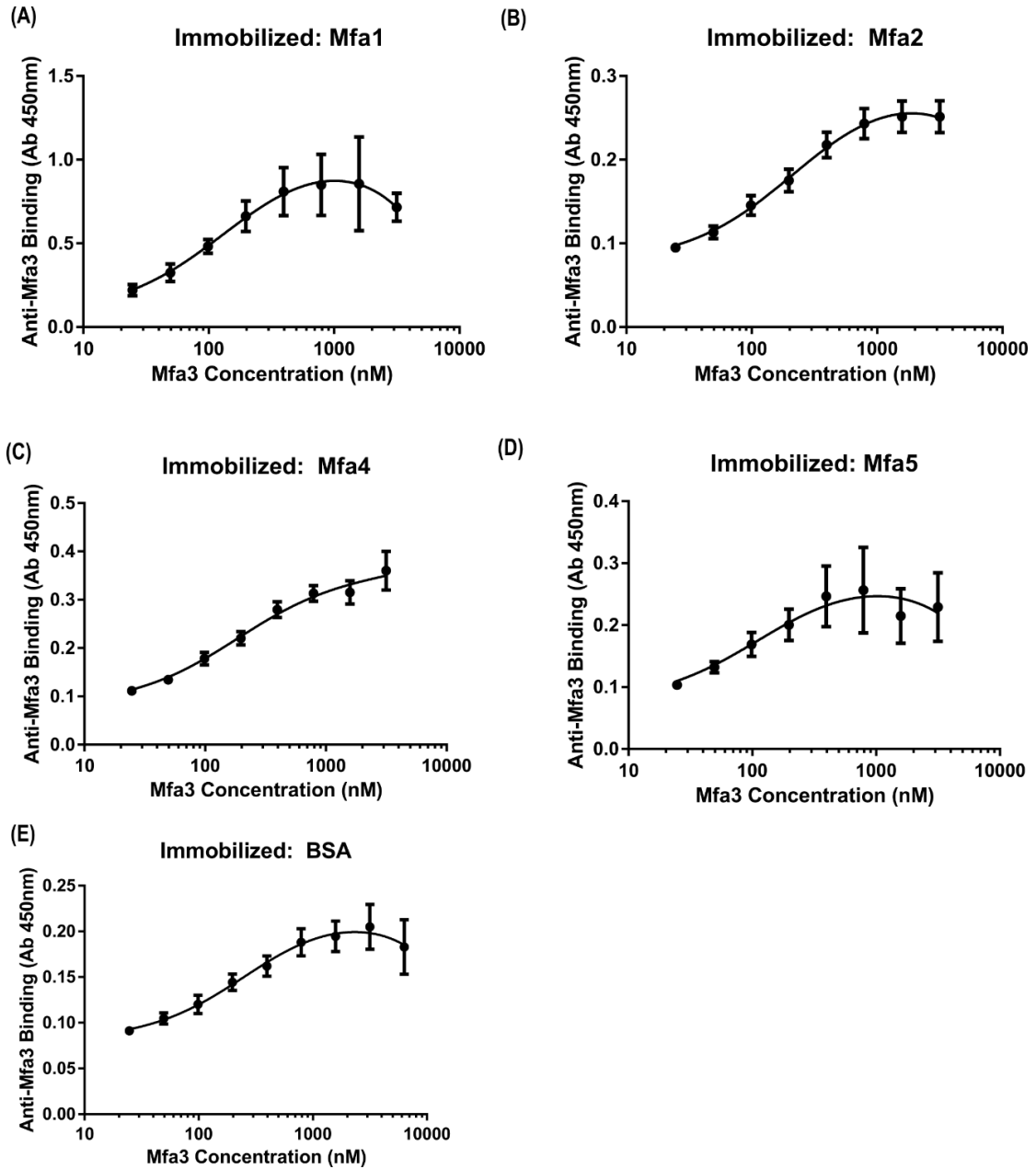


Figure 6. Pre-Rgp processed Mfa saturation binding ELISA. Recombinant Mfa1, Mfa2, Mfa4, Mfa5, or BSA (0.1 μ g) were immobilized on an ELISA plate through passive absorption. Ten-fold less protein was immobilized compared to the previous binding ELISA to mitigate a potential ligand depletion effect, which can skew the estimation of dissociation constants (48). Binding of recombinant Mfa3 at various concentrations to the immobilized proteins was detected with antibodies to Mfa3 (1:5000) followed by secondary anti-rabbit IgG HRP-linked antibodies (1:5000). Signals were developed for 10 min with the TMB substrate and stopped with 0.1 M sulfuric acid. Absorbance values were measured at 450 nm. Error bar = SEM. N=3+ experiments.

Table 4. Estimated apparent dissociation constants (K_D) from the saturation binding ELISA with pre-Rgp processed recombinant Mfa proteins.

Binding Pairs	Apparent K_D (nM)	Standard Error	R^2
Mfa1-Mfa3	145.7	31.81	0.8269
Mfa2-Mfa3	230.6	93.32	0.6891
Mfa4-Mfa3	182.4	66.01	0.7577
Mfa5-Mfa3	120.4	49.19	0.7156
BSA-Mfa3	270.1	124.8	0.5484

Data points from the saturation binding ELISA were non-linearly fitted with one-site binding model of GraphPad Prism. The estimated apparent dissociation constants along with the standard error and goodness-of-fit values from the binding model are shown.

Next, the binding interaction between Mfa2 and precursor Mfa proteins and the interaction between Mfa2 and Mfa5 were examined. Mfa2 exhibited concentration-dependent specific binding activities to Mfa1, Mfa3, and Mfa5 (Figure 7). A lower level of binding was seen between Mfa2 and Mfa4 although it was still higher compared to that between Mfa2 and BSA (Figure 6). It is possible that the interaction between Mfa2 and Mfa4 is non-specific, and the biological significance of such interaction remains unclear.

The binding interaction between precursor Mfa1 and Mfa2 was subsequently examined. Mfa1 showed concentration-dependent specific binding activity to Mfa2 (Figure 8). This is consistent with the previous binding experiment between Mfa1 and Mfa2 in which configuration of immobilization was reversed with precursor Mfa1 on the plate. However, no binding was observed between precursor Mfa1 to precursor Mfa3 and Mfa4 (data not shown). Furthermore, there was no binding activity between precursor Mfa1 and Mfa5 (data not shown). The inconsistent binding activity between Mfa1 and Mfa3 may be attributed to potentially blocked and inaccessible binding site resulting from the passive adsorption process of Mfa3 to the plate.

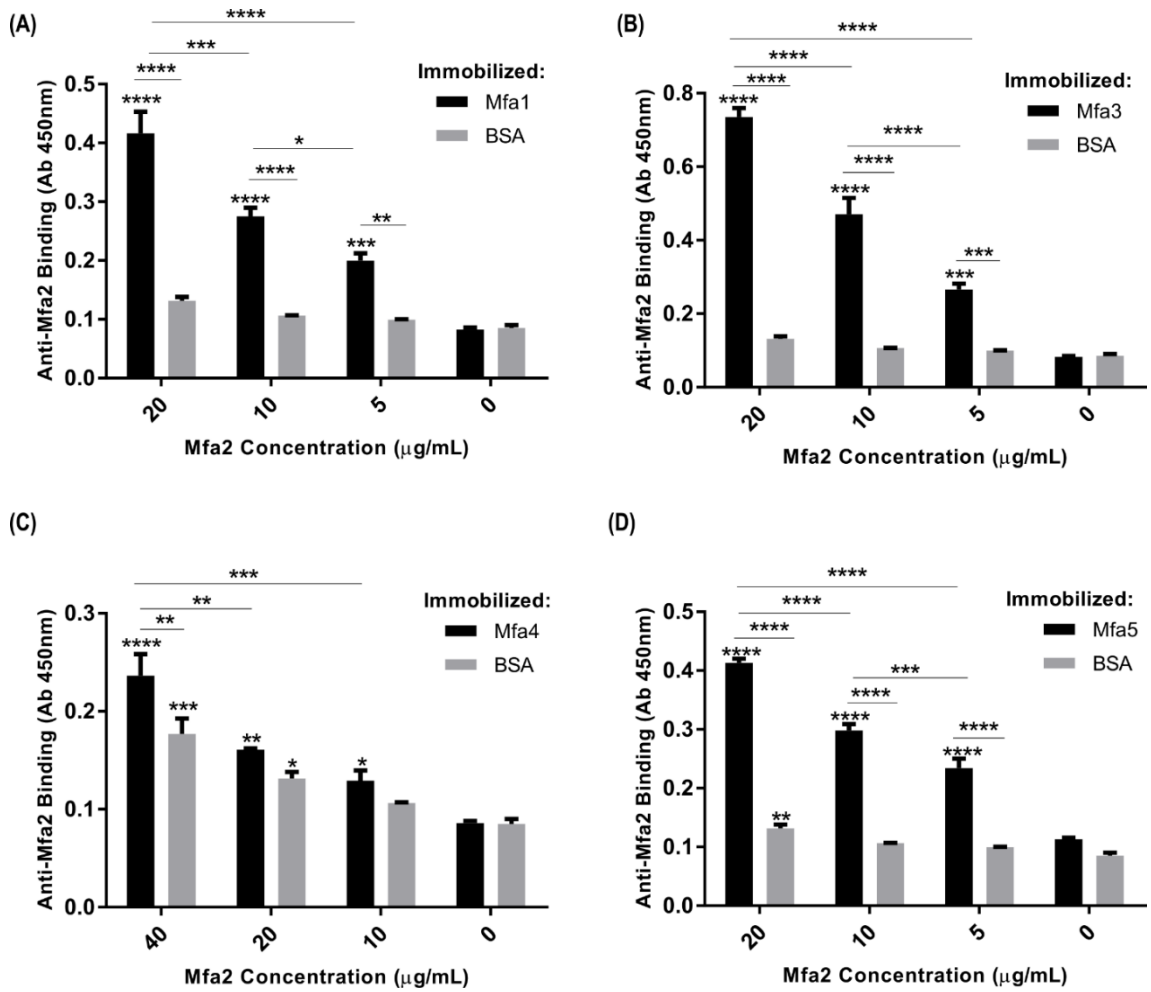


Figure 7. Binding ELISA between Mfa2 and other pre-Rgp processed Mfa proteins. Recombinant Mfa1, Mfa3, and Mfa4 representing pre-Rgp processed forms and Mfa2 and Mfa5 (1 µg each) were immobilized on a plate through passive absorption. BSA (1 µg) was also immobilized as a specificity control. Binding of recombinant Mfa3 at various concentrations to the immobilized proteins was detected with antibodies to Mfa2 (1:10000) followed by secondary anti-rabbit IgG HRP-linked antibodies (1:5000). Signals were developed for 10 min with the TMB substrate and stopped with 0.1 M sulfuric acid. Absorbance values were measured at 450 nm. Error bar = SD (measured in duplicate wells). One representative result of two independent experiments is shown. Statistical significance was tested via two-way ANOVA. Asterisk(s) directly above a bar indicates statistical significance compared to the background control.

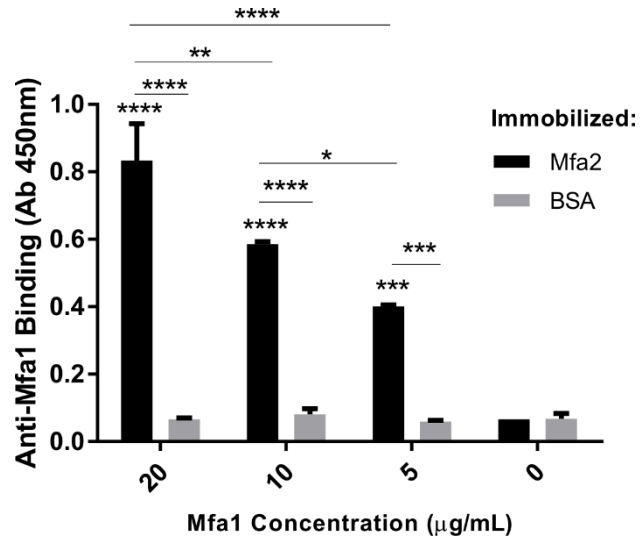


Figure 8. Binding ELISA between pre-Rgp processed Mfa1 and Mfa2. Recombinant Mfa1 representing the pre-Rgp processed form and Mfa2 (1 µg each) were immobilized on a plate through passive absorption. BSA (1 µg) was also immobilized as a specificity control. Binding of recombinant Mfa3 at various concentrations to the immobilized proteins was detected with antibodies to Mfa1 (1:10000) followed by secondary anti-rabbit IgG HRP-linked antibodies (1:5000). Signals were developed for 10 min with the TMB substrate and stopped with 0.1 M sulfuric acid. Absorbance values were measured at 450 nm. Error bar = SD (measured in duplicate wells). One representative result of two independent experiments is shown. Statistical significance was tested via two-way ANOVA. Asterisk(s) directly above a bar indicates statistical significance compared to the background control.

Finally, the binding of precursor Mfa4 to other Mfa proteins were examined. Interestingly, Mfa4 did not show any binding activity to any of the Mfa proteins (data not shown). Given the previous binding results between precursor Mfa4 to Mfa3 and Mfa2 (Figure 5C and 7C), the inconsistency may again be due to potentially blocked binding site during passive adsorption process of Mfa3 and Mfa2 to the plate.

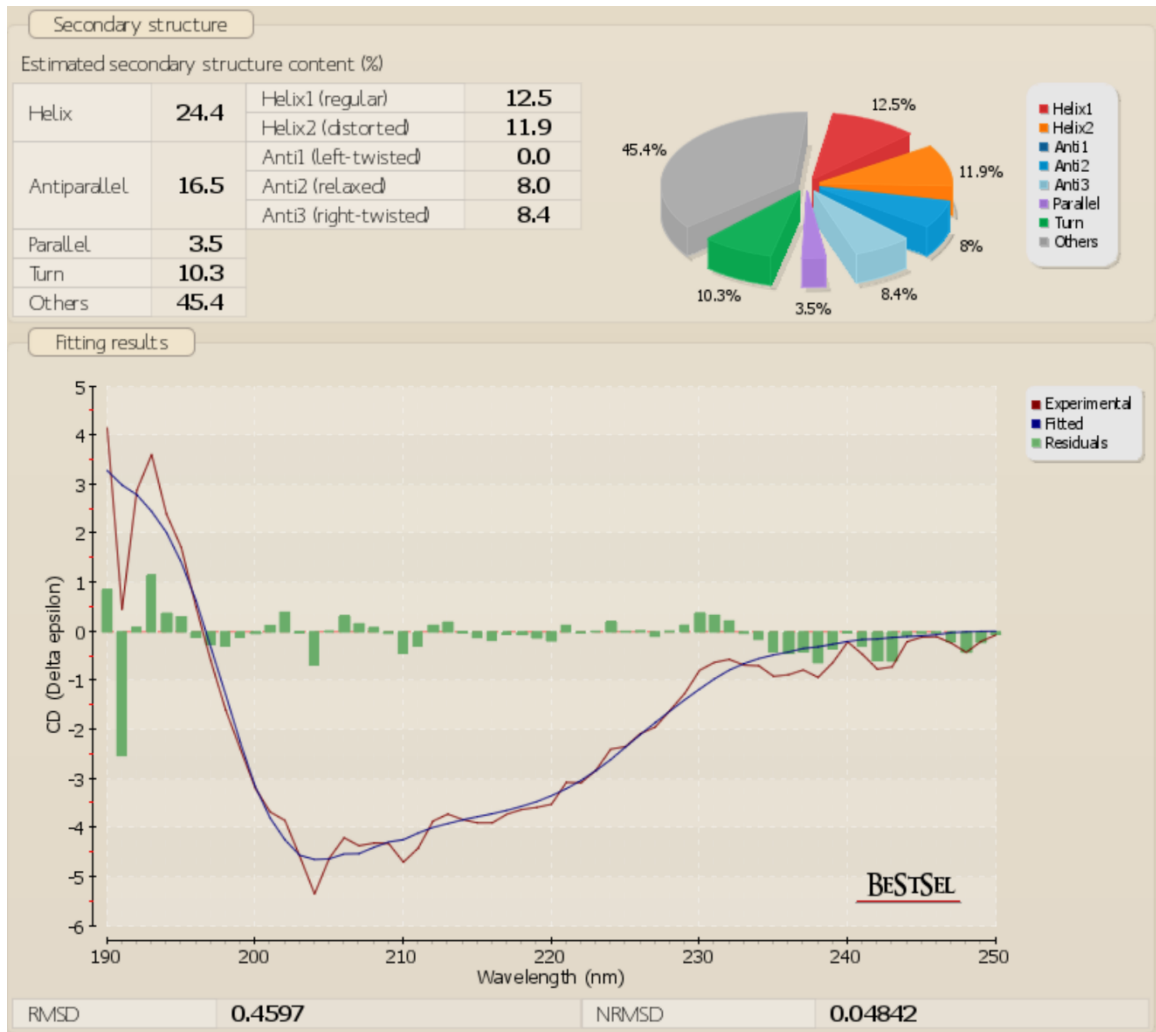
Collectively, the results confirm our hypothesis that the assembly of the Mfa1 fimbriae is initiated with precursor Mfa proteins interacting with each other and that Mfa3 serves as an adaptor protein that interlinks other fimbrial subunits. Precursor Mfa3 thus may form a pre-assembly complex along with precursor Mfa1, Mfa4, and Mfa5 in the periplasm. The binding interaction between Mfa2 and other Mfa proteins may allow Mfa2 to serve its putative role as an assembly terminator more efficiently through its binding to multiple fimbrial subunits rather than to just Mfa1.

Secondary structure estimation of recombinant Mfa proteins

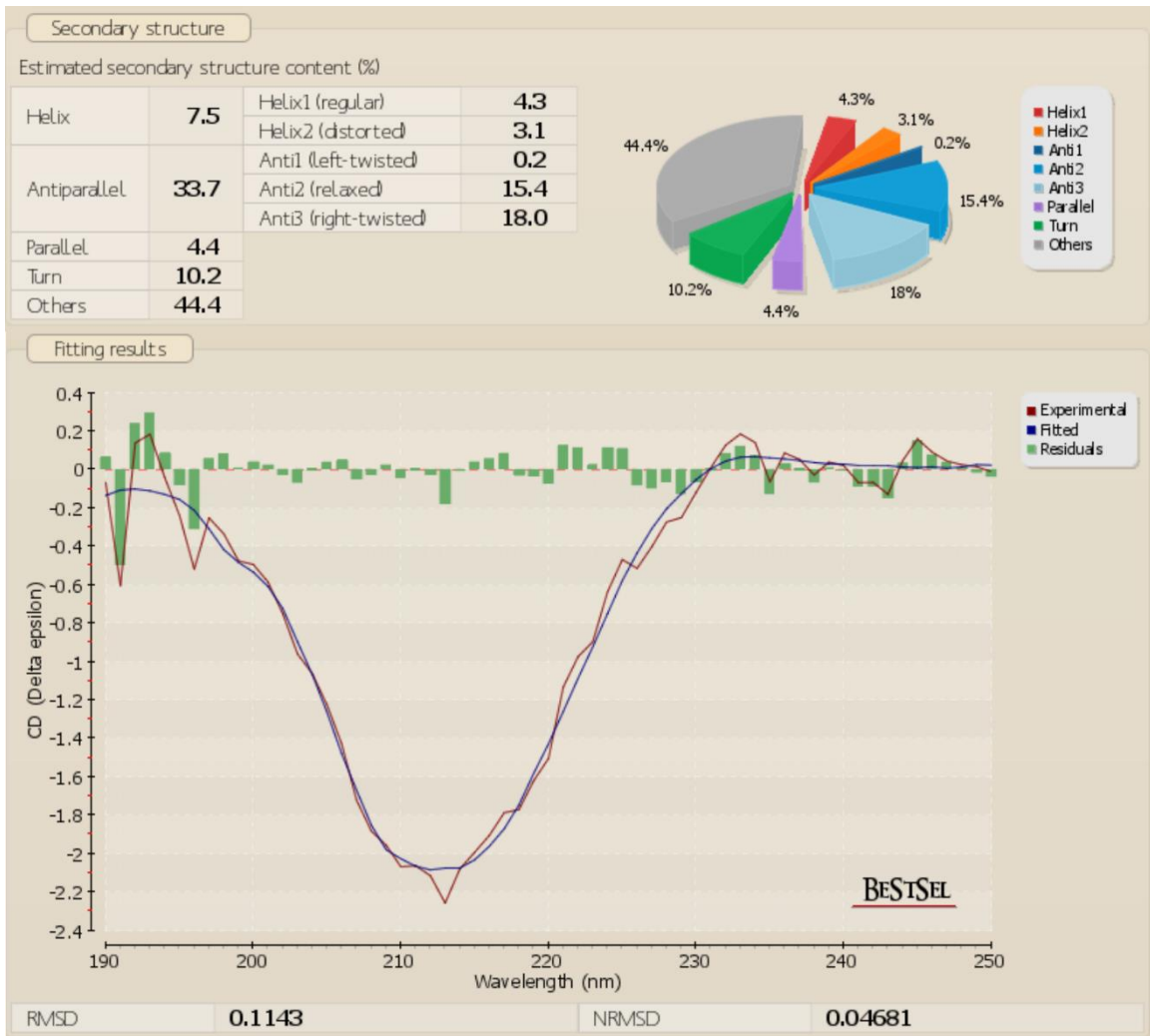
It is possible that binding activities of recombinant Mfa proteins is impacted by conformational changes occurring in recombinant proteins. To address this possibility and to better appreciate biochemical nature of Mfa proteins, secondary structure analyses of each of the recombinant Mfa proteins used in the binding ELISA were carried out via circular-dichroism (CD) spectroscopy. The resulting blank-subtracted spectra were analyzed via BeStSel for secondary structure prediction (49). Recombinant precursor Mfa1 exhibited a content of approximately 24% helices, 20% beta-sheets, 10% turns, and 45% disordered structure (Figure 9A). Recombinant Mfa2 showed 7% helices, 38% beta-sheets, 10% turns, and 44% disordered structure (Figure 9B). Recombinant precursor Mfa3 showed 8% helices, 32% beta-sheets, 14% turns, and 47% disordered structure (Figure 9C).

Recombinant precursor Mfa4 exhibited 17% helices, 18% beta-sheets, 12% turns, and 54% disordered structure (Figure 9D). Recombinant Mfa5 showed 17% helices, 31% beta-sheets, 11% turns, and 41% disordered structure (Figure 9E). Overall, each of the recombinant Mfa proteins showed various secondary structures without any indication of total denaturation.

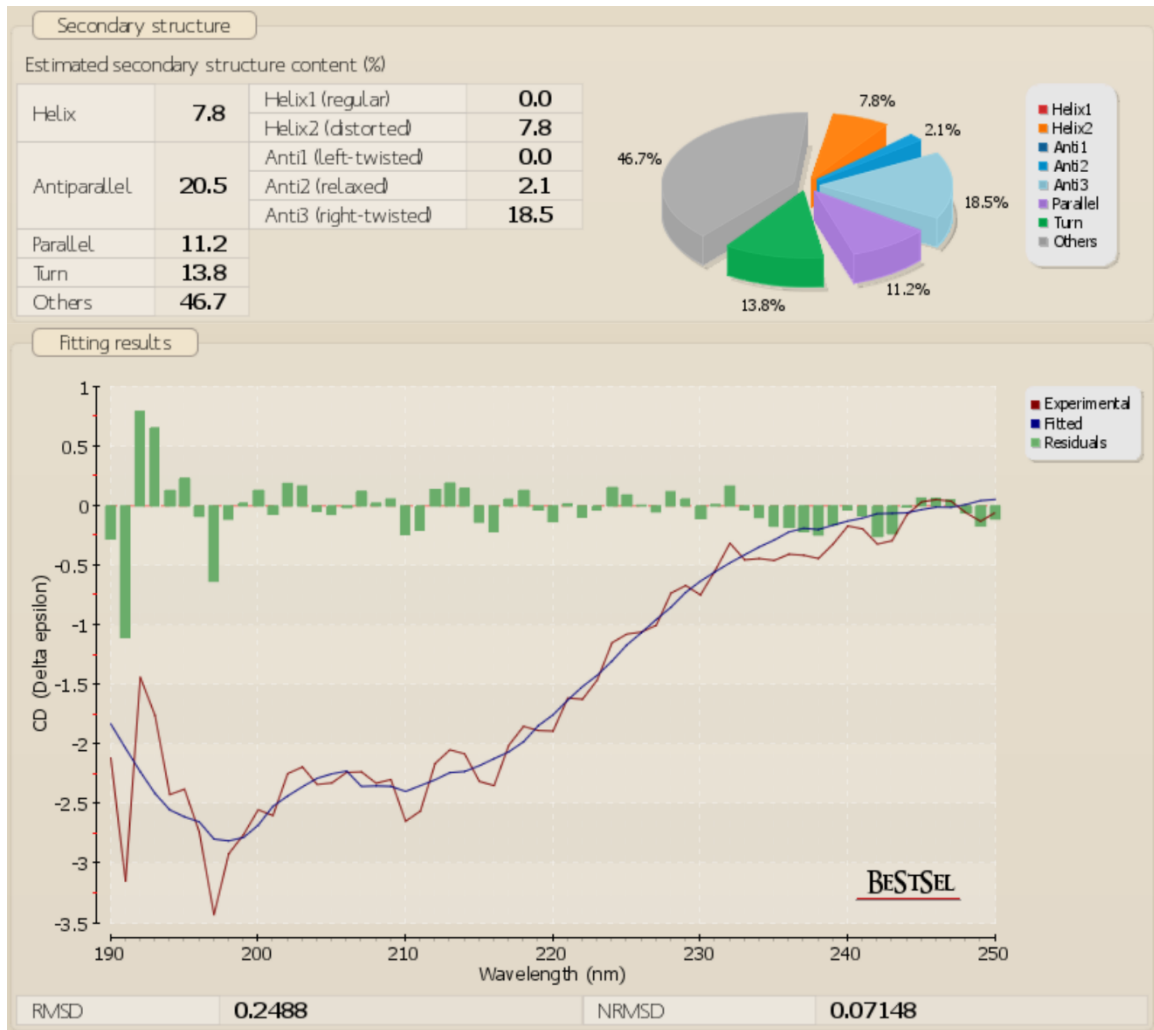
(A) CD spectrum of Mfa1



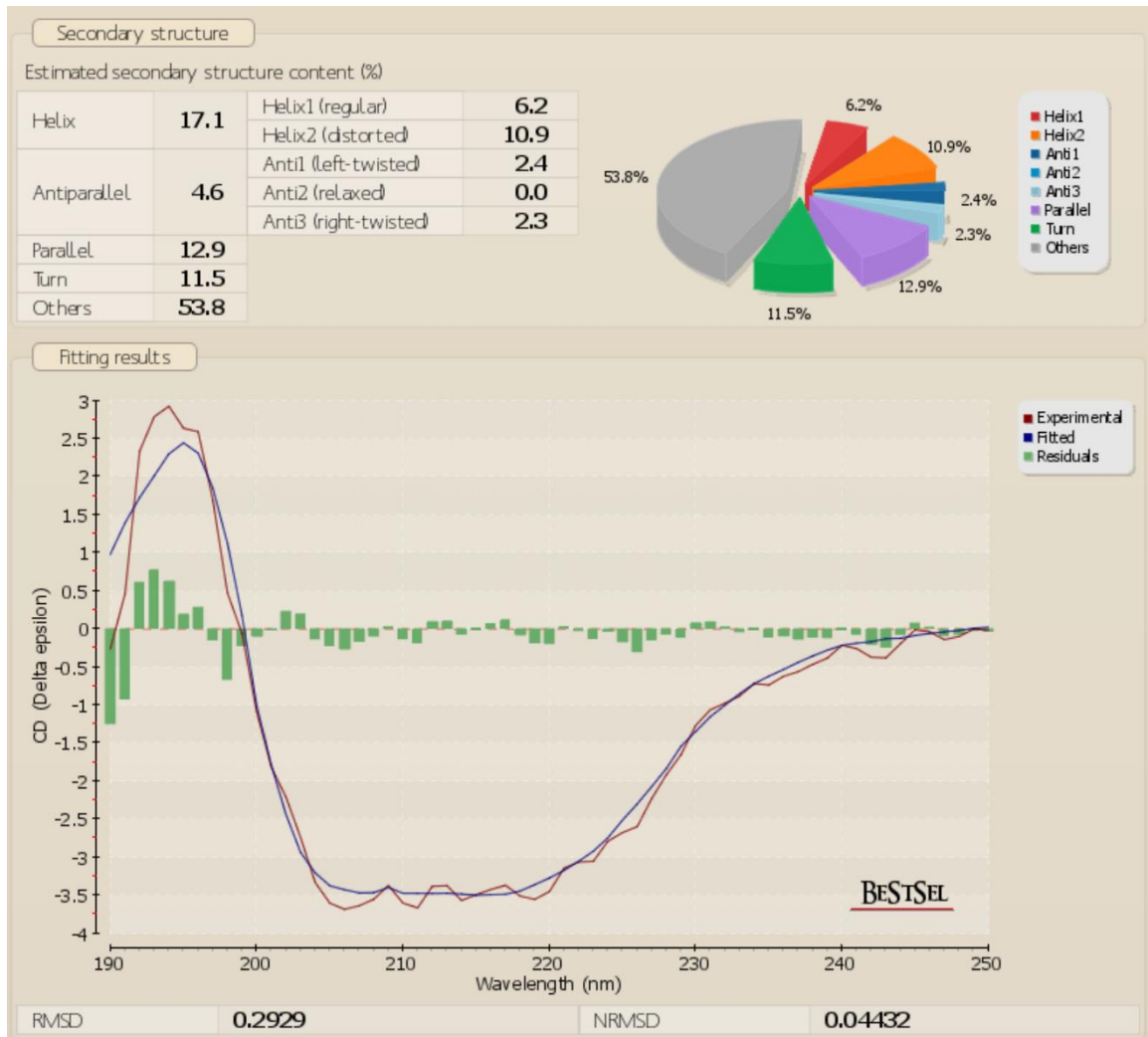
(B) CD spectrum of Mfa2



(C) CD spectrum of Mfa3



(D) CD spectrum of Mfa4



(E) CD spectrum of Mfa5

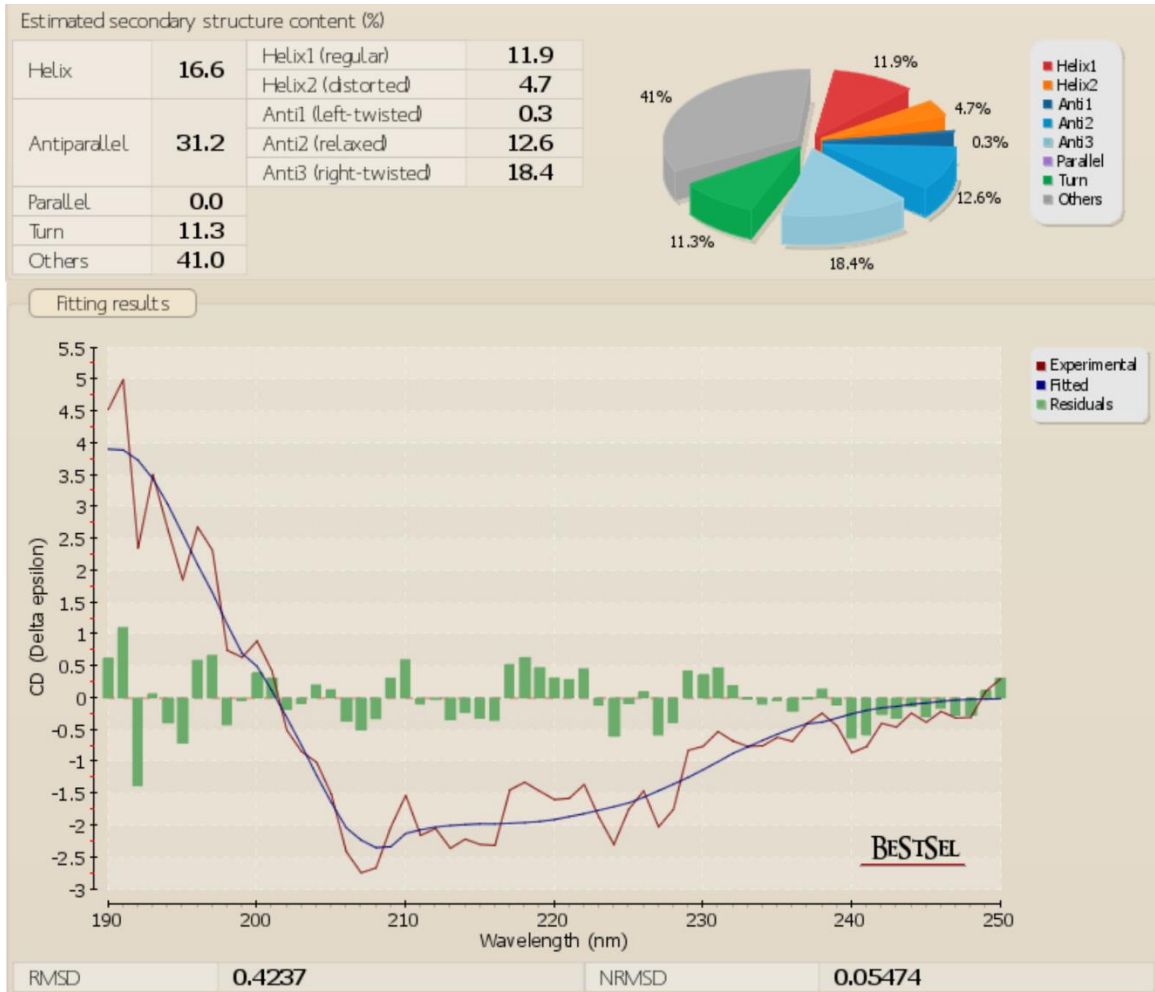


Figure 9. Secondary structure estimation of recombinant Mfa proteins via circular-dichroism (CD) spectroscopy. (A-E) Recombinant Mfa proteins in PBS were analyzed through CD spectroscopy. Upon subtracting the spectrum for the PBS, the resulting spectra were used for secondary structure prediction through the BeSTSEL server.

Binding interactions amongst post-Rgp processed Mfa proteins

To determine whether the Rgp processing of Mfa proteins affects the interaction amongst fimbrial subunits, additional binding ELISAs were carried out with recombinant mature Mfa proteins. The binding of mature Mfa3 to Mfa2 and Mfa5 in addition to mature Mfa1 and Mfa4 were still evident. Specifically, mature Mfa3 showed concentration-dependent specific binding activities to all the other Mfa proteins (Figure 10). We then examined the interaction between Mfa2 and mature Mfa1, Mfa3, and Mfa4. Mfa2 also showed concentration-dependent specific binding activities to all the other Mfa proteins (Figure 11). Furthermore, no binding activity was observed between the mature Mfa4 and other Mfa proteins when the mature Mfa4 was used as a ligand (data not shown). Moreover, no binding activity was seen between mature Mfa1 and other Mfa proteins when mature Mfa1 was used as a ligand (data not shown). The inconsistent binding results when immobilization configurations are reversed may again be attributed to inaccessible binding site resulting from the passive adsorption process. Overall, the results indicate that Rgp-processing does not affect the binding interactions initiated amongst the precursor Mfa proteins and does not initiate interactions between pairs that originally did not show any binding activity as precursor forms.

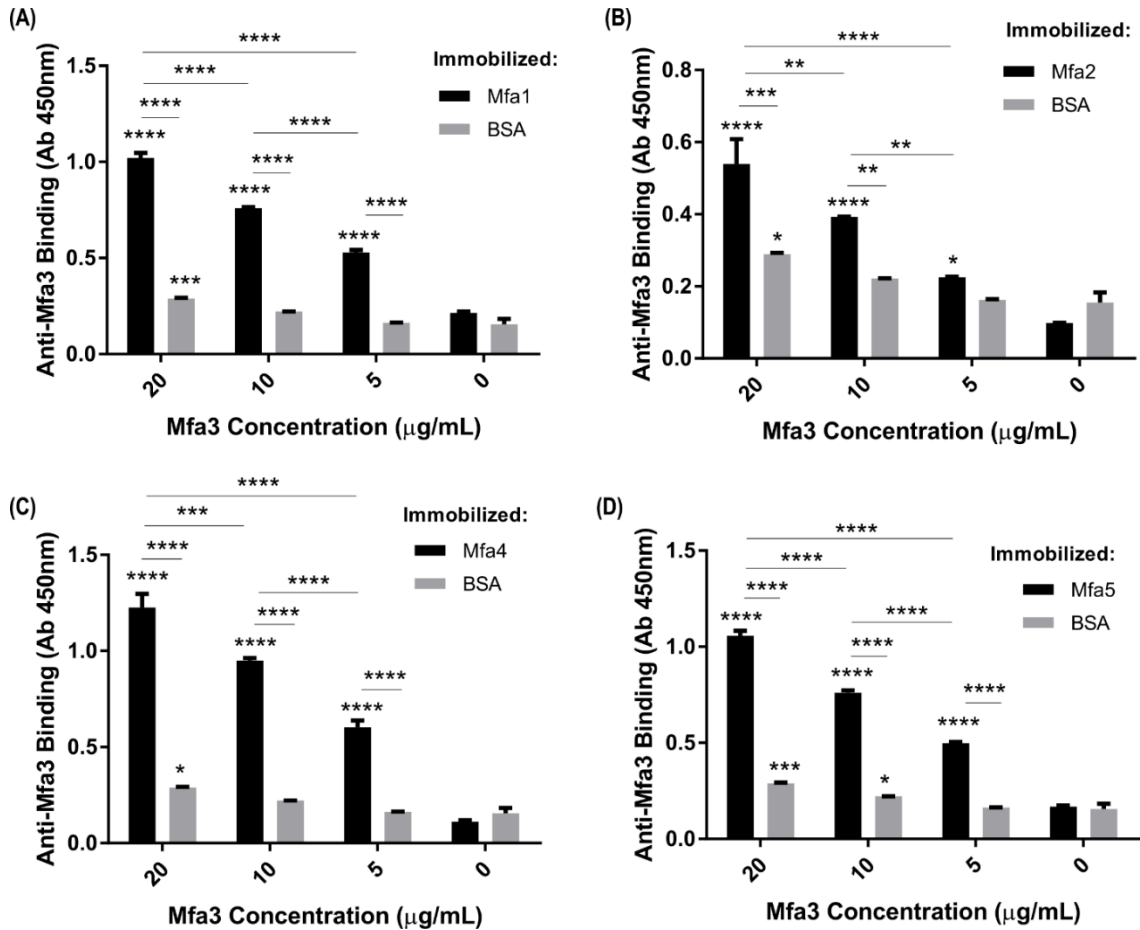


Figure 10. Binding ELISA between post-Rgp processed Mfa3 and other post-Rgp processed Mfa proteins. Recombinant Mfa1 representing the post-Rgp processed forms and Mfa2 and Mfa5 (1 μg each) were immobilized on a plate through passive absorption. BSA (1 μg) was also immobilized as a specificity control. Binding of recombinant Mfa3 at various concentrations to the immobilized proteins was detected with antibodies to Mfa3 (1:5000) followed by secondary anti-rabbit IgG HRP-linked antibodies (1:5000). Signals were developed for 10 min with the TMB substrate and stopped with 0.1 M sulfuric acid. Absorbance values were measured at 450 nm. Error bar = SD (measured in duplicate wells). One representative result of two independent experiments is shown. Statistical significance was tested via two-way ANOVA. Asterisk(s) directly above a bar indicates statistical significance compared to the background control.

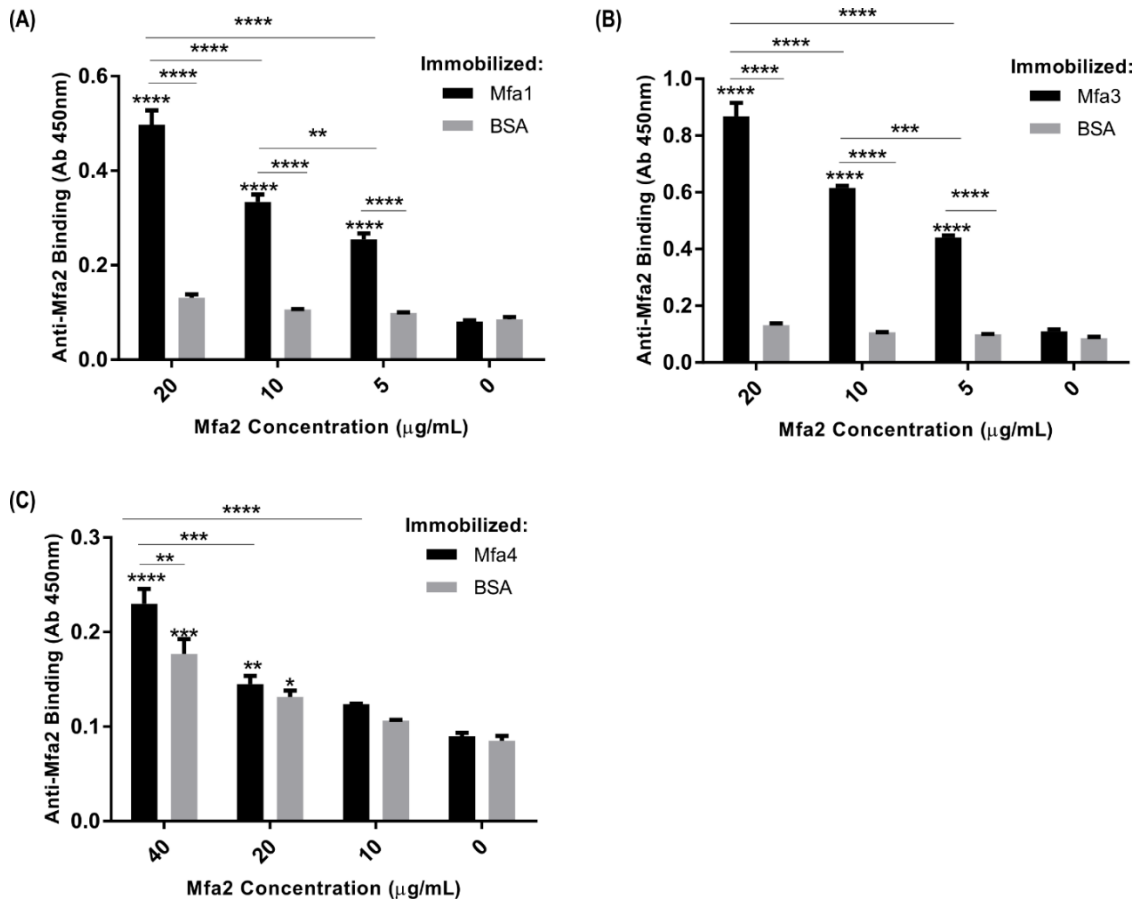


Figure 11. Binding ELISA between Mfa2 and other post-Rgp processed Mfa proteins. Recombinant Mfa1, Mfa3, and Mfa4 representing post-Rgp processed forms and Mfa2 and Mfa5 (1 μg each) were immobilized on a plate through passive absorption. BSA (1 μg) was also immobilized as a specificity control. Binding of recombinant Mfa3 at various concentrations to the immobilized proteins was detected with antibodies to Mfa2 (1:10000) followed by secondary anti-rabbit IgG HRP-linked antibodies (1:5000). Signals were developed for 10 min with the TMB substrate and stopped with 0.1 M sulfuric acid. Absorbance values were measured at 450 nm. Error bar = SD (measured in duplicate wells). One representative result of two independent experiments is shown. Statistical significance was tested via two-way ANOVA. Asterisk(s) directly above a bar indicates statistical significance compared to the background control.

Processing and surface presentation of Mfa1-4

It was previously shown that the lack of either Mfa4 or Mfa5 precludes the full proteolytic processing of Mfa3, indicating there may be an intricate interplay amongst accessory fimbrial proteins prior to incorporation into the Mfa1 fimbriae (30, 34). Furthermore, the surface expression of Mfa1 was reduced in the absence of either Mfa4 or Mfa5, suggesting the biogenesis of Mfa1 fimbriae is interlinked between the major subunit and accessory subunits (30, 34). Moreover, our binding ELISA data with precursor recombinant Mfa proteins indicated that the fimbrial biogenesis may indeed be initiated within the periplasm. A disrupted periplasmic assembly process amongst key, putative interacting Mfa proteins would then lead to an abnormal surface presentation of one or more of the Mfa proteins to ultimately yield structurally incomplete Mfa1 fimbriae, with remnant Mfa proteins either lingering on the surface unincorporated into the fimbriae, trapped within the periplasm as individual subunits, or potentially tagged for degradation. Extensive analyses of processing and surface presentation of Mfa1-4 utilizing all five *mfa* mutants have not been previously reported. Therefore, to expand on our findings from the binding ELISA experiments and to further characterize the Mfa fimbrial biogenesis on the surface and within the periplasm, we employed whole cell ELISAs and immunoblotting analyses of whole cell cultures of isogenic *mfa* mutants.

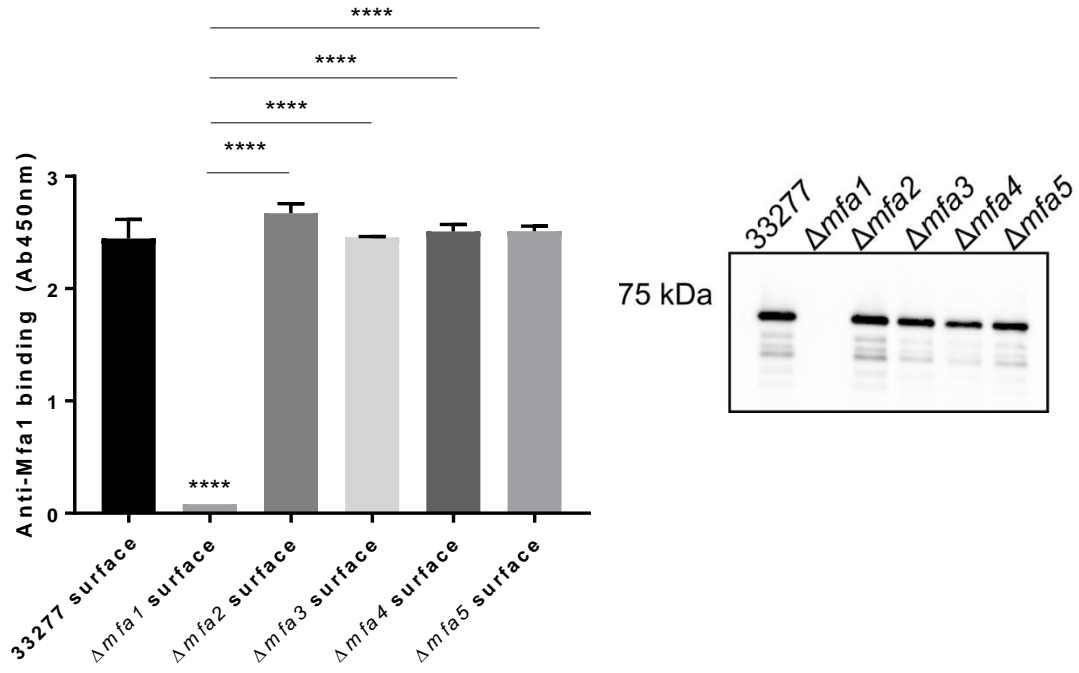
Given that the *fim* operon, encoding for FimA fimbrial proteins, and *mfa* operon, encoding for Mfa1 fimbrial proteins, are situated at different loci on the *P. gingivalis* chromosome, the FimA major subunit protein was deemed as a viable surface marker to ensure equal immobilization of cells in the case of whole cell ELISAs and equal sample loading in the case of immunoblotting of whole cell cultures. Hence, the surface

presentation and expression of FimA in *mfa* mutants were also examined. As expected, FimA surface presentation was comparable across the *mfa* mutants in the whole cell ELISA, and FimA expression was also comparable across the *mfa* mutants in the immunoblotting analyses of whole cell cultures (Figure 12E).

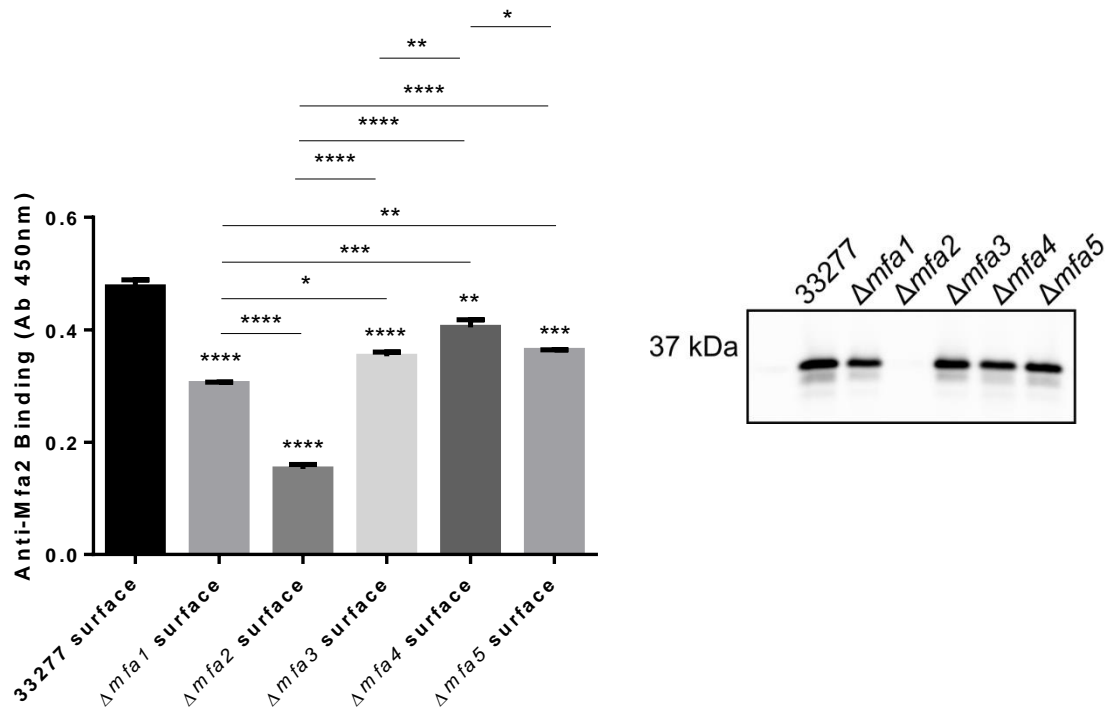
From the whole cell ELISA, we found that the surface expression of Mfa1 was comparable across all *mfa* mutants (Figure 12A). In addition, immunoblotting analyses of whole cell cultures of *mfa* mutants, which include both the whole cells and their culture supernatant, revealed that accessory fimbrial proteins Mfa2-5 do not affect the proteolytic processing of Mfa1. Hence, Mfa1 surface presentation and its proteolytic processing occurs independently of Mfa2-Mfa5.

In contrast, the surface expression of Mfa2 was reduced in all the *mfa* mutants compared to the wild-type, with *mfa1* mutant exhibiting the most significant reduction in surface presentation level other than the *mfa2* mutant (Figure 12B). Immunoblotting analyses of whole cell cultures of *mfa* mutants showed that Mfa2 is not proteolytically processed by other Mfa proteins (Figure 12B). It should be noted that the relatively low overall signals in the whole cell ELISA for Mfa2 may be attributed to its localization in the basal portion of the fimbriae which likely renders detection by the antibodies more challenging. The results indicate Mfa2 translocation onto the surface is mediated most prominently by Mfa1 but also partly by Mfa3, Mfa4, and Mfa5, and that the proteolytic processing of Mfa2, if any occurs at all, does not necessitate other Mfa proteins.

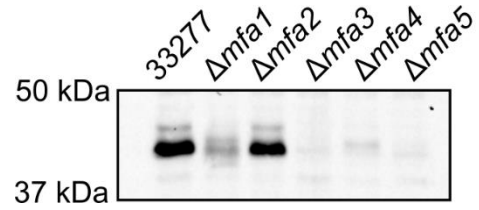
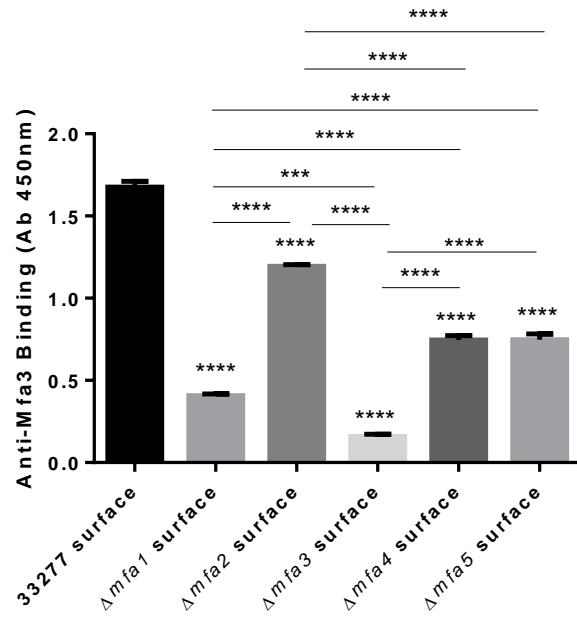
(A) Mfa1



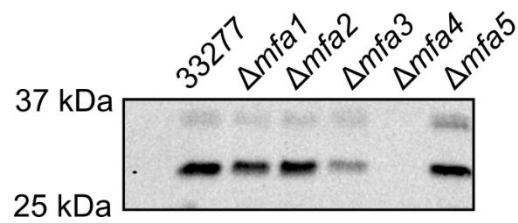
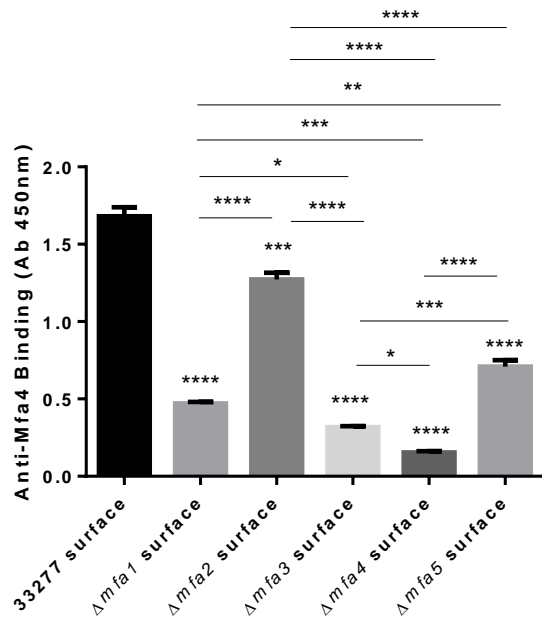
(B) Mfa2



(C) Mfa3



(D) Mfa4



(E) FimA

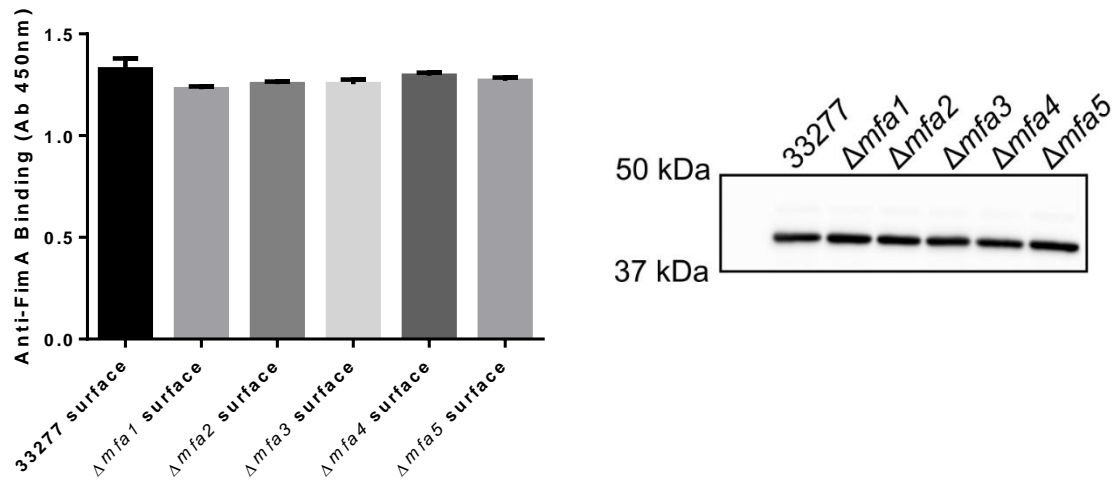


Figure 12. Mfa surface presentation and expression in *mfa* mutants via whole cell ELISA and immunoblotting analyses. (A-E) WT (33277) and *mfa* mutants were immobilized on an ELISA plate as whole cells for surface detection of Mfa1-4 or FimA (control) with specific antibodies. Signals were developed with TMB substrate for 10 min and stopped with 0.1 M sulfuric acid. Absorbance values were measured at 450 nm. Error bars = SD. One representative whole cell ELISA for each protein of at least 3 biological replicates, is shown. Statistical significance was tested via one-way ANOVA. Asterisk(s) directly above a bar indicates statistical significance compared to the wild-type. Right panels show whole cell cultures including whole cells and supernatants of 33277 and *mfa* mutants analyzed via immunoblotting with antibodies to Mfa1-4 or FimA. One representative blot of at least 3 biological replicates for each protein is shown.

For Mfa3, surface presentation was reduced most prominently compared to the wild-type in *mfa1* mutant followed by *mfa4* and *mfa5* mutants (Figure 12C). The *mfa2* mutant also exhibited reduced surface presentation level of Mfa3 although it was higher than that of Mfa3 in the *mfa1*, *mfa4*, and *mfa5* mutants (Figure 12C). Interestingly, immunoblotting analyses showed that Mfa3 was expressed and fully processed in the *mfa2* mutant but could only be detected in a minute quantity in the *mfa1* mutant or not all in *mfa4* and *mfa5* mutants (Figure 12C). This suggests that Mfa2 does not affect the processing of Mfa3, whereas Mfa1, Mfa4 and Mfa5 either directly or indirectly associate with Mfa3 in a manner essential for proper processing and efficient surface presentation of Mfa3. It should be noted that such direct interaction may indeed be possible as our binding ELISA data indicated that Mfa3 adheres to Mfa1, Mfa4, and Mfa5. Considering Mfa3 is still detected on the surface of *mfa1*, *mfa4* and *mfa5* mutants albeit at a significantly reduced level compared to the wild-type, Mfa3 is most likely translated and translocated into the periplasm where Mfa3 proteins that failed to be exported to the surface are accumulating in the absence of Mfa1, Mfa4, or Mfa5. Such accumulation would likely activate a degradation pathway facilitated through a periplasmic protease resembling DegP of *E. coli*, a protease known to degrade accumulating proteins in the periplasm (44). This would account for the minute quantity of Mfa3 detected for the *mfa1* mutant and no Mfa3 detected for the *mfa4* and *mfa5* mutants in immunoblotting analyses of whole cell cultures. In support of this explanation, the protein Basic Local Alignment Search Tool (BLAST) queried with the DegP sequence of *E. coli* in search of homologous *P. gingivalis* gene products revealed HsdR of *P. gingivalis* as a homologous gene product to DegP with 37%

sequence identity (Figure 13), suggesting HsdR, which has an annotated periplasmic serine protease region, may degrade accumulating fimbrial proteins including Mfa3 that failed to translocate to the surface. Our transcriptional analyses of *mfa* gene cluster in *mfa* mutants also indicated that *mfa* genes are transcribed properly in all the *mfa* mutants (Figure 14), demonstrating that Mfa proteins are likely translated and that any absence of Mfa proteins in the immunoblotting analyses of *mfa* mutants is likely a result of an activated degradation pathway in the periplasm potentially involving HsdR.

type I deoxyribonuclease HsdR [Porphyromonas gingivalis]

Sequence ID: [WIP_004585130.1](#) Length: 498 Number of Matches: 1

[▶ See 10 more title\(s\)](#)

Range 1: 51 to 468		GenPept	Graphics			▼ Next Match	▲ Previous Match
Score	Expect	Method	Identities	Positives	Gaps		
247 bits(631)	2e-76	Compositional matrix adjust.	163/441(37%)	241/441(54%)	37/441(8%)		
Query 25	TAAETSSAITAQQMPSLAPMLEKVMPSVVSINVEGSTIVNTPRMPRNFQQFFGDDSPFCQ					84	
Sbjct 51	T+ I+S +A +P+L E + +VV I VE +++ + F+ FFG +S Q						109
Query 85	EGSPFQSSPFCQGGQGGNGGGQQKFMALGSGVIIADADKGYVVTNNHVVDNATVIKVLQ					144	
Sbjct 110	R-----P-----QTRQVVVYGGSGVIISTD-GYIITNNHVVKGAKEMTVILN						149
Query 145	DGRKFDKAMVGGKDPKRSIALIQIQNPKNLTAIKMADSDALRVGDYTVVAIGNPFGLGETVT					204	
Sbjct 150	DNRF AK++G D +DIAL+++ + K L I DSD LRVG++ +A+GNPF L TVT						208
Query 205	SGIVSALGRSGLNAEN-----YENFIQTDAAINRGNSSGALVNLNDELIGINTAILAPDG					259	
Sbjct 209	+GIVSA GRS E+FIQTDAA+N GNSGGALVN GELIGINT I + G						268
Query 260	GNIGIGFAIPSNMVKNLTSQMVEYGVKRGELGIMGTELNSELAKAMKVDAQRGAFVSVQV					319	
Sbjct 269	G FA+P ++ + + +YGV+R LGI G +++ E K + + GA V+						328
Query 320	LPNSSAAKAGIKAGDVITSLNGKPISSFAALRAQVGTMPVGSKLTGLLRDG--KQVNVN					377	
Sbjct 329	S+A AG++ GDVIT++ GK I SF L+ + G K+ L + R G K++ V						388
Query 378	LELQQSSQNQVDSSSI-----FNGIEGAEMSNGKDKQGVVVNVKGTGTPAAQIGLKKG					430	
Sbjct 389	L+ + S + + S F + +M + G GV V +V +G G+KKG						447
Query 431	DVIIGANQQAVKNIAELRKVL 451						
Sbjct 448	+I+ N+Q V + A++ ++						468

Figure 13. Homology search of *E. coli* DegP against the *P. gingivalis* 33277 genome via NCBI BLAST. Protein sequence of DegP was used to search for a homologous gene product of *P. gingivalis*. The result for the top hit from the search is shown. HsdR displays 37% identity to DegP.

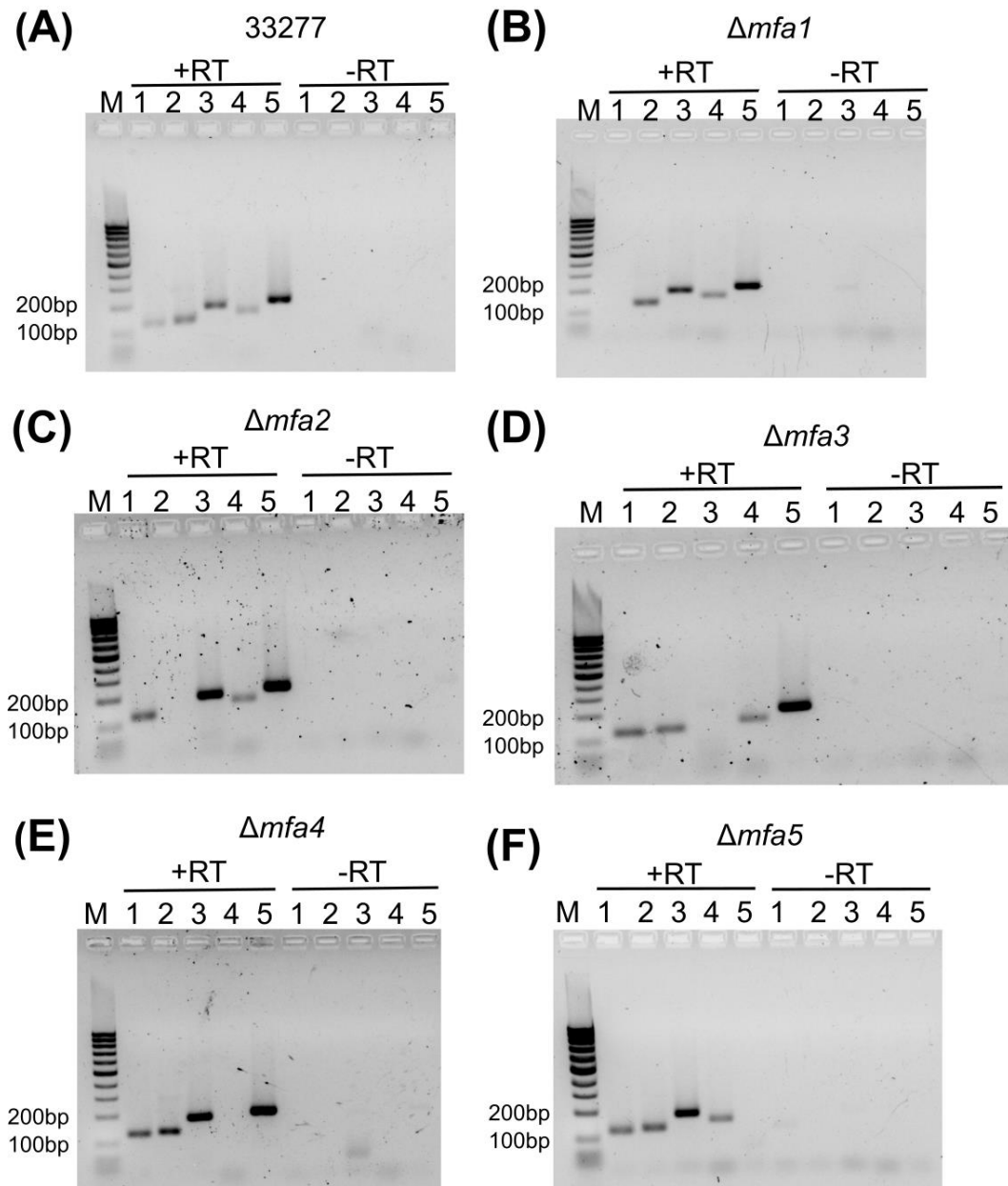


Figure 14. Transcriptional analyses of *mfa* gene cluster in *mfa* mutants. Total RNA was extracted from 33277 WT (A), $\Delta mfa1$ (B), $\Delta mfa2$ (C), $\Delta mfa3$ (D), $\Delta mfa4$ (E), and $\Delta mfa5$ (F) and was used for RT-PCR of *mfa* gene cluster. A no-reverse transcriptase (-RT) control was used to rule out the possibility of genomic DNA contamination. Numbers above gels represent *mfa* gene numbers (e.g. 1 = *mfa1*, 2=*mfa2*, etc). Results are representative of 3 biological replicates.

Mfa4 surface presentation was also reduced across all *mfa* mutants compared to the wild-type but most prominently for *mfa3* mutant followed by *mfa1*, *mfa5*, and *mfa2* mutants (Figure 12D). Immunoblotting analyses revealed that Mfa4 processing does not necessitate the presence of other Mfa proteins (Figure 12D). However, the Mfa4 band of the *mfa3* mutant whole cell culture appeared in lower intensity than in wild-type and other *mfa* mutants (Figure 12D), suggesting that Mfa4 may have been partially degraded in the absence of Mfa3 potentially also via a degradation pathway involving HsdR. Thus, Mfa4 translocation is mediated most prominently by Mfa3 and partly by Mfa1, Mfa5, and Mfa2, but its proteolytic processing occurs independently of other Mfa proteins.

Collectively, the results demonstrate intricate interactions amongst Mfa fimbrial proteins within the periplasm and on the surface. Notably, the Mfa1 major subunit did not necessitate Mfa2-5 for its surface presentation and proteolytic processing, suggesting that its biogenesis pathway is independent of the downstream accessory proteins. In contrast, the surface expression of Mfa2-4 and, to an extent, their proteolytic integrity in the whole cell culture appeared to depend on each other.

Role of accessory proteins in Mfa1 polymerization

Our whole cell ELISA and immunoblotting analysis of *mfa* mutants indicated that the Mfa1 major subunit does not necessitate accessory fimbrial proteins for its proteolytic processing and for its efficient surface presentation. However, it was unclear whether the polymerization of Mfa1, rather than the mere surface presentation, was influenced by the accessory proteins. As the Mfa1 subunit protein constitutes the backbone of the Mfa1 fimbriae in a heteropolymeric form with at least Mfa3 and Mfa4, as evidenced in our immuno-TEM experiments, in addition to Mfa5 and possibly Mfa2 (31), we investigated

the role of accessory fimbrial proteins Mfa2-5 in the polymerization of Mfa1. Because the role of Mfa2-5 did not appear essential in the surface presentation of Mfa1 as shown by our whole cell ELISA experiment, we hypothesized that the polymerization of Mfa1 entails an accessory fimbrial protein-independent mechanism. It should be noted that subjecting whole cell lysates to sodium dodecyl sulfate (SDS) and subsequent electrophoresis and immunoblotting has been the standard approach in investigating both FimA and Mfa1 polymers as they are SDS-resistant at sub-boiling temperatures, exhibiting distinct ladder-like patterns on an immunoblot when probed with either FimA or Mfa1 antibodies (32, 34). We thus employed the traditional SDS-based immunoblotting analyses of whole cell lysates of *mfa* mutants processed at different temperatures to exploit the non-covalent and thus heat-sensitive nature of the Mfa1 polymer; sonication on ice rather than boiling was chosen as the method of cell lysis to prevent any heat-induced premature dissociation of Mfa1 polymer prior to sample processing. Consistent with our hypothesis, the ladder-like polymerization pattern was observed in *mfa3-5* mutants at sub-boiling temperatures (65°C and 80°C), suggesting that Mfa1 polymerization occurs independently of Mfa3-5 (Figure 15). The specificity of Mfa1 antibodies was confirmed through the inclusion of *mfa1* mutant, for which no bands were observed (Figure 15). Intriguingly, neither a prominent ladder-like pattern nor a monomeric band was observed for *mfa2* mutant at 65°C (Figure 15). Given that Mfa2 has been shown to regulate fimbrial length and since its absence leads to a longer phenotype (31), it may be the case that the Mfa1 polymer failed to enter the electrophoretic gel due to its longer length and potentially having a higher affinity amongst individual Mfa1 subunits from positive cooperativity that precluded the dissociation of the Mfa1 polymer at 65°C. Nonetheless, the ladder-pattern was evident for

the *mfa2* mutant at 80°C (Figure 15). Furthermore, the characteristic ladder-like pattern was eliminated and was converted to a monomeric band upon sample processing at 100°C for the wild type and *mfa2-5* mutants, confirming the non-covalent nature of the Mfa1 polymer (Figure 15). Therefore, we conclude that Mfa1 polymerization does not involve any of the accessory proteins and occurs solely by an Mfa1 subunit-mediated polymerization mechanism.

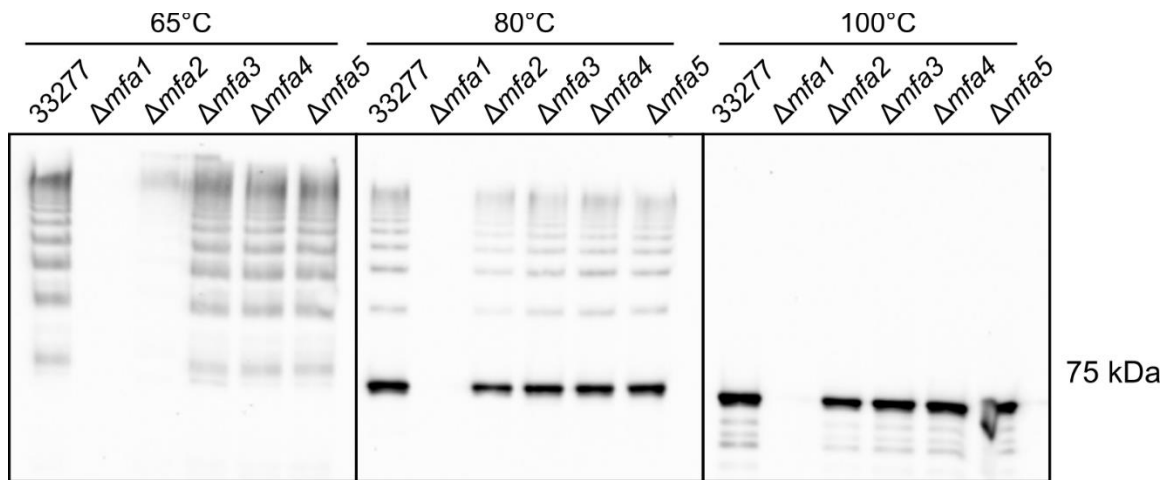


Figure 15. Mfa1 polymerization in *mfa* mutants. Whole cell sonicates of 33277 WT and *mfa* mutants were processed at 65°C, 80°C, and 100°C prior to SDS-PAGE and immunoblotting with antibodies to Mfa1. One representative blot of 3 biological replicates is shown. The Mfa1 monomer is at 67 kDa and the higher molecular weight ladder-like bands represent different polymerization states.

Role of Rgp processing and Mfa1 terminal regions in Mfa1 polymerization

Because the Mfa1 polymerization mechanism appeared independent of the accessory fimbrial proteins, we postulated that the process was solely mediated by intrinsic features of individual Mfa1 subunits. A previous electron microscopic examination of a *P. gingivalis* mutant lacking arginine gingipains revealed a cell surface significantly devoid of fimbriations (41), suggesting a direct involvement of arginine gingipains in fimbrial assembly and as a potential Mfa1 polymerization initiation mechanism. However, a definitive biochemical evidence showing Rgp processing of Mfa1 as the mechanism responsible for the polymerization initiating event of Mfa1 has not been reported. Notably, structural evidence from FimA and Mfa4 crystals have suggested DSE as a likely mechanism for *P. gingivalis* fimbriae (32, 38). In the case of Mfa1 fimbriae, this implies the involvement of terminal beta-strand regions for polymerization. However, due to the lack of Mfa1 crystal structure, no definitive evidence implicating DSE as the Mfa1 polymerization mechanism is available. A biochemical approach involving truncations of Mfa1 terminal beta-strand regions would provide additional evidence either for or against DSE as the Mfa1 polymerization mechanism. Furthermore, Xu *et al.* reported that the truncation of a C-terminal region of Mfa1 abrogated its polymerization, but no experimental data were provided (32). Thus, we hypothesized that the polymerization of Mfa1 is initiated with Rgp processing of Mfa1 and that subsequent polymerization involves either N or C-terminal regions of the Mfa1 subunit in a process identical to, or resembling, DSE. Secondary structure prediction of Mfa1 revealed putative beta-strand regions immediately following arginine 49, which is the putative Rgp processing site, and in the C-terminus (Figure 16). This information was used to generate corresponding N or C-

terminally truncated recombinant Mfa1 proteins such that the terminal regions containing two consecutive beta-strands that may act as donor-strands were deleted. Additional recombinant Mfa1 proteins corresponding to pre-Rgp processed form and post-Rgp processed form denoted as precursor and mature, respectively, were also generated. Immunoblotting analyses of purified recombinant Mfa1 proteins representing precursor, mature, and N or C-terminally truncated forms revealed monomeric bands for precursor and N or C-terminally truncated Mfa1 proteins and a characteristic ladder-like pattern for mature Mfa1 protein when the proteins were processed at 60°C prior to electrophoresis (Figure 17). Only monomeric bands were observed when the proteins were processed at 100°C (Figure 17), confirming that the ladder pattern for the mature Mfa1 protein was indicative of the Mfa1 polymer. The involvement of Rgp processing in Mfa1 polymerization was further confirmed with a *P. gingivalis* mutant lacking both *rgpA* and *rgpB*. As Kgp was shown not to be involved in the processing of Mfa1 (42), a *kgp* mutant was included as a specificity control for a gingipain knockout. *P. gingivalis* wild-type and *kgp* mutant exhibited a characteristic ladder-like pattern when whole cell sonicates were processed at 60°C prior to electrophoresis without any apparent monomeric band (Figure 18). In contrast, the whole cell sonicate of the *rgpA/B* mutant exhibited a monomeric band corresponding to the pre-Rgp processed form of Mfa1 (Figure 18). As expected, only the monomeric bands were present when the whole cell sonicates of wild-type and gingipain mutants were processed at 100°C, and the monomeric band for the *rgpA/B* mutant appeared at a higher molecular weight than that for the wild-type and *kgp* mutant (Figure 18), demonstrating the pre-Rgp processed nature of the higher molecular-weight Mfa1 monomer. Interestingly, some evidence of ladder-like pattern was observed

in the whole cell sonicate of *rgpA/B* mutant at 60°C. Although the precise nature of such ladder-like pattern in *rgpA/B* mutant is unclear, it may be attributed to Kgp rescuing the processing of Mfa1 albeit inefficiently since the monomeric band corresponding to pre-Rgp processed form of Mfa1 is still evident. Collectively, these results suggest that Rgp processing is indeed the initiating event for Mfa1 polymerization and that upon Rgp processing, N and C-terminal beta-strand regions are essential for Mfa1 polymerization, reminiscent of DSE of type I and P pili of *E. coli*.

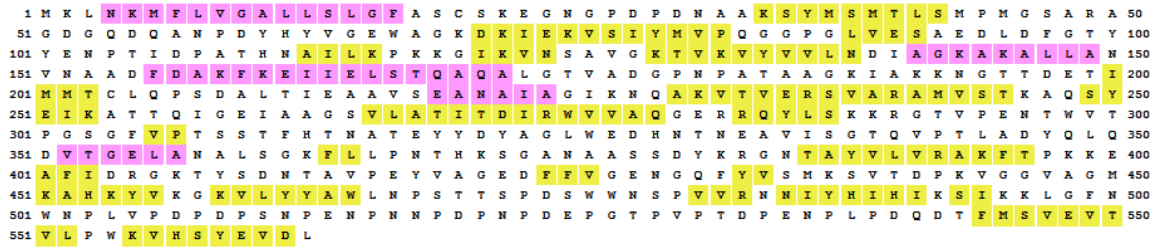


Figure 16. Predicted secondary structure of Mfa1. The full-length sequence of Mfa1 was used to predict its secondary structure via PSIPRED. Pink regions indicate helices. Yellow regions denote beta-strands. Numbers on the left and right sides indicate amino acid residue positions. Arginine 49 is the putative Rgp processing site. The pre-Rgp processed form of recombinant Mfa1 does not contain a signal peptide, which are predicted to be the first twenty amino acid residues from methionine 1 to cysteine 20. The post-Rgp processed form of recombinant Mfa1 contains the remaining residues from alanine 49. C-terminally truncated recombinant Mfa1 is a post-Rgp processed form of Mfa1 and additionally does not contain phenylalanine 544 through leucine 563. N-terminally truncated recombinant Mfa1 is also a post-Rgp processed form of Mfa1 and does not contain alanine 50 through serine 91.

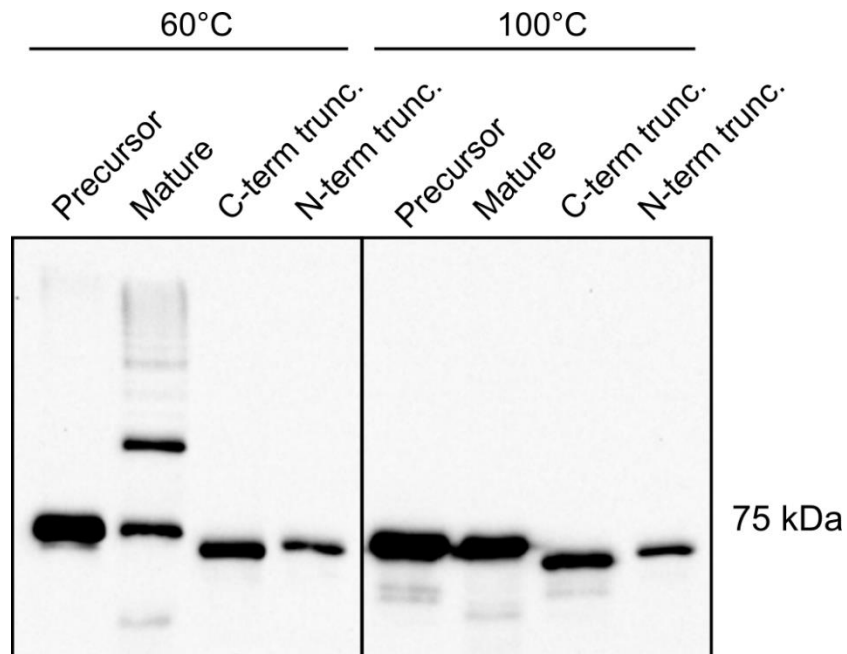


Figure 17. Mfa1 polymerization assay with recombinant Mfa1 proteins. Purified recombinant Mfa1 proteins corresponding to pre-Rgp processed form (precursor), post-Rgp processed form (mature), and either C-terminally truncated (C-term trunc) or N-terminally truncated (N-trunc) forms were processed at either 60°C or 100°C prior to SDS-PAGE and immunoblotting with antibodies to Mfa1. One representative blot of 3 biological replicates is shown.

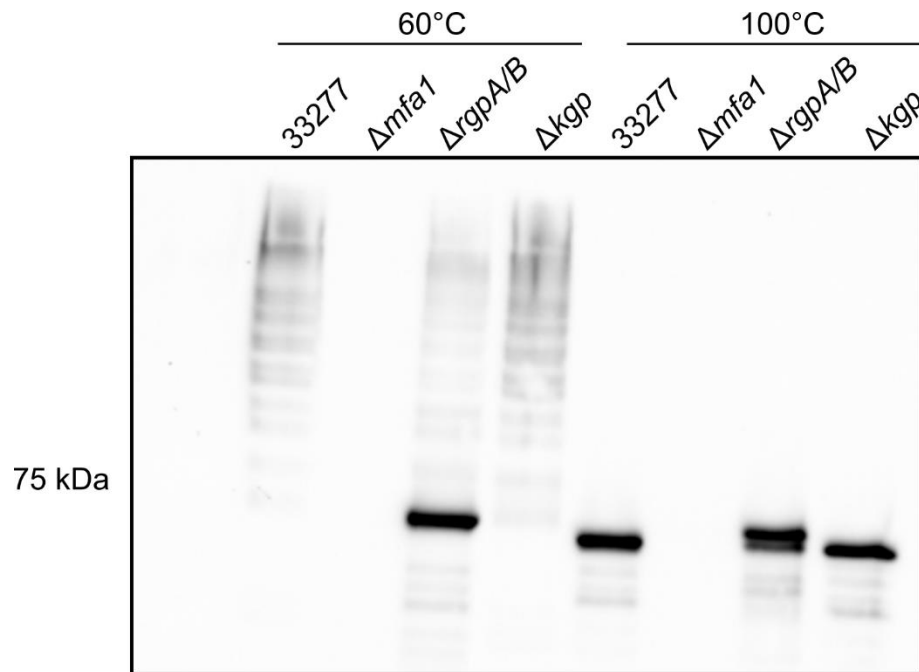


Figure 18. Mfa1 polymerization assay with 33277, *mfa1* mutant, *rgpA/B* mutant, and *kgp* mutant. Whole cell sonicates of 33277, *mfa1* mutant, *rgpA/B* mutant, and *kgp* mutant were processed at 60°C and 100°C prior to SDS-PAGE followed by immunoblotting with antibodies to Mfa1.

Role of Mfa1 terminal beta-strands in Mfa1 polymerization

In the well-characterized *E. coli* type I and P pili system, DSE entails a direct insertion of the N-terminal beta-strand of a pilin into the hydrophobic groove of another pilin for their polymerization to complete the characteristic IgG fold that each of the pilin subunits was lacking prior to the beta-strand insertion (44). Hence, to investigate the role of the beta-strands located in the terminal regions of Rgp-processed Mfa1 in polymerization, two additional recombinant Mfa1 proteins were generated with strategically placed amino acid substitutions to disrupt either N or C-terminal beta-strands. Specifically, two serine residues located in the putative beta-strand regions were replaced with prolines in either N or C-terminus of recombinant Mfa1 proteins via site-directed mutagenesis, on the basis that prolines are established beta-strand disruptors (50). Soluble fractions of *E. coli* expressing the proline substituted recombinant Mfa proteins were subjected to immunoblotting analyses with antibodies to Mfa1 to investigate the polymerization pattern of the proteins. Interestingly, both the N-terminal proline substituted Mfa1 and the C-terminal proline substituted Mfa1 exhibited the characteristic ladder-like pattern identical to the control recombinant Mfa1 without any amino acid substitution at 60°C (Figure 19). All proteins yielded a monomeric band at 100°C (Figure 19). The results thus indicated that the beta-strands in either terminus of Mfa1 are not essential in the polymerization of Mfa1.

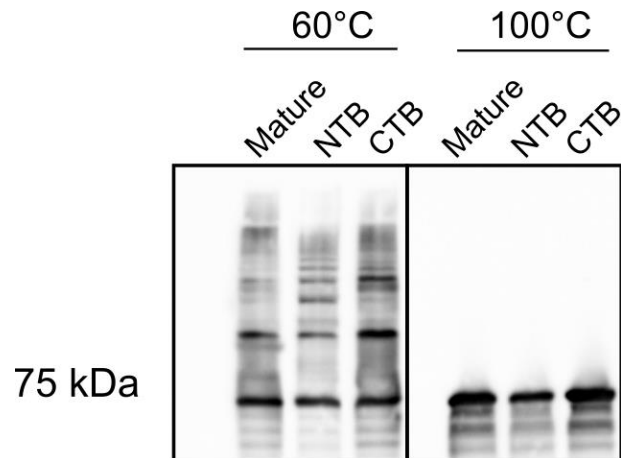


Figure 19. Mfa1 polymerization assay with N-terminal or C-terminal beta-strand disrupted Mfa1. Soluble fractions of *E. coli* BL21 sonicates containing the post-Rgp processed form of recombinant Mfa1 (mature), the N-terminal beta-strand recombinant Mfa1 (NTB), or the C-terminal beta-strand disrupted recombinant Mfa1 (CTB) were heated to either 60°C or 100°C prior to SDS-PAGE followed by immunoblotting with antibodies to Mfa1. One representative blot of 3 biological replicates is shown.

To further confirm that the beta-strands are indeed disrupted, circular-dichroism spectroscopy was carried out to estimate the secondary structures of the proline-substituted Mfa1 proteins. The blank-adjusted CD spectra of the proline substituted proteins revealed differential spectral patterns not only compared to each other but also compared to the control recombinant Mfa1 without any amino acid substitution, most prominently in lower absorbance regions (Figure 20). This suggests that the beta-strands in N and C-terminus of Mfa1 are most likely disrupted by the proline substitutions.

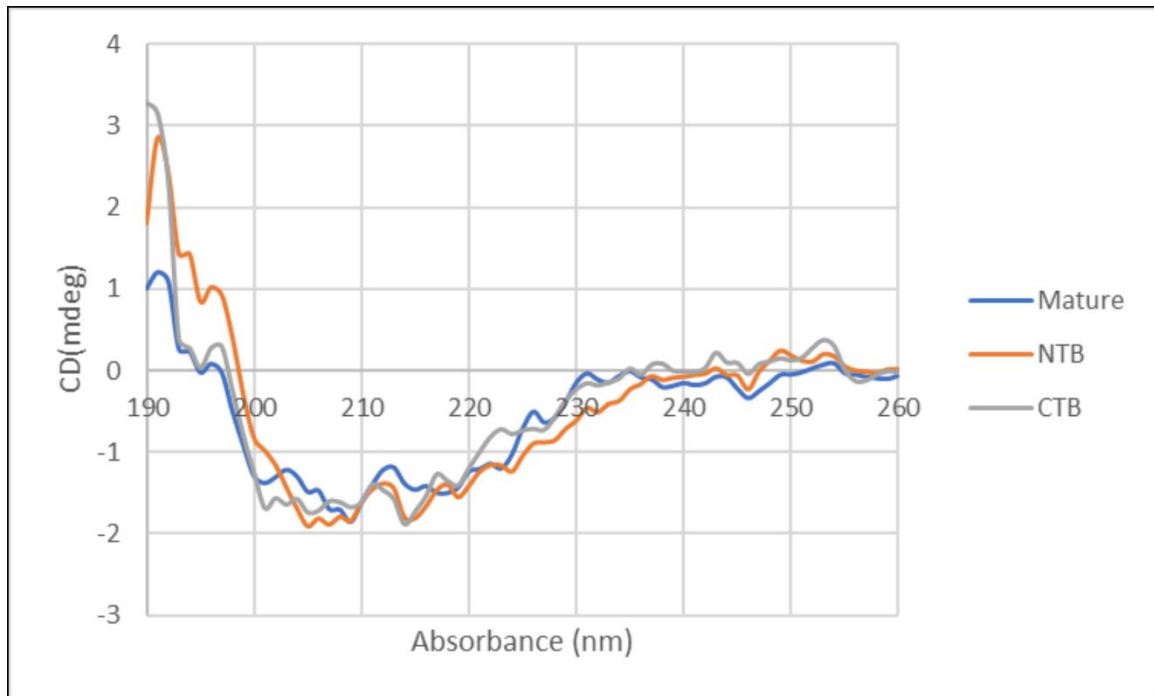


Figure 20. CD spectra of post-Rgp processed recombinant Mfa1 and its derivative with N-terminal or C-terminal beta-strand disruption. To confirm that the N-terminal beta-strands or C-terminal beta-strands of post-Rgp processed recombinant Mfa1 with proline substitutions are indeed disrupted, CD spectroscopy was carried out from absorbance 190nm to 260nm with the mature, NTB, and CTB recombinant Mfa1's.

Collectively, our results suggest that the beta-strands located in N and C-termini of the Rgp-processed Mfa1 are not essential in the polymerization of Mfa1. While this may appear contrary to our initial hypothesis that the Mfa1 polymerization occurs via DSE, no study to the best of our knowledge has demonstrated that the beta-strands are indeed essential features of DSE specifically through a beta-strand disruption approach. It should be noted that the beta-strands in the specific case of *E. coli*'s type I and P pili are important, but perhaps not necessarily required, only in the context that they complete the structural IgG fold when the pilins are assembled with each other. However, because no definitive structural evidence for Mfa1 is currently available in the form of a crystal, at least to the best of our knowledge, our result still does not necessarily refute the hypothesis that Mfa1 polymerization occurs via DSE. Specifically, the terminal beta-strands of Mfa1 may not be involved in completing an intrinsic structural fold or a domain that an Rgp-processed monomeric Mfa1 protein may lack, and it is possible that other secondary structural elements that may be present in the terminal regions including a coil or, to a less likely extent, a helix may participate in completing a certain fold or a domain. Nonetheless, that the terminal regions are essential in the polymerization of Mfa1 as shown by our N/C terminally truncated recombinant Mfa1 proteins still supports the DSE-mediated Mfa1 polymerization hypothesis. It should be noted that a truncation of either termini may have led to a significant loss of tertiary structure, yielding an artificial non-native conformation that nullified the polymerization competent state. Hence, rather than relying on the truncation assay as the definitive means for probing the role of Mfa1 termini in its polymerization, it should be taken as a complementary evidence to other biochemical assays. Despite the disrupted secondary structural elements in N and C-termini, Mfa1 may

still be able to dock either the N or C-terminus extension to the hydrophobic groove of another Mfa1, especially if the DSE in the case of Mfa1 is a beta-strand-independent process but rather a process more dependent on another feature of DSE involving the hydrophobicity of select alternating residues on the protein terminus.

Role of hydrophobic residues in Mfa1 termini in its polymerization

To further ascertain that the Mfa1 polymerization takes place via a DSE-like process, another feature of DSE of *E. coli* type P pili that involves alternating hydrophobic residues on the N-terminus was deemed as an appropriate readout to investigate with recombinant Mfa1 proteins. We hypothesized that Rgp-processed Mfa1 possesses alternating hydrophobic residues at either N or C-terminus that participate in a DSE-like polymerization process by forming a binding interface between individual Mfa1 subunits. Because our truncation data indicated that both the N and C-termini are essential in the Mfa1 polymerization, hydrophobic residues in both terminal regions were considered during an *in silico* analysis of the biochemical nature of Mfa1. The analysis showed there are several alternating amino acid residues in both N and C termini that are predicted to be buried without access to the solvent, thus exhibiting hydrophobic properties (Figure 21). Strategic amino acid substitutions were carried out via site-directed mutagenesis whereby alternating hydrophobic residues in either N or C-terminus of recombinant Mfa1 were replaced with either aspartic acid, serine, or alanine (Figure 22). Aspartic acid, serine, and alanine contain charged, polar, and hydrophobic side chains, respectively, and represent a decreasing likelihood of disrupting hydrophobic interactions, with aspartic acid most likely to disrupt them. In immunoblotting analyses of the soluble fractions of *E. coli* expressing the recombinant Mfa1 proteins, the aspartic acid-substituted Mfa1 in either terminus did

not exhibit any ladder-like pattern while the serine-substituted Mfa1 and the alanine substituted Mfa1 in either terminus showed the characteristic polymerization pattern at 60°C (Figure 23). All the Mfa1 proteins only showed monomeric bands at 100°C as expected (Figure 23). The results indicate that introduction of charged residues, but not polar or hydrophobic residues, in either N or C-terminus of Mfa1 in place of putative buried and thus hydrophobic residues disrupts the polymerization of Mfa1. In addition, because substitutions with serine, which possesses polar side-chains, did not disrupt the polymerization of Mfa1, the results also indicate that the hydrophobicity in the binding interface can tolerate some degree of polarity prior to dissociation when the polarity is increased with an introduction of charged residues. Thus, the polymerization interface surrounding the alternating hydrophobic residues in either terminus of Rgp-processed Mfa1 likely does not involve a strict hydrophobic milieu but rather a state intermediate between strict hydrophobicity and strict hydrophilicity. Nonetheless, the results still underscore the essential aspect of the biochemical characteristics of alternating hydrophobic residues in either terminus in the polymerization of Mfa1, supporting the DSE-like process as the Mfa1 polymerization mechanism.

(A) Predicted biochemical characteristics of N-terminus of Mfa1

	1	11	21	31	41	51	61	71
SEQ	MKLNKMFVLG	ALLSLGFASC	SKEGNGPDPD	NAAKSYMSMT	LSMPMGSARA	GDGQDQANPD	YHYVGEWAGK	DKIEKVSIIYM
SS3	C H H H H H H H H H	H H H H H H H H H C	C C C C C C C C C C	C C C C E E E E E E	E E C C C C C C C C	C C C C C C C C C C	C C C C C C C C C C	C C E E E E E E E E
SS8	L H H H H H H H H H	H H H H H H H H L L	L L L L L L L L L L	L L L L E E E E E E	E E L L L L L L L L	L L L L L L L L L L	L L L L L L L L L L	L E E E E E E E E E
ACC	E E E E E M B E E B B	E E B B B B B B M	M E E E E E E E E E	E E E E B M B M B M	B M B E E E E E E E	E E E E E E E E E E	E E E E E E E E E E	E M B M M B B B B B
DISO	* * * * * * * * * *	* * * * * * * * * *	* * * * * * * * * *	* * * * * * * * * *	* * * * * * * * * *	* * * * * * * * * *	* * * * * * * * * *	* * * * * * * * * *

	81	91	101	111	121	131	141	151
SEQ	VPQGGPGLVE	SAEDLDFGTY	YENPTIDPAT	HNAILKPKKG	IKVNSAVGKT	VKVYVVLNDI	AGKAKALLAN	VNAADFDAKF
SS3	E C C C C C C C E E	E E E E C C C C C C	C C C C C C C C C C	C C C C E E E E E E	E E C C C C C C C E	E E E E E E E E C C	H H H H H H H C C C	C C H H H H H H H H
SS8	E L L T T S S E E E E	E E E E L L L T L L	E S L L L L L T L L	L L L E E E E E E E	E E L L L L L T T L E	E E E E E E E E L L	H H H H H H H H T	L L H H H H H H H H
ACC	B M E E E E E M M M	M M M B E E E E M	M E E E M M E E E E	E E E E E B E M E M E	B E B M M E M E E E	B M B B B B B B M	E E E B E E B M E E	M M M E E B M E M B
DISO

(B) Predicted biochemical characteristics of C-terminus of Mfa1

	481	491	501	511	521	531	541	551
SEQ	VVRNNIYHIH	IKSIKKLGFN	WNPLVPDPDP	SNPENPNPND	PNPDEPGTPV	PTDPENPLPD	QDIFMSVEVT	VLPWKVHSYE
SS3	C C C C C E E E E E	E E E E C C C C C C	C C C C C C C C C C	C C C C C C C C C C	C C C C C C C C C C	C C C C C C C C C C	C C C E E E E E E E	E E C C E E E C C C
SS8	L L L T T L E E E E E	E E E E E S T T L L	L L L L L L L L L L	L L L L L L L L L L	L L L L L L L L L L	L L L L L L L L L L	L L L L L L L L L L	L L L E E E E E E E
ACC	B B B B B B B M B M	B M M B E E M M M E	M M E E E E E E E E	E E E E E E E E E E	E E E E E E E E E E	E E E E E E E E E E	E E E E E E E E E E	E E M E B M B E B M
DISO * * * * *	* * * * * * * * * *	* * * * * * * * * *	* * * * * * * * * *	* * * * * * * * * *	* * * * * * * * * *

	561
SEQ	VDL
SS3	C C C
SS8	L L L
ACC	E E E
DISO	* * *

Figure 21. Predicted biochemical characteristics of Mfa1 termini. Full-length Mfa1 sequence was used to generate biochemical property predictions via RaptorX Property Prediction. Numbers indicate amino acid residue positions. SEQ line indicates amino acid sequences. SS3 and SS8 indicate secondary structure predictions with following notations: H=alpha-helix, E=beta-sheet, C= coil, L=loop, T=hydrogen bonded turn, and S=bend. ACC indicates solvent accessibility with following notations: B=buried, M=medium, and E=exposed. DISO denotes order/disorder state.

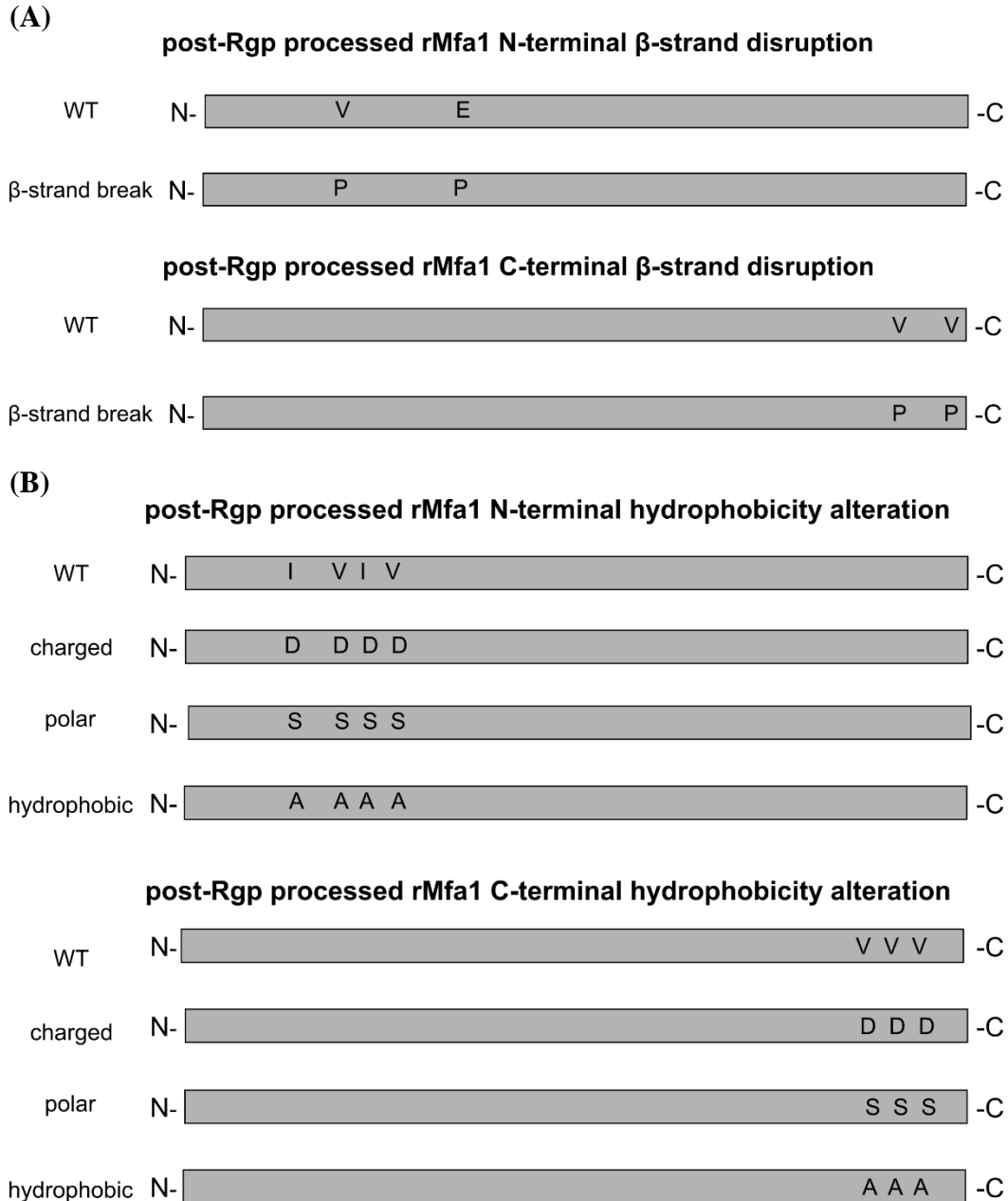


Figure 22. Beta-strand disruption and hydrophobicity alteration on post-Rgp processed rMfa1 termini. Amino acid substitutions in either N-terminus or C-terminus of post-Rgp processed form of recombinant Mfa1 were carried out via site-directed mutagenesis. (A) To disrupt N-terminal beta-strands, valine 76 and glutamic acid 90 were substituted with prolines. To disrupt C-terminal beta-strands, valine 549 and valine 556 were substituted with prolines. (B) N-terminal hydrophobicity was altered by substituting isoleucine 73, valine 76, isoleucine 78, and valine 81 with either aspartic acid or serine. As a substitution control that maintains hydrophobicity, an alanine substitution construct was also generated. C-terminal hydrophobicity was altered by substituting valine 547, valine 549, and valine 551 with either aspartic acid or serine. An alanine substituted construct was also generated.

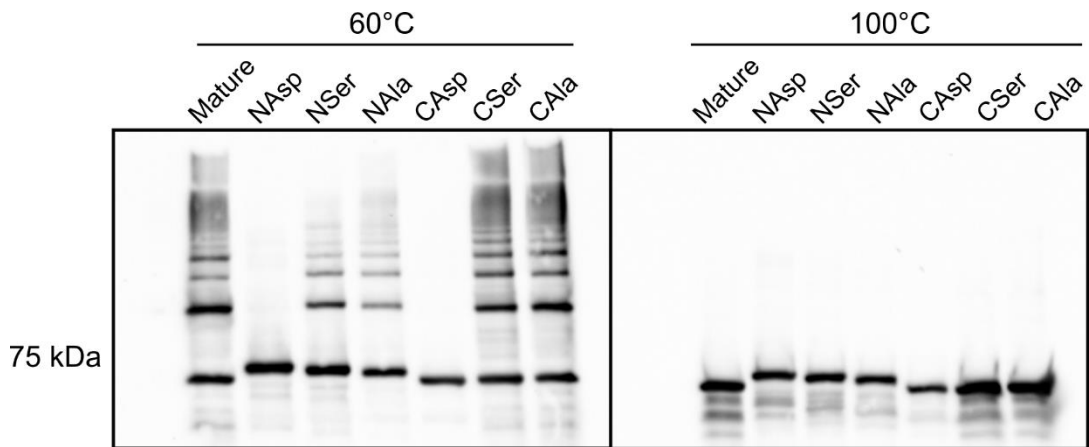


Figure 23. Mfa1 polymerization with hydrophobicity altered post-Rgp processed recombinant Mfa1. Soluble fractions of *E. coli* BL21 sonicates containing post-Rgp processed recombinant Mfa1 with N-terminal or C-terminal substitutions were heated to either 60°C or 100°C prior to SDS-PAGE, followed by immunoblotting with antibodies to Mfa1. N-terminal aspartic acid, serine, or alanine substituted constructs are denoted as NAsp, NSer, or NAla, respectively. C-terminal aspartic acid, serine, or alanine substituted constructs are denoted as CAsp, CSer, or CAla, respectively. Post-Rgp processed recombinant Mfa1 without any substitutions is denoted as mature. One representative blot of 3 biological representatives is shown.

CHAPTER 4 DISCUSSION

Mfa1 fimbriae of *P. gingivalis* are an important virulence factor that enhance the pathogenicity of the bacterium and contributes to the pathogenesis of the adult chronic periodontitis (2, 24, 27). As a peritrichous fimbrial structure protruding from the surface of *P. gingivalis*, Mfa1 fimbriae represents a heteropolymeric protein complex comprising the Mfa1 major subunit protein along with accessory proteins Mfa2-5. The interacting partners amongst the Mfa subunits and the mechanism of Mfa1 fimbrial biogenesis have remained elusive. In this study, the spatial relationships amongst Mfa subunits and their assembly mechanism were investigated using a combination of molecular, biochemical, and biophysical approaches.

Immuno-transmission electron microscopic examinations of *P. gingivalis* wild-type and individual *mfa* mutants revealed the localization of Mfa1-4. Consistent with previously reported findings (31, 33), Mfa1 was localized throughout the fimbrial structure, whereas Mfa2 was localized in the basal portion of the fimbriae. Also in agreement with the previous result (33), Mfa3 was located at the tip portion of the fimbriae. Similarly, Mfa4 was determined to be at the distal portion of the fimbriae. As noted earlier, because the TEM experiments were carried out without thin-sectioning, the cells in the TEM images represent structurally intact cells. This means that there may be some areas in images where fimbriae are overlapping. Furthermore, given the variable length of the Mfa1 fimbriae, gold particles may appear to be localizing throughout the fimbrial structure when in fact they are the result of overlapped fimbriae with differing lengths. While the use of

ultra-thin sectioning may eliminate such overlap issue, it may be more challenging to observe fimbrial structure with the use of sectioning as the fimbriae are surface structures that are capable of being sheared into the extracellular milieu. Nonetheless, the resolution provided by the transmission electron microscopy is unparalleled for the maximally retained fimbrial structures due to no sectioning and is appropriate for precise determination of fimbrial subunit localization.

From the ELISA-based binding assays using recombinant Mfa proteins, it was found that pre-Rgp processed Mfa3 adheres to other precursor Mfa proteins including Mfa1 and Mfa4 in addition to Mfa2 and Mfa5. Similarly, Mfa2 adhered to Mfa5 and to precursor Mfa1 and Mfa3. Mfa2 showed relatively weak binding suggestive of non-specific interaction with precursor Mfa4 compared to its binding to other precursor Mfa proteins. Rgp-processing did not appear to affect the binding results observed with pre-Rgp processed Mfa proteins as recombinant mature Mfa3 still adhered to mature Mfa1, Mfa4 in addition to Mfa2 and Mfa5. Moreover, Mfa2 showed binding activity to mature Mfa1 and Mfa3 but only exhibited what appeared to be non-specific interaction with mature Mfa4. Secondary structure estimations through circular-dichroism analyses of precursor recombinant Mfa proteins revealed that the proteins were most likely in their native forms and that the binding events observed in ELISA experiments were not due to altered conformation or complete denaturation. No other binding activity was observed with Mfa proteins. Hence, the binding data demonstrated that the interaction amongst Mfa proteins, and by corollary the assembly process, is initiated prior to Rgp processing and thus within the periplasm as precursor forms. Although the relative affinity was estimated via saturation binding ELISA experiments with select binding pairs, it is imperative that more

biophysical assays be carried out for richer characterization of the binding events amongst Mfa proteins, especially given that the saturation binding ELISA relied on the one-site binding model that may or may not be valid within the *in vivo* context (i.e. in the periplasm of *P. gingivalis* or on the surface of the bacterium in the oral cavity within biofilm). Specifically, the binding stoichiometry may be best determined through analytical ultracentrifugation based on distinct sedimentation velocity values of binding pairs (51).

Whole cell ELISA experiments showed Mfa1 surface expression occurs independently of Mfa2-5. In contrast, Mfa2 surface expression was partially dependent on other Mfa proteins. Similarly, Mfa3 and Mfa4 surface expression was also at least partially dependent on other Mfa proteins. Because the reduced surface presentation could be the result of reduced protein expression or protein degradation in the periplasm, whole cell cultures of *mfa* mutants, which comprised both whole cell lysates and culture supernatants, were analyzed through immunoblotting. The results indicated that Mfa1 and Mfa2 were unperturbed in terms of protein expression and integrity in all the *mfa* mutants except for *mfa1* and *mfa2* mutants, which served as negative controls. In the case of Mfa2, this means the reduced surface presentation level is partly due to the failure of Mfa2 to either directly or indirectly interact with other Mfa proteins. Interestingly, Mfa3 showed markedly lowered expression level in the whole cell culture of *mfa1* mutant and no expression at all in *mfa4* and *mfa5* mutants. In contrast, its expression appeared normal in *mfa2* mutant. Given the normal transcriptional activity of *mfa* gene cluster in all five *mfa* mutants as evidence by the RT-PCR results, it was reasonable to presume proteolytic degradations as the cause of such aberrant immunoblot profile for Mfa3 with *mfa1*, *mfa4*, and *mfa5* mutants. A homology search of serine protease DegP of *E. coli* against *P. gingivalis* genome

revealed HsdR as the likely periplasmic protease that may degrade accumulating Mfa3 that failed to translocate to the surface. Similarly, Mfa4 expression appeared to be reduced in the whole cell culture of *mfa3* mutant. This may also be attributed to an increased sensitivity to proteolytic degradation of Mfa4 to periplasmic protease in the absence of Mfa3.

Next, the polymerization mechanism of Mfa1 major subunit was investigated. Mfa2-5 were found not to be essential in the polymerization of Mfa1, suggesting an intrinsic feature present on the Mfa1 subunit itself as the driving force for fimbrial elongation. On the other hand, Rgp processing was found to be essential for the polymerization of Mfa1. Furthermore, the terminal regions of Mfa1 were determined to be crucial as recombinant proteins lacking either of these regions failed to show characteristic ladder-like pattern in immunoblotting analyses. Two specific features of DSE, namely beta-strand involvement and alternating hydrophobic residues at a protein terminus, were used as readouts to further determine whether the polymerization of Mfa1 is a DSE-like process. Interestingly, recombinant Mfa1 proteins with disrupted putative beta-strand regions in either N-/C-terminus still exhibited polymerization pattern, indicating that the beta-strands are not essential features in Mfa1 polymerization. Beta-strand disruptions were confirmed via circular-dichroism spectroscopy. Yet, when alternating hydrophobic residues in either termini were altered to charged residues, no polymerization pattern was observed, reminiscent of DSE in type P pili of *E. coli*. It is possible that Mfa1 may utilize alternative secondary structural feature other than beta-strands to polymerize. Furthermore, to the best of our knowledge, no study has demonstrated that the beta-strands are indeed a require feature for DSE in type I and P pili

systems of *E. coli* using a beta-strand disruption approach. Provided that certain biochemical features are maintained such as alternating hydrophobicity in a protein terminus and that there are no drastic alterations to a tertiary structure, the presence of beta-strands may not be crucial in the DSE process. Importantly, that the terminal regions are directly involved in the polymerization is in support of DSE-like process as the polymerization mechanism of Mfa1. It is particularly interesting to note that both termini of Mfa1, rather than just one terminus, appear to be involved in the DSE-like polymerization process, suggesting that either N- or C- terminus are equally likely to serve as the donor-strand. According to the *P. gingivalis* FimA polymerization model, the C-terminus is likely the donor-strand, whereas the polymerization model based on Mfa4 crystal structure posits that the N-terminus is likely the donor-strand. Nonetheless, both models implicate DSE as the polymerization mechanism in *P. gingivalis* fimbrial system. While it is not currently possible to definitively conclude which terminus is the donor-strand in the case of Mfa1 fimbrial polymerization, our data overall further supports the notion that DSE is the likely mechanism used by the Mfa1 fimbriae for its polymerization. For a more definitive determination of the donor-strand side, solving of the Mfa1 crystal structure may prove to be the most useful. It should be emphasized that despite the use of the term donor-strand in describing DSE as the likely polymerization mechanism of Mfa1, given the biochemical evidence that negated the importance of beta-strands in either terminus of Mfa1 in its polymerization, the term should only be used to refer to a protruding element of the protein that coincidentally possesses beta-strands as secondary structures. Hence, the use of the term donor-strand itself should not imply the importance of beta-strands in Mfa1 polymerization. Lastly, the involvement of both termini in Mfa1

polymerization suggests that the N-terminus may directly interact with the C-terminus. This was the case in *P. gingivalis* FimA major subunit in its polymerization (32). To further probe this possibility, a cysteine-substitution based crosslinking experiment whereby cysteines are introduced in N and C-termini of Mfa1 in an oxidizing condition or in the presence of a short-arm sulfhydryl specific crosslinker may provide definitive evidence for the interaction between the two termini. Similarly, a more sophisticated approach involving high-resolution mass spectrometry and chemical crosslinking (commonly referred to as XL-MS) may be used to complement the results from the cysteine-substitution based crosslinking assay (52, 53). In this approach, no alteration to the primary structure is needed, and it only requires that the polymer be crosslinked using a specific short-arm (or zero-length) crosslinker, which is then analyzed via high-resolution mass-spectrometer for determination of the amino acid sequence of the crosslinked peptides. The same approach may also be used to determine binding sites amongst other Mfa binding pairs.

Based on our findings, we propose an assembly model of the Mfa1 fimbriae involving a pre-assembly complex within the periplasm amongst the subunits and the elongation of Mfa1 major subunit via a DSE-like process with alternating hydrophobic residues on both termini forming a binding interface (Figure 24). Nascent Mfa proteins are guided by their N-terminal signal peptides for transport into the periplasm aided by the SecYEG translocon located in the inner membrane. Given that Mfa1-4 contain lipoprotein signal peptides, type II signal peptidase within the periplasm cleaves the N-terminal signal peptides of Mfa1-4, which are then lipidated at their N-terminus cysteine residues that immediately follow the signal peptides. For Mfa5, a known protein that utilizes the Type

IX secretion system, it still undergoes N-terminal signal peptide processing in the periplasm but via type I signal peptidase rather than type II signal peptidase. It should be noted that although Mfa5 may use the dedicated outer membrane channel comprising Por proteins, it may also interact with other Mfa proteins within the periplasm and consequently circumvent the utilization of Type IX secretion system. Within the periplasm, precursor Maf3 binds precursor Mfa1 and Mfa4 in addition to Mfa5 to form a pre-assembly complex, designated as such to underscore the periplasmic assembly prior to presentation on the surface and extracellular milieu. Because Mfa3-5 are quantitatively less abundant subunits relative to Mfa1 (31), the pre-assembly complex comprising Mfa1, Mfa3, Mfa4, and Mfa5 also exists in lesser amount relative to unbound precursor Mfa1 in the periplasm. Furthermore, Mfa1, Mfa3, and Mfa4 are lipoproteins with N-terminal lipidation, and thus the pre-assembly complex likely exhibits more hydrophobic properties due to additional lipidation compared to individual Mfa subunits alone. Therefore, despite the relative quantitative paucity of the pre-assembly complex, it likely has a higher affinity for the outer membrane given the additional lipidation present on the complex than individual Mfa1 subunits, which only possesses single lipidation. Such a higher affinity of the pre-assembly complex towards the outer membrane likely allows it to initiate the fimbrial assembly on the surface and consequently be localized on the distal portion of the fimbriae. It is probable that there may be a structure on the surface that serves flippase-like function to transport the pre-assembly complex in addition to individual Mfa1 and Mfa2 subunits from the periplasm to the surface. Once the pre-assembly complex localizes on the surface, proteolytic processing by either RgpA or B will initiate, and subsequently the N-terminal lipid will be eliminated, allowing the complex to either completely be detached from the

surface or only attached to it with reduced affinity. Next, individual precursor Mfa1 subunits will be transported to the surface where they will undergo Rgp processing to assume a polymerization competent state. Mature Mfa1 then polymerizes with the mature Mfa1 subunit that is part of the already transported pre-assembly complex, and the elongation of Mfa1 continues with incoming mature Mfa1 subunits. The elongation of Mfa1 is mediated by the terminal regions with alternating hydrophobic residues forming the core of a binding interface between Mfa1 subunits with biochemical property that is intermediate of complete hydrophilicity and hydrophobicity. The elongation is terminated when Mfa2 is transported to the surface and binds to Mfa1. In addition, an early termination seems feasible when Mfa2 interacts with the pre-assembly complex, specifically with Mfa1, Mfa3, and Mfa5, prior to the elongation of Mfa1. It is likely that the anchoring of Mfa1 fimbriae is mediated partly by an unknown molecule(s) on the surface and not solely by Mfa2 as our surface expression data indicated that *mfa2* mutant still expressed Mfa1 on the surface. With regards to a potential degradation pathway that exists with the periplasm for accumulating Mfa3, an incomplete pre-assembly complex such as a binary complex between Mfa3 and Mfa4 or between Mfa3 and Mfa5 or a tertiary complex amongst Mfa1, Mfa3, and Mfa4 or amongst Mfa1, Mfa3, and Mfa5 may be targeted by a DegP-like periplasmic protease such as HsdR, which would specifically degrade Mfa3 and hence negating its function as an adaptor protein.

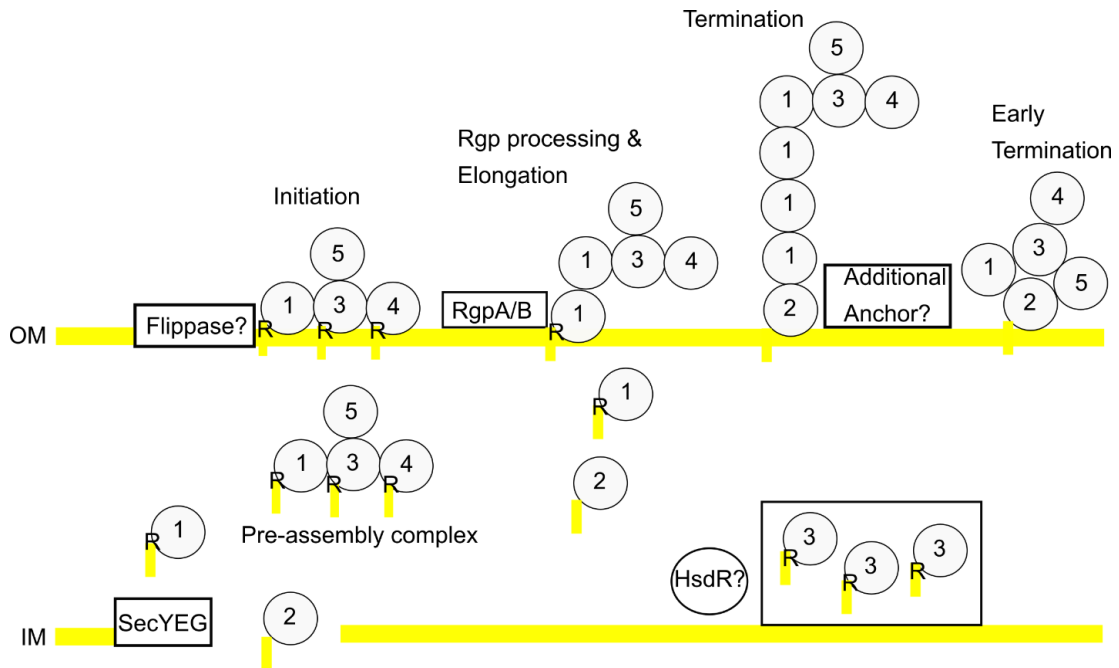


Figure 24. Proposed assembly model of Mfa1 fimbriae. Nascent Mfa proteins are transported into the periplasm via SecYEG translocon. Upon translocation, signal peptides are cleaved by type II signal peptidase for Mfa1-4 and type I signal peptidase for Mfa5. Mfa1-4 are subsequently lipidated. Mfa3 binds Mfa1, 4, and 5 to form a pre-assembly complex and directs the complex to the outer membrane. The complex is presented to the surface through a currently unknown mechanism that may involve a flippase-like protein. On the surface, all Mfa proteins except Mfa2 undergo processing by either RgpA or B that results in the release of N-terminal lipid, enabling the detachment of the complex from the surface and the elongation of Mfa1 to continue. Individual units of Mfa1 are presented to the surface and processed by RgpA/B in the same manner. Upon processing by RgpA/B, Mfa1 assumes a polymerization competent state. Through its terminal regions involving alternating hydrophobic residues reminiscent of DSE, Mfa1 attaches to previous Mfa1 subunit to continue the elongation. Mfa2 is presented to the surface and adheres to Mfa1 to terminate the elongation of Mfa1. In the case that Mfa2 directly interacts with pre-assembly complex, the fimbrial elongation results in early termination. Additional unknown anchoring molecules may help stabilize the fimbrial structure on the surface. Excess Mfa3 that failed to form a pre-assembly complex may be tagged for degradation by a periplasmic protease such as HsdR. Numbers correspond to *mfa* gene number (e.g. 1=Mfa1, 2=Mfa2 etc). Figure not drawn to scale. OM=outer membrane. IM=inner membrane. R=arginine residue targeted by RgpA/B.

CHAPTER 5 CONCLUSION

Here, we demonstrated that the Mfa1 fimbrial biogenesis involves complex protein-protein interactions that entail participation of all proteins of Mfa1 fimbriae with their initial interaction in the periplasm followed by their proteolytic processing by Rgp gingipains on the surface that in turn initiates the Mfa1 polymerization, the mechanism of which necessitates terminal regions with alternating hydrophobic residues forming the core of the likely binding interface reminiscent of DSE-like polymerization mechanism. Importantly, our findings may aid in the development of oral therapeutics that target the assembly mechanisms of Mfa1 fimbriae to ultimately render the assembly process dysfunctional resulting in *P. gingivalis* less likely to interact with primary colonizers and form pathogenic biofilm. However, more studies are needed as the crystal structure of Mfa1 is still unavailable, which would yield additional evidence into the polymerization mechanism, and the mechanism of elongation termination (i.e. how Mfa2 expression and/or activation, if any, is regulated) remains unclear. Moreover, the physiological significance of the pre-assembly complex, which serves as a fimbrial cap at the distal portion of the fimbriae, needs further investigation although the complex likely serves a virulence role through its participation in biofilm formation and interbacterial adhesion.

REFERENCES

1. Eke PI, Dye BA, Wei L, Slade GD, Thornton-Evans GO, Borgnakke WS, et al. Update on Prevalence of Periodontitis in Adults in the United States: NHANES 2009 – 2012. *Journal of periodontology*. 2015;86(5):611-22.
2. Lamont RJ, Hajishengallis G. Polymicrobial synergy and dysbiosis in inflammatory disease. *Trends in molecular medicine*. 2015;21(3):172-83.
3. Kuboniwa M, Lamont RJ. Subgingival biofilm formation. *Periodontology 2000*. 2010;52(1):38-52.
4. Dixon DR, Darveau RP. Lipopolysaccharide heterogeneity: innate host responses to bacterial modification of lipid A structure. *Journal of dental research*. 2005;84(7):584-95.
5. Burns E, Bachrach G, Shapira L, Nussbaum G. Cutting Edge: TLR2 is required for the innate response to *Porphyromonas gingivalis*: activation leads to bacterial persistence and TLR2 deficiency attenuates induced alveolar bone resorption. *Journal of immunology (Baltimore, Md : 1950)*. 2006;177(12):8296-300.
6. Rangarajan M, Aduse-Opoku J, Paramonov N, Hashim A, Bostanci N, Fraser OP, et al. Identification of a Second Lipopolysaccharide in *Porphyromonas gingivalis* W50. *Journal of bacteriology*. 2008;190(8):2920-32.
7. Zhang Y, Gaekwad J, Wolfert MA, Boons GJ. Synthetic tetra-acylated derivatives of lipid A from *Porphyromonas gingivalis* are antagonists of human TLR4. *Organic & biomolecular chemistry*. 2008;6(18):3371-81.
8. Sawada N, Ogawa T, Asai Y, Makimura Y, Sugiyama A. Toll-like receptor 4-dependent recognition of structurally different forms of chemically synthesized lipid As of *Porphyromonas gingivalis*. *Clinical and experimental immunology*. 2007;148(3):529-36.
9. Coats SR, Jones JW, Do CT, Braham PH, Bainbridge BW, To TT, et al. Human Toll-like receptor 4 responses to *P. gingivalis* are regulated by lipid A 1- and 4'-phosphatase activities. *Cellular microbiology*. 2009;11(11):1587-99.
10. Slaney JM, Gallagher A, Aduse-Opoku J, Pell K, Curtis MA. Mechanisms of Resistance of *Porphyromonas gingivalis* to Killing by Serum Complement. *Infection and immunity*. 2006;74(9):5352-61.
11. Gorasia DG, Veith PD, Chen D, Seers CA, Mitchell HA, Chen YY, et al. *Porphyromonas gingivalis* Type IX Secretion Substrates Are Cleaved and Modified by a Sortase-Like Mechanism. *PLoS pathogens*. 2015;11(9):e1005152.
12. How KY, Song KP, Chan KG. *Porphyromonas gingivalis*: An Overview of Periodontopathic Pathogen below the Gum Line. *Frontiers in microbiology*. 2016;7:53.
13. Brunner J, Scheres N, El Idrissi NB, Deng DM, Laine ML, van Winkelhoff AJ, et al. The capsule of *Porphyromonas gingivalis* reduces the immune response of human gingival fibroblasts. *BMC microbiology*. 2010;10:5.
14. Laine ML, van Winkelhoff AJ. Virulence of six capsular serotypes of *Porphyromonas gingivalis* in a mouse model. *Oral microbiology and immunology*. 1998;13(5):322-5.

15. Guo Y, Nguyen KA, Potempa J. Dichotomy of gingipains action as virulence factors: from cleaving substrates with the precision of a surgeon's knife to a meat chopper-like brutal degradation of proteins. *Periodontology* 2000. 2010;54(1):15-44.
16. Glew MD, Veith PD, Peng B, Chen YY, Gorasia DG, Yang Q, et al. PG0026 is the C-terminal signal peptidase of a novel secretion system of *Porphyromonas gingivalis*. *The Journal of biological chemistry*. 2012;287(29):24605-17
17. Enersen M, Nakano K, Amano A. *Porphyromonas gingivalis* fimbriae. *Journal of oral microbiology*. 2013;5.
18. Watanabe K, Onoe T, Ozeki M, Shimizu Y, Sakayori T, Nakamura H, et al. Sequence and product analyses of the four genes downstream from the fimbriin gene (*fimA*) of the oral anaerobe *Porphyromonas gingivalis*. *Microbiology and immunology*. 1996;40(10):725-34.
19. Yilmaz O, Watanabe K, Lamont RJ. Involvement of integrins in fimbriae-mediated binding and invasion by *Porphyromonas gingivalis*. *Cellular microbiology*. 2002;4(5):305-14.
20. Maeda K, Nagata H, Nonaka A, Kataoka K, Tanaka M, Shizukuishi S. Oral streptococcal glyceraldehyde-3-phosphate dehydrogenase mediates interaction with *Porphyromonas gingivalis* fimbriae. *Microbes and infection*. 2004;6(13):1163-70.
21. Pierce DL, Nishiyama S, Liang S, Wang M, Triantafilou M, Triantafilou K, et al. Host adhesive activities and virulence of novel fimbrial proteins of *Porphyromonas gingivalis*. *Infection and immunity*. 2009;77(8):3294-301.
22. Nagano K, Hasegawa Y, Murakami Y, Nishiyama S, Yoshimura F. *FimB* regulates *FimA* fimbriation in *Porphyromonas gingivalis*. *Journal of dental research*. 2010;89(9):903-8.
23. Hamada N, Sojar HT, Cho MI, Genco RJ. Isolation and characterization of a minor fimbria from *Porphyromonas gingivalis*. *Infection and immunity*. 1996;64(11):4788-94.
24. Park Y, Simionato MR, Sekiya K, Murakami Y, James D, Chen W, et al. Short fimbriae of *Porphyromonas gingivalis* and their role in coadhesion with *Streptococcus gordonii*. *Infection and immunity*. 2005;73(7):3983-9.
25. Demuth DR, Irvine DC, Costerton JW, Cook GS, Lamont RJ. Discrete Protein Determinant Directs the Species-Specific Adherence of *Porphyromonas gingivalis* to Oral Streptococci. *Infection and immunity*. 2001;69(9):5736-41.
26. Brooks W, Demuth DR, Gil S, Lamont RJ. Identification of a *Streptococcus gordonii* SspB domain that mediates adhesion to *Porphyromonas gingivalis*. *Infection and immunity*. 1997;65(9):3753-8.
27. Daep CA, Novak EA, Lamont RJ, Demuth DR. Structural dissection and in vivo effectiveness of a peptide inhibitor of *Porphyromonas gingivalis* adherence to *Streptococcus gordonii*. *Infection and immunity*. 2011;79(1):67-74.
28. Zeituni AE, Jotwani R, Carrion J, Cutler CW. Targeting of DC-SIGN on human dendritic cells by minor fimbriated *Porphyromonas gingivalis* strains elicits a distinct effector T cell response. *Journal of immunology (Baltimore, Md : 1950)*. 2009;183(9):5694-704.
29. Naito M, Hirakawa H, Yamashita A, Ohara N, Shoji M, Yukitake H, et al. Determination of the genome sequence of *Porphyromonas gingivalis* strain ATCC 33277 and genomic comparison with strain W83 revealed extensive genome rearrangements in *P. gingivalis*. *DNA research : an international journal for rapid publication of reports on genes and genomes*. 2008;15(4):215-25.
30. Hasegawa Y, Iijima Y, Persson K, Nagano K, Yoshida Y, Lamont RJ, et al. Role of *Mfa5* in Expression of *Mfa1* Fimbriae in *Porphyromonas gingivalis*. *Journal of dental research*. 2016;95(11):1291-7.

31. Hasegawa Y, Iwami J, Sato K, Park Y, Nishikawa K, Atsumi T, et al. Anchoring and length regulation of *Porphyromonas gingivalis* Mfa1 fimbriae by the downstream gene product Mfa2. *Microbiology (Reading, England)*. 2009;155(Pt 10):3333-47.
32. Xu Q, Shoji M, Shibata S, Naito M, Sato K, Elsliger MA, et al. A Distinct Type of Pilus from the Human Microbiome. *Cell*. 2016;165(3):690-703.
33. Hasegawa Y, Nagano K, Ikai R, Izumigawa M, Yoshida Y, Kitai N, et al. Localization and function of the accessory protein Mfa3 in *Porphyromonas gingivalis* Mfa1 fimbriae. *Molecular oral microbiology*. 2013;28(6):467-80.
34. Ikai R, Hasegawa Y, Izumigawa M, Nagano K, Yoshida Y, Kitai N, et al. Mfa4, an Accessory Protein of Mfa1 Fimbriae, Modulates Fimbrial Biogenesis, Cell Auto-Aggregation, and Biofilm Formation in *Porphyromonas gingivalis*. *PloS one*. 2015;10(10):e0139454.
35. Daep CA, James DM, Lamont RJ, Demuth DR. Structural characterization of peptide-mediated inhibition of *Porphyromonas gingivalis* biofilm formation. *Infection and immunity*. 2006;74(10):5756-62.
36. Daep CA, Lamont RJ, Demuth DR. Interaction of *Porphyromonas gingivalis* with oral streptococci requires a motif that resembles the eukaryotic nuclear receptor box protein-protein interaction domain. *Infection and immunity*. 2008;76(7):3273-80.
37. Chung WO, Demuth DR, Lamont RJ. Identification of a *Porphyromonas gingivalis* receptor for the *Streptococcus gordonii* SspB protein. *Infection and immunity*. 2000;68(12):6758-62.
38. Klopsteck P, Hall M, Hasegawa Y, Persson K. Structure of the fimbrial protein Mfa4 from *Porphyromonas gingivalis* in its precursor form: implications for a donor-strand complementation mechanism. *Scientific reports*. 2016;6:22945.
39. Shoji M, Naito M, Yukitake H, Sato K, Sakai E, Ohara N, et al. The major structural components of two cell surface filaments of *Porphyromonas gingivalis* are matured through lipoprotein precursors. *Molecular microbiology*. 2004;52(5):1513-25.
40. Zuckert WR. Secretion of bacterial lipoproteins: through the cytoplasmic membrane, the periplasm and beyond. *Biochimica et biophysica acta*. 2014;1843(8):1509-16.
41. Nakayama K, Yoshimura F, Kadowaki T, Yamamoto K. Involvement of arginine-specific cysteine proteinase (Arg-gingipain) in fimbriation of *Porphyromonas gingivalis*. *Journal of bacteriology*. 1996;178(10):2818-24.
42. Kadowaki T, Nakayama K, Yoshimura F, Okamoto K, Abe N, Yamamoto K. Arg-gingipain acts as a major processing enzyme for various cell surface proteins in *Porphyromonas gingivalis*. *The Journal of biological chemistry*. 1998;273(44):29072-6.
43. Proft T, Baker EN. Pili in Gram-negative and Gram-positive bacteria - structure, assembly and their role in disease. *Cellular and molecular life sciences : CMLS*. 2009;66(4):613-35.
44. Waksman G, Hultgren SJ. Structural biology of the chaperone-usher pathway of pilus biogenesis. *Nature reviews Microbiology*. 2009;7(11):765-74.
45. Remaut H, Rose RJ, Hannan TJ, Hultgren SJ, Radford SE, Ashcroft AE, et al. Donor-strand exchange in chaperone-assisted pilus assembly proceeds through a concerted beta strand displacement mechanism. *Molecular cell*. 2006;22(6):831-42.
46. Diaz AA, Tomba E, Lennarson R, Richard R, Bagajewicz MJ, Harrison RG. Prediction of protein solubility in *Escherichia coli* using logistic regression. *Biotechnology and bioengineering*. 2010;105(2):374-83.
47. Nishiyama M, Vetsch M, Puorger C, Jelesarov I, Glockshuber R. Identification and characterization of the chaperone-subunit complex-binding domain from the type 1 pilus assembly platform FimD. *Journal of molecular biology*. 2003;330(3):513-25.

48. Hulme EC, Trevethick MA. Ligand binding assays at equilibrium: validation and interpretation. *British Journal of Pharmacology*. 2010;161(6):1219-37.
49. Micsonai A, Wien F, Kernya L, Lee YH, Goto Y, Refregiers M, et al. Accurate secondary structure prediction and fold recognition for circular dichroism spectroscopy. *Proceedings of the National Academy of Sciences of the United States of America*. 2015;112(24):E3095-103.
50. Li SC, Goto NK, Williams KA, Deber CM. Alpha-helical, but not beta-sheet, propensity of proline is determined by peptide environment. *Proceedings of the National Academy of Sciences of the United States of America*. 1996;93(13):6676-81.
51. Lebowitz J, Lewis MS, Schuck P. Modern analytical ultracentrifugation in protein science: A tutorial review. *Protein science : a publication of the Protein Society*. 2002;11(9):2067-79.
52. Sriswasdi S, Harper SL, Tang HY, Speicher DW. Enhanced identification of zero-length chemical cross-links using label-free quantitation and high-resolution fragment ion spectra. *Journal of proteome research*. 2014;13(2):898-914.
53. Holding AN. XL-MS: Protein cross-linking coupled with mass spectrometry. *Methods (San Diego, Calif)*. 2015;89:54-63.

CURRICULUM VITA

Name: Jae Y. Lee

Email: jae.lee@louisville.edu

Education

University of Louisville, Louisville, KY May 2020 (expected)

- D.M.D./Ph.D. (dual-degree program)
- Dissertation advisor: Richard J. Lamont, Ph.D.

University of Kentucky, Lexington, KY May 2013

- B.S. Mathematics

The Gatton Academy of Mathematics and Science, Bowling Green, KY May 2011

- High school diploma
- Early college program

Conferences and Presentations

IADR/AADR General Session & Exhibitions (oral presentation) 2017

Kentucky Academy of Science Annual Meeting (oral presentation) 2016

Hinman Student Research Symposium (oral presentation) 2016

Research!Louisville (poster presentation) 2016

Colgate Dental Students' Conference on Research 2015

Awards and Honors

American Association for Dental Research Bloc Travel Grant 2016

- Awarded a travel grant from the AADR to present research findings at 2017 IADR/AADR General Session & Exhibitions in San Francisco, CA

1st Place, Microbiology Section, Kentucky Academy of Science Annual Meeting 2016

Graduate Student of the Month 2016

- Selected amongst the graduate students in the School of Interdisciplinary and Graduate Studies for the month of February

Basic Sciences Award 2016

- Finished in the top 10% of the class in biochemistry, physiology, and anatomy courses in the first year of dental school

F30 Ruth L. Kirschstein National Research Service Award 2015

- Awarded a four-year fellowship grant from the NIH to characterize fimbrial proteins of periodontal pathogen *Porphyromonas gingivalis*

Academic Merit Scholarship 2014

- Awarded a one-year merit scholarship from the School of Dentistry based on undergraduate GPA and DAT score

Languages

- Korean (native language)
- English (full professional proficiency)